AN ABSTRACT OF THE THESIS OF

Karen M. Radakovich for the degree of Doctor of Philosophy in Chemistry
presented on May 26, 2005.

Title: Quantifying *In Situ* β-Glucosidase and Phosphatase Activity in Groundwater.

Abstract approved: _Redacted for Privacy____

Jennifer A. Field

Enzymes play an important role in the environment, they breakdown natural-occurring and anthropogenic molecules so that they can be transported into cells and utilized. Enzyme assays are routinely used in soil science and oceanography to measure the activities of specific processes and to serve as general indicators of microbial activity. Conventional enzyme assays are conducted as batch incubation of sediment and water samples. During these assays the concentration of product is measured and enzyme activity is then determined as the rate of product formation. Few studies have measured enzyme activities of groundwater. This work investigates the use of β-glucosidase and phosphatase assays for quantifying *in situ* enzyme activities in groundwater. Improvements to conventional enzyme assays using *p*-nitrophenyl substituted compounds were made by developing a high performance liquid chromatography method to improve quantitation limits of the product and to quantify concentrations of both the substrate and the product. An *in situ* single-well push pull test was then conducted to measure β-glucosidase activity *in situ* and to estimate the Michaelis constant (K_m) and the maximum reaction velocity (V_{max}) in petroleum-contaminated groundwater at a field site near

Newberg, Oregon. An important feature of the single-well push pull test is the nonlinear drop in pore water velocity that the test solution experiences as it moves out from the injection point. The nonlinear drop in pore water velocity is of particular interest because enzyme-mediated reactions are very fast and changes in the hydraulic properties during the test may give rise to mass-transport limitations. Fast reactions lead to the simultaneous depletion of substrate and accumulation of product at the site of the reaction so substrate and product concentrations near the enzyme can be different then the concentrations in bulk solution. And the rates obtained from a single-well push pull tests may be a combination of the rates at which substrate diffuses to the microorganism and at which the reaction occurs. Laboratory experiments with sediment-packed columns were conducted with a range of pore water velocities typically achieved in the subsurface during as push-pull test as a means for examining the potential effects of inhibition and diffusion on phosphatase enzyme kinetics. In this set of column experiments rates of phosphatase-mediated reactions were investigated instead of β-glucosidase, which is an inducible enzyme. Numerical investigations were then conducted to examine the importance of diffusion limitations for describing the influence of transport processes on the observed rates of reaction. The theoretical investigation was conducted by formally upscaling the proposed sub-pore-scale processes to develop a macroscale (or Darcy scale) description of the transport of the substrate. These results indicate that mass-transfer limitations due to the diffusion of the substrate to the enzyme cause an increase in the apparent K_m but have no effect on V_{max}. In this study an analytical method was developed to measure rates of enzyme-mediated reaction *in situ* so that the measured rates reflected actual rates of microorganism in their natural environment. More carefully

controlled laboratory experiments demonstrated that rates of enzyme-mediated reactions measured at low substrate concentrations depended on the flow properties of the test solution.

Quantifying In Situ β-Glucosidase and Phosphatase Activity in Groundwater

by

Karen M. Radakovich

A THESIS

submitted to

Oregon State University

in partial fulfillment of
the requirements for the
degree of

Doctor of Philosophy

Presented May 26, 2005
Commencement June 2006

<u>Doctor of Philosophy</u> thesis of <u>Karen M. Radakovich</u> presented on <u>May 26, 2005</u>.

APPROVED:

Redacted for Privacy

Major Professor, representing Chemistry

Redacted for Privacy

Chair of the Department of Chemistry

Redacted for Privacy

Dean of the Graduate School

I understand that my thesis will become part of the permanent collection of Oregon State University libraries. My signature below authorizes release of my thesis to any reader upon request.

Redacted for privacy

Karen M. Radakovich, Author

CONTRIBUTION OF AUTHORS

Dr. Jack Istok provided access to the Newberg and Beatty field sites as well as assistance with the design and logistics of laboratory column and field experiments. Dr. Brian Wood and Dr. Fabrice Golfier provided mathematical support and the associated numerical evaluations.

TABLE OF CONTENTS

TABLE OF CONTENTS (Continued)

LIST OF FIGURES

LIST OF TABLES

QUANTIFYING IN SITU β-GLUCOSIDASE AND PHOSPHATASE ACTIVITY IN GROUNDWATER

Chapter 1

Introduction

Groundwater systems are important because they supply drinking water to nearly half of the world's population. Surface activities and disposal practices have resulted in the contamination of groundwater. Microorganisms catalyze a number of processes that dictate geochemical changes in the subsurface [1, 2]. Many methods like direct counts, culture methods, and biochemical markers focus on identifying the types of organisms present in an aquifer while other methods such as activity measurements focus on the net effects of microbial processes. More information on the identity and actions of subsurface microorganisms in both pristine and contaminated aquifers is needed to support site evaluations and monitor bioremediation efforts. Because the subsurface is vast and access is limited, it is difficult and expensive to interrogate the subsurface microbial community. One fundamental problem encountered by scientists studying the role of microorganisms in subsurface environments is that while aquifer systems are large, most methods used to interrogate the microbial community are carried out on relatively small amounts of collected groundwater and sediments. *In situ* test methods are desirable because they are carried out in the subsurface and measure processes carried out by microorganisms in their native environment. Microorganisms are now recognized for their ability to breakdown numerous contaminants such as BTEX (Benzene, Toluene, Ethyl benzene, and Xylene) compounds [3, 4], as well as compounds like CAHs

(Chlorinated Aliphatic Hydrocarbons) [5-7] and MTBE [8, 9] that initially were considered to be immune to degradation in subsurface environments.

One strategy microorganisms employ to degrade compounds is to speed up reactions by catalyzing reactions with enzymes. Enzymes from subsurface organisms have been shown to degrade contaminants as a carbon and energy source coincidentally due to co-metabolism. Enzymes are specialized proteins that catalyze biochemical reactions that would otherwise proceed too slowly to be of metabolic consequence. Hydrolases are one class of enzymes microorganisms use to break down large molecules into smaller molecules that can be taken into the cell and utilized. Hydrolases break down molecules by adding a water molecule across a covalent bond. Phosphatase and β-glucosidase enzymes are two types of hydrolases that are investigated in this study; they are responsible for the hydrolysis of ester linked organic phosphate and β -linked polysaccharides [10].

Viable cells contain at least four distinct types of enzymes and are classified by location as: intracellular enzyme, which function within the cytoplasm of Gram-positive bacteria; periplasmic enzymes, which are restricted to the periplasmic space in Gram-negative bacteria; surface-bound enzymes which are attached to the outer surface of the cell; and extracellular enzyme, which were secreted by living cells and are free in solution [11]. The term ectoenzymes is often applied to describe both periplasmic and surface-bound enzymes. In aquatic environments 85 to 92% of the total enzyme activity was attributed to ectoenzymes, with the remaining activity due to extracellular enzymes [10]. Activities of a variety of ecto- and extracellular enzymes have been measured on numerous environmental samples including soils [12-14], subsurface sediments [15],

stream sediments [16], marine sediments [17], groundwater [18], lake water [19, 20], and sea water [21, 22].

Enzyme-catalyzed reactions can be described by the following equation

$$E + S \underset{k_{-1}}{\overset{k_1}{\leftrightarrow}} ES \overset{k_2}{\rightarrow} E + P \qquad \text{(Eq. 1)}$$
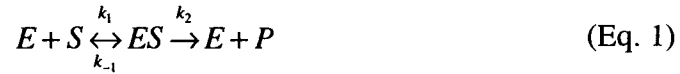
where the concentrations of the free enzyme and substrate are represented by E and S, the enzyme-substrate complex is ES, and the product is P. The rate constants for the formation and breakdown of the enzyme-substrate are k_1 and k_{-1}, and the transformation of the enzyme-substrate complex to product is k_2. The rate of an enzyme catalyzed reaction (v) typically is defined by the Michealis-Menten equation

$$v = \frac{V_{max} \cdot S}{K_m + S} \qquad \text{(Eq. 2)}$$

where K_m is $(k_2 + k_{-1})/k_1$ with units of substrate concentration, and V_{max} is $k_2(E + ES)$ with units of moles of product per unit time. Although the Michaelis-Menton equation was derived to express the rates of reaction catalyzed by enzymes that are free in a homogenous solution, it has been used to describe the kinetics of enzyme-mediated reactions of more complex heterogeneous systems like soil and sediment samples [14, 23]. The use of kinetic analysis of enzyme-mediated reaction rates for heterogeneous microbial populations was shown provide a good fit to the Michaelis-Menton equation with some deviations in rates observed at low substrate concentrations [24].

A lack of specificity at the active sites of some enzymes allows substances that are structurally similar to the substrate, including the end product, to bind reversibly with the enzyme. This situation, known as competitive inhibition, reduces the concentration of enzyme available to bind with the substrate. The rate of an enzyme catalyzed reaction (v)

which includes the effects of competitive inhibition is defined by a modified Michaelis-Menten equation give by

$$v = \frac{V_{max} \cdot S}{K_m(1 + \dfrac{I}{K_i}) + S}$$

(Eq. 3)

where I is the concentration of the inhibitor in moles per liter, and K_i is the dissociation constant for the enzyme-inhibitor complex. When $I \ll K_i$, then Eq. 3 reduces to the Michaelis-Menten equation. When $I \gg K_i$, the observed reaction rate is decreased. It should be noted that in either case, when $S \gg K_m$ the rate of the reaction approaches V_{max} and is independent of the inhibition effects and substrate concentration. The value of K_i determines how sensitive the rate of the reaction will be to the presence of the inhibitor.

While many methods like direct counts, culture methods, and biochemical markers focus on identifying the types of organisms present in an aquifer other methods such as activity measurements focus on the net effects of microbial processes. The measurement of specific enzyme activities as a surrogate for microbial activity has been widely used in soil science, oceanography, and limnology. Enzyme assays used to measure activity employ substrates that are transformed by a number of different enzymes to allow for a broader spectrum of enzyme activity and thus microbial activity to be measured. Some of the enzymes used for this purpose include dehydrogenase, esterase, protease, and phosphatase [25]. Enzyme assays are routinely conducted to assess the microbial activity of surface soils and water from collected samples but few studies have attempted to measure microbial activity of subsurface microorganisms *in situ*.

Methods used to quantify enzyme activities are based on the enzymatic conversion of chromogenic, fluorogenic, or radiolabeled substrates. Incubations with

these substrates are carried out at elevated temperatures and pH to give optimum rates. The rates of these enzyme-mediated reactions are measured by quantifying the increase in the concentration of the products. Reviews of these methods have been conducted by Tabatabai [14] and Chróst [26]. Many of these methods are able to measure nanomolar product concentrations and therefore can quantify reaction rates in samples that have very low enzyme activities. Although these methods have assayed enzyme activities on a wide range of samples in microcosm studies, few studies have attempted to measure enzyme activities *in situ*. Our interest is to select and optimize current enzyme assays so that *in situ* measurements of enzyme activity of subsurface microorganisms can be made.

Methods for measuring *in situ* enzyme activity in aquifers require substrates that have chemical properties that make them compatible with use in the subsurface, and a method that can quantify both the substrate and product concentrations. Substrates must be able to be transported out into the aquifer to contact sediment-bound microorganisms. Substrates will therefore need to have high water solubility and a low affinity for sorption to the aquifer solids. While fluorogenic substrates such as florescein diacetate and 4-methyl-umbelliferone substituted substrates produce products with superior detection limits, they have high affinities for solids that make them poor candidates for *in situ* test methods. Soil scientists have used *p*-nitrophenyl substituted substrates in enzyme assays. These compounds have high aqueous solubility and exhibit very little sorption, which makes them an excellent choice for *in situ* use. In soil science enzyme activities are large enough that low detection limits are not required. Enzyme activities have been shown to decrease down the soil profile [15] and in the saturated subsurface activities are expected to be even lower due to low nutrient availability, low temperature, and low oxygen

concentrations. Subsurface environments typically have reduced enzyme activities; therefore, methods to interrogate this environment require lower detection limits. Moreover, methods developed for *in situ* use in groundwater need to separate and quantify both substrate and product concentrations.

An improved method for assaying β-glucosidase activity using *p*-nitrophenyl-β-D-glucopyranoside coupled with high performance liquid chromatography (HPLC) was developed to support *in situ* measurement of enzyme activity. The method offers improvements to conventional soil methods by reducing detection limits by first chromatographically separating the product prior to detection and quantitation. This HPLC method allows the simultaneous quantitation of both substrate and product, which is essential for *in situ* testing applications. This method is demonstrated on groundwater samples and sediment cores, and then used to measure *in situ* β-glucosidase activities in petroleum-contaminated groundwater at a site near Newberg, OR.

The single well push pull test method was selected as the field method for this study. Push-pull tests have been used to study numerous processes that occur in the subsurface under *in situ* conditions [27-29]. Push-pull tests eliminate many disadvantages of laboratory-based microcosm studies including; the need for core material, small volume of samples, disturbance and contamination during sample collection, handling, and testing, artificial laboratory environment. A typical push-pull test consists of four phases; a pretest purging and sampling, an injection, a rest, and sampling phase. During the purging and sampling phase, the water contained in the well casing is removed and native groundwater is sampled to obtain background information. A test solution containing one or more reactive solutes and a nonreactive solute is

pumped into the subsurface at a constant rate where it mixes with native groundwater and is exposed to the subsurface microorganisms. The injection phase may or may not be followed by a rest phase depending on the rate of the reaction of interest. The rest phase is omitted for *in situ* studies of fast reaction, like the transformation of a substrate by enzymes or the utilization of oxygen or nitrate as terminal electron acceptors. Conversely, the rest phase is included for *in situ* studies of slow reactions, like the degradation of trichloroethene and BTEX compounds, so the injected test solution can be exposed to subsurface microorganisms long enough to undergo transformation in measurable quantities. Finally, a volume equivalent to 2 to 3 injection volumes is removed as a mixture of the test solution and groundwater during the extraction phase. Then extraction phase samples are analyzed for tracer, reactant, and product concentrations. Conservative tracer concentrations indicated how much of each sample is test solution and how much is groundwater so that reactant and product concentrations can be corrected for dilution due to mixing with groundwater. Breakthrough curves can be constructed to show the relative concentrations C/C_0 against the ratio of the volume extracted to volume injected, which serves as a measure of dimensionless time. A single well push-pull test conducted at petroleum-contaminated site to measure *in situ* β-glucosidase activity is described in Chapter 2.

A feature of the single-well push-pull test is the nonlinear drop in the pore water velocity of the injected solution as it moves out radially from the injection point. Pore water velocity is inversely related to residence time. As the concentration of substrate decreases as it moves outward from the well during a push-pull test and is converted to product by the indigenous microorganisms. A small percent of the injected substrate is

converted to product that substrate concentration is relatively unaffected by the enzyme-mediated reaction. However, the concentration of the product builds up as the test solution moves outward from the well. Increases in the concentration of the product, phosphate, are of interest because phosphate is a known competitive inhibitor of phosphatases. So the measured phosphatase rates depend on the concentrations of substrate and product, according to equation 3. The pore water velocity ($v(r)$) experienced by the test solution is given by the following equation,

$$v(r) = \frac{Q}{2\pi r h \eta} \qquad \text{(Eq.4)}$$

where Q is the pumping rate ($m^3 s^{-1}$), h is the vertical thickness of the injection/extraction zone, and η is the porosity. Figure 1 shows pore water velocities as a function of radial distance from the well. The pore water velocities were calculated with typical test conditions including a vertical thickness of 1 m, a porosity of 0.30, and an injection pumping rate of 1.6 x 10^{-5} m^3/s (1L/min). The four data points in Figure 1 represent pore water velocities selected for use in laboratory column experiments conducted to investigate the effects of pore water velocity on observed reaction rates, which are discussed in Chapter 3.
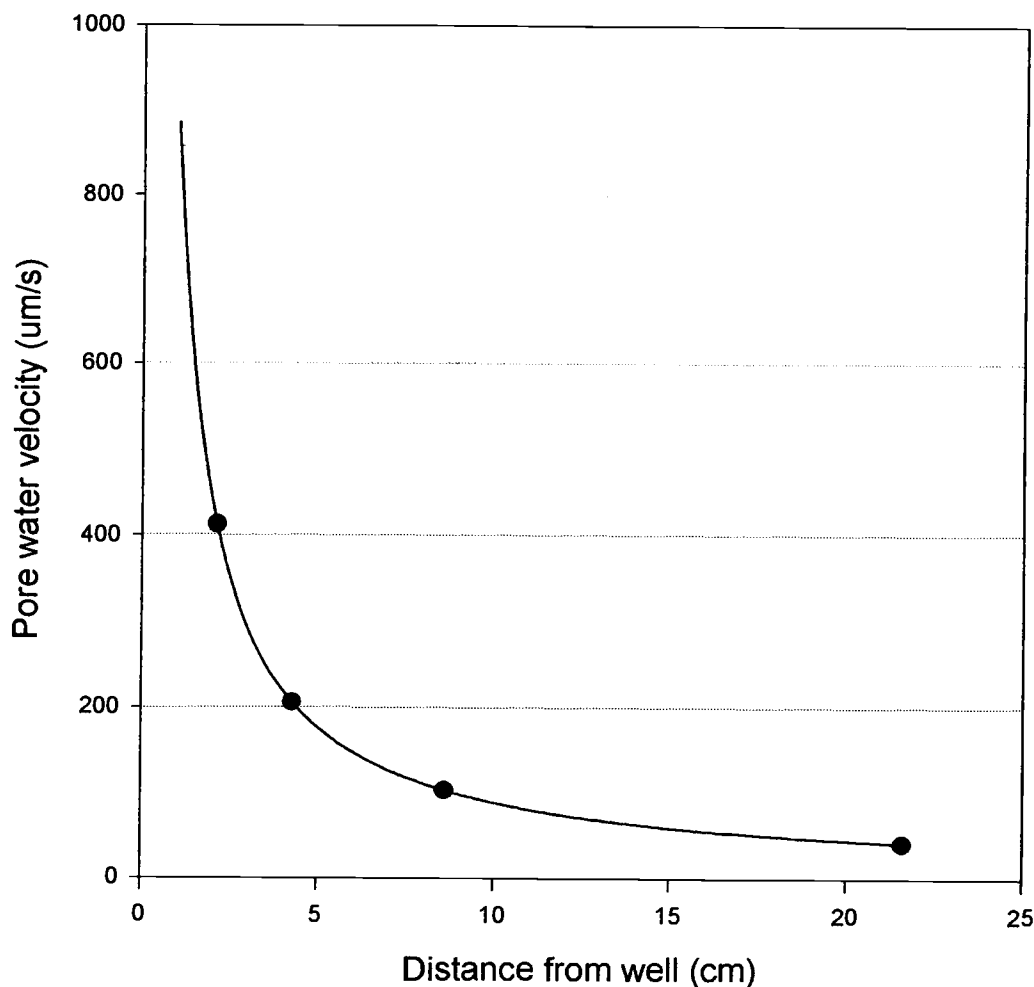
Figure 1.1. Subsurface pore water velocity as a function of distance from the injection well during a single well push-pull test.

Another potential effect of varying pore water velocity is mass transfer limitations due to diffusion [30, 31]. The rate of any reaction is dictated by the reaction mechanisms slowest step. Difference in the pore water velocities experienced during a push-pull test lead to hydrodynamic variation in the test, such as the thickness of the stagnant layer surrounding sediment particles. The effects of diffusion have been investigated for a number of bound enzyme systems [32-38]. Soil scientists have documented changes in

observed reaction rates due to shaking in batch experiments [39] and flow rate in column experiments [40, 41], suggesting that the reactions are mass transfer limited. Diffusion effects along with the simultaneous depletion of the substrate and accumulation of the product at the enzyme can lead to concentration gradients being established between the local environment of the enzyme and bulk solution. If the rate of delivery of substrate to the microbes on the surface of the particle is slower than the rate of enzymatic transformation then the observed rate is due to diffusion and not reaction. In Chapter 4 the potential effects of mass transfer limitations are investigated to determine if results obtained from column are consistent with the presence of diffusional resistances.

Many studies have investigated the role of diffusion in processes that occur in heterogeneous systems such as diffusion and dispersion in porous media [42], mass transfer and reaction in biofilms [43, 44], and the dissolution of dense non-aqueous phase liquids during flow in porous media [45]. All of these studies use the method of volume averaging to develop a macroscopic representation of pore scale processes. The volume averaging theorem allows multiphase transport problems to be simplified to a single phase transport problem [46]. Numerical methods were used to create models that consider the effect of diffusion in porous media with heterogeneous irreversible reaction.

Chapter 2 describes the analytical method developed to quantify β-glucosidase in groundwater, and the demonstration of this method. The reproducibility of method was investigated by measuring β-glucosidase on increasing amounts of biomass collected by filtration from a single sample of groundwater. The ability of the method to quantify spatial variability within a site is demonstrated at two sites one contaminated with petroleum and the other contaminated with chlorinated aliphatic hydrocarbon. Finally the

method was demonstrated on groundwater samples collected during an *in situ* single well push-pull test to measure the β-glucosidase activity of both sediment-bound and free living microorganisms.

The work presented in Chapters 3 and 4 was conducted to examine the potential for measuring enzyme reactions in natural porous media. The third chapter describes laboratory experiments using sediment-packed columns to investigate the affect changing pore water velocity has on the observed rates of enzyme-mediated reactions. The column experiments were conducted with air-dried sediment and air-dried sediment that was autoclaved to determine the relative contribution of abiotic rates to the total observed rates and to determine if pore water velocity affects both biotic and abiotic rates. Inhibition effects due to the build up in product concentrations in columns with lower pore water velocities is evaluated to determine if the decreases in rates can be attributed to increase in the concentration of the inhibitor.

In Chapter 4 a theoretical and numerical investigation is conducted to determine the importance of diffusion limitations for describing the influence of transport processes on the observed rate of reaction. Our theoretical investigation will be conducted by formally upscaling the proposed sub-pore-scale processes to develop a macroscale (or Darcy scale) description of the transport of the reactive chemical species. The goal is to determine if the experimentally observed dependence of the kinetic parameters K_m and V_{max} can be reasonably explained by a diffusive mass transfer limitation in the laboratory studies detailed in Chapter 3.

Literature Cited

[1]   Madsen, E.L. Epistemology of Environmental Microbiology. Environ. Sci. Technol., 1998, **32**(4), p. 429-439

[2]   Chapelle, F.H. Ground-Water Microbiology and Geochemistry. John Wiley and Sons, Inc., Englewood Cliffs, NJ., 1993,

[3]   Costura, R.K. and Alvarez, P.J.J. Expression and longevity of toluene dioxygenase in Pseudomonas putida F1 induced at different dissolved oxygen concentrations. Water Research, 2000, **34**(11), p. 3014-3018

[4]   Prenafeta-Boldu, F.X., Vervoort, J., Grotenhuis, J.T.C., and van Groenenstijn, J.W. Substrate interactions during the biodegradation of benzene, toluene, ethylbenzene, and xylene (BTEX) hydrocarbons by the fungus Cladophialophora sp strain T1. Applied and Environmental Microbiology, 2002, **68**(6), p. 2660-2665

[5]   Leahy, J.G., Byrne, A.M., and Olsen, R.H. Comparison of factors influencing trichloroethylene degradation by toluene-oxidizing bacteria. Applied and Environmental Microbiology, 1996, **62**(3), p. 825-833

[6]   Magnuson, J.K., Romine, M.F., Burris, D.R., and Kingsley, M.T. Trichloroethene reductive dehalogenase from Dehalococcoides ethenogenes: Sequence of tceA and substrate range characterization. Applied and Environmental Microbiology, 2000, **66**(12), p. 5141-5147

[7]   Magnuson, J.K., Stern, R.V., Gossett, J.M., Zinder, S.H., and Burris, D.R. Reductive dechlorination of tetrachloroethene to ethene by two-component enzyme pathway. Applied and Environmental Microbiology, 1998, **64**(4), p. 1270-1275

[8]   Deeb, R.A., Scow, K.M., and Alvarez-Cohen, L. Aerobic MTBE biodegradation: an examination of past studies, current challenges, and future research directions. Biodegradation, 2000, **11**(2-3), p. 171-186

[9]   Fayolle, F., Vandecasteele, J.P., and Monot, F. Microbial degradation and fate in the environment of methyl tert-butyl ether and related fuel oxygenates. Applied Microbiology and Biotechnology, 2001, **56**(3-4), p. 339-349

[10]   Chróst, R.J. Environmental Control of Microbial Ectoenzymes. in *Microbial Enzymes in Aquatic Environmentsl*, Chròst, R.J., Editor. 1991, Speinger-Verlag: New York, p. 30-59

[11]   Burns, R.G. Enzyme Activity in Soil: Location and a Possible Role in Microbial Ecology. Soil Biol. Biochem., 1982, **14** p. 423-427

[12]   Eivazi, F. and Tabatabai, M.A. Phosphatases in Soils. 1976

[13]   Eivazi, F. and Tabatabai, M.A. Glucosidases and galactosidases in soils. Soil Biol. Biochem., 1988, **20**(5), p. 601-606

[14]   Tabatabai, M.A. Soil Enzymes. in *Methods of Soil Analysis, Part 2. Microbiological and Biochemical Properties.* 1994: Madison, p. 775-835

[15]   Taylor, J.P., Wison, B., Mills, M.S., and Burns, R.G. Comparison of microbial numbers and enzymatic activities in surface soils and subsoils using various techniques. Soil Biol. Biochem., 2002, **34**(3), p. 387-401

[16]   Scholz, O. and Marxsen, J. Sediment phosphatases of the Breitenbach, a first-order Central European stream. Arch. Hydrobiol., 1996, **135**(4), p. 433-450

[17]   King, G.M. Characterization of b-glucosidase activity in intertidal marine sediments. Applied and Environmental Microbiology, 1986, **51**(2), p. 373-380

[18]   Hendel, B. and Marxsen, J. Measurement of low-level extracellular enzyme activity in natural waters using fluorigenic model substrates. Acta hydrochim. hydrobiol., 1997, **25**(5), p. 253-258

[19]   Cotner, J.B. and Wetzel, R.G. Bacterial Phosphatases from Different Habitats in a Small, Hardwater Lake. in *Microbial Enzymes in Aquatic Environments*, Chròst, R.J., Editor. 1991, Springer-Verlag: New York, p. 187-205

[20]   Chróst, R.J. Characterization and significance of β-glucosidase activity in lake water. Limnol. Oceanogr., 1989, **34**(4), p. 660-672

[21]   Christian, J.R. and Karl, D.M. Bacterial ectoenzymes in marine waters: activity ratios and temperature responses in three oceanographic provinces. Limnol. Oceanogr., 1995, **40**(6), p. 1042-1049

[22]   Somville, M. Measurement and Study of Substrate Specificity of Exoglucosidase Activity in Eutrophic Water. Applied and Environmental Microbiology, 1984, **48**(6), p. 1181-1185

[23]   Chróst, R.J. Ectoenzymes in aquatic environments: Microbial strategy for substrate supply. Verh. Internat. Verein. Limnol., 1991, **24** p. 2597-2600

[24]   Williams, P.J. The validity of the application of simple kinetic analysis to heterogeneous microbial populations. Limnol. Oceanogr., 1973, **18**(1), p. 159-165

[25] Atlas, R.M. and Bartha, R. Microbial Ecology Fundamentals and Applications. 4th ed. Benjamin/Cunnings Science Publishing, Menlo Park, California, 1998,

[26] Chróst, R.J. Microbial ectoenzymes in aquatic environments. in *Aquatic Microbial Ecology: Biochemical and Molecular Approaches*, Chróst, R.J., Editor. 1990, Springer-Verlag: New York, p. 47-78

[27] Istok, J.D., Humphrey, M.D., Schroth, M.H., Hyman, M.R., and O'Reilly, K.T. Single-Well "Push-Pull" Test for In Situ Determination of Microbial Activities. Groundwater, 1997, **35**(4), p. 619-631

[28] Istok, J.D., Field, J.A., and Schroth, M.H. In Situ Determination of Subsurface Microbial Enzyme Kinetics. Ground Water, 2000, **39**(3), p. 348-355

[29] Schroth, M.H., Istok, J.D., Conner, G.T., Hyman, M.R., Haggerty, R., and O'Reilly, K.T. Spatial variability in in situ aerobic respiration and denitrification rates in a petroleum-contaminated aquifer. Groundwater, 1998, **36**(6), p. 924-937

[30] Bailey, J.E. and Ollis, D.F. Biochemical Engineering Fundamentals. 2nd ed. McGraw-Hill Book Company, New York, 1986, 202-223

[31] Engasser, J.-M. and Horvath, C. Applied Biochemistry and Bioengineering. in *Immobilized Enzyme Principles*, Goldstein, L., Editor. 1976, Academic Press: New York, p. 144-167

[32] Laidler, K.J. and Bunting, P.S. The Kinetics of Immobilized Enzyme Systems. in *Immobilized Enzyme Kinetics*. 1980, Academic Press: New York

[33] Goldstein, L. Kinetic Behavior of Immobillized Enzyme Systems. in *Kinetics of Immobilzed Enzymes*. 1980, Academic Press: New York, p. 397443

[34] Marrazzo, W.N., Merson, R.L., and McCoy, B.J. Enzyme Immobilized in a Packed-Bed Reactor: Kinetic Parameters and Mass Transfer Effects. Biotechnol. Bioeng., 1975, **17**(10), p. 1515-28

[35] Nelsestuen, G.L. and Martinez, M.B. Steady State Enzyme Velocities That Are Independent of [Enzyme]: An Important Behavior in Many Membrane and Particle-Bound States. Biochemistry, 1997, **36**(30), p. 9081-9086

[36] Horvath, C. and Engasser, J.-M. External and Internal Diffusion in Heterogeneous Enzymes Systems. Biotechnology and Bioengineering, 1974, **16** p. 909-923

[37]   Patwardhan, V.S. and Karanth, N.G. Film diffusional influences on the kinetic parameters in packed-bed immobilized enzyme reactors. Biotechnol. Bioeng., 1982, **24**(4), p. 763-80

[38]   Engasser, J.M. and Horvath, C. Inhibition of bound enzymes. II. Characterization of product inhibition and accumulation. Biochemistry, 1974, **13**(19), p. 3849-54.

[39]   Tabatabai, M.A. and Bremner, J.M. Michaelis Constants of Soil Enzymes. Soil Biology and Biochemistry, 1971, **3** p. 317-323

[40]   Marxsen, J. and Schmidt, H. Extracellular phosphatase activity in sediments of the Breitenbach, a Central European mountain stream. Hydrobiologia, 1993, **253** p. 207-216

[41]   Brams, W.H. and McLaren, A.D. Phosphatase Reactions in Columns of Soil. Soil Biol. Biochem., 1974, **6** p. 183-189

[42]   Whitaker, S. Diffusion and dispersion in porous media. A.I.Ch.E. J., 1967, **13** p. 420-427

[43]   Wood, B.D., Quintard, M., and Whitaker, S. Calculation of Effective Diffusivities for Biofilms and Tissues. Biotechnology and Bioengineering, 2002, **77**(5), p. 495-514

[44]   Wood, B.D. and Whitaker, S. Cellular growth in biofilms. Biotechnology and Bioengineering, 1999, **64**(6), p. 656-668

[45]   Quintard, M. and Whitaker, S. Dissolution of an immobile phase during flow in porous media. Ind. and Engng Chem. Res., 1999, **38**(3), p. 833-844

[46]   Whitaker, S. A simple geometrical derivation of the spatial averaging theorem. Chemical Engineering Education, 1985, **19** p. 18-21, 50-52

Chapter 2

Quantifying *In Situ* β-Glucosidase Activity In Groundwater

Karen M. Radakovich[1] and Jennifer A. Field[2], Jonathon D. Istok [3], Brian D. Wood [3]

[1] Department of Chemistry

[2] Department of Environmental and Molecular Toxicology

[3] Department of Civil Engineering

Oregon State University, Corvallis, Oregon 97331

Abstract

In this study we develop a method that permits the measurement of *in situ* enzyme activities in the saturated subsurface. The method uses *p*-nitrophenyl-β-D-glucopyranoside (PNG) as a model substrate to demonstrate the compatibility of *p*-nitrophenyl substituted substrates with an *in situ* single well push-pull test. PNG is one substrate of many *p*-nitrophenyl-substituted compounds that are used in soil science to measure enzyme activity. To enable the coupling of enzyme activity measurements with an *in situ* test we extend the soil science method by chromatographically separating and quantifying both substrate and product concentrations. Laboratory experiments were conducted on groundwater samples to develop and validate the method. β-Glucosidase activities measured on groundwater samples collected from two sites ranged from 0.12 to 29.4 μM PNP/h. An *in situ* demonstration of this method was carried out in an aquifer at one of the sites, which was contaminated with petroleum products. From the extraction-phase data of this test the Michaelis-Menton parameters were determined to be $K_m = 49$ μM PNG and $V_{max} = 1.47$ μM PNP/h. This approach allows the enzyme activities of subsurface microorganism to be measure *in situ*.

Introduction

Enzyme activities have been used as surrogates for microbial metabolic activities [1, 2]. Measurements made of general enzymes like dehydrogenase, esterase, and phosphatase reflect activities of a large portion of the microbial community and serve as quantitative measures of microbial activity [3]. A number of methods have been previously employed to measure enzyme activities on a variety of water and sediment samples, and a review of these methods can be found in Chröst [4] and Tabatabai [5]. These methods are carried out in laboratories with small soil samples as batch incubation experiments with elevated temperature and optimized pH to facilitate sample comparison. The main differences among these methods are the types of substrates used and the detection method employed for quantifying the products.

Our goal is to develop a method for assaying subsurface enzyme activities *in situ*, with a particular emphasis on methods that can be used with single well push-pull tests. A push-pull test is an *in situ* test for interrogating the physical, chemical, and microbial properties of subsurface materials in the field [6-10]. In these tests, reactive and conservative aqueous species are injected into the subsurface (the 'push' phase) and then quantitatively extracted by pumping (the 'pull' phase). Measurements of microbial activity [6] can be made by injecting biologically reactive substrates which are then transported through the subsurface to sediment-bound microorganisms. During injection, these substrates undergo transformation, and the original substrate plus any transformation products formed are recovered during the extraction phase.

Our interest is to effectively measure enzyme activity of microorganisms in the subsurface using push-pull tests. For this approach to be successful we need a method

that (1) can quantify both substrate and product concentration, (2) is sensitive enough to quantify low activities by improving the quantitation limits of the product and (3) employs enzyme substrates that are suitable for *in situ* testing. Suitable enzyme substrates should be chemically stable, have high aqueous solubility, exhibit low sorption, and have low toxicity. Of the methods reviewed by Chróst and Tabatabai, the *p*-nitrophenyl substituted compounds offer the best transport properties and exhibit high aqueous solubility and low sorption to subsurface sediments.

The approach for this research was to modify and optimize conventional soil assays based on the use of *p*-nitrophenyl substituted compounds [11] for use with an *in situ* push-pull test. We modified the previously reported soil enzyme assay by chromatographically separating the substrate and the common product with high performance liquid chromatography (HPLC). This modification enables us to increase the assays sensitivity and to quantify both the substrate and the product. Our goal is to measure enzyme activity *in situ* by injecting substrates into the subsurface, where they mix with groundwater and are transformed by the indigenous microorganisms. Because we are conducting experiments in an open system, we need to quantify both substrate and product concentrations and, account for processes such as dilution as well as transformation. Substrates such as *p*-nitrophenyl-β-D-glucopyranoside (PNG), *p*-nitrophenyl phosphate, and *p*-nitrophenyl sulfate have been used to measure glucosidase, phosphatase and sulfatase activity (respectively) in a variety of soil samples [11-16]. For this work a method was developed to quantify β-glucosidase activity with PNG used as the substrate, and then the method was tested by measuring β-glucosidase activity and kinetics on groundwater and sediment samples from two field sites. Finally, an *in situ*

assay was conducted to demonstrate that the optimized method could successfully measure β-glucosidase activity of indigenous microorganism in the subsurface on one of the field sites.

Experimental

Chemicals and Materials. Standards of PNG (99 %) and PNP (99+ %) were purchased from Aldrich Chemical Co. (Milwaukee, WI). An aqueous quench solution consisted of 0.25 M calcium chloride and 0.20 M tris[hydroxymethyl]amino-methane (Tris) adjusted to pH 12 with NaOH. A 50 mM phosphate buffer (pH 2.5) was prepared in deionized water from monobasic sodium phosphate monohydrate and dibasic sodium phosphate. HPLC grade methanol was obtained from Fisher Scientific.

Groundwater and Sediment Samples. In this study groundwater samples were collected from two field sites, one located in Newberg, Oregon and the other located in Beatty, Oregon. Sediment cores were collected from the Beatty, Oregon site only. The push-pull test conducted as a demonstration of the ability to measure β-glucosidase activity *in situ* was conducted at the Newberg site.

The Newberg site is a former gasoline/diesel fuel distribution center. The site was contaminated by leaky storage tanks and surface spills that occurred between the 1930 and 1991. Ten monitoring wells designated MW-1 through MW-10 were installed between 1991 and 1995. Monitoring wells were constructed with a 5.1-cm internal diameter poly(vinyl chloride) casing and screen. Boring logs indicate that the unconfined aquifer consists primarily of lacustrine deposits of clayey silt and silt, with occasional traces of fine sand, gravel, and peat. Water table depths range from 0.59 to 1.24 m below

land surface. Regional groundwater flow is generally from north to south; the hydraulic gradient is approximately 0.01m/m, and the average groundwater velocity is approximately 10^{-3} m/d. A variety of *in situ* biological and chemical test have been conduct in previous studies at the site [6, 9, 10, 17].

The Beatty site is an industrial site that was contaminated with chlorinated aliphatic hydrocarbons (CAHs). The site was undergoing remediation with soil vapor extraction and a pilot study was being conducted to investigate *in situ* technologies for transforming CAHs to nonhazardous compounds. Thirty-five monitoring wells were installed at this site. Two wells are screened in the upper aquitard, near the CAHs source area where dissolved, sorbed, and free-phase CAHs are located. Twenty-three other wells are screened in the upper and ten in the intermediate zone. Groundwater samples were collected from the seven wells screened in the upper and intermediate zones and are designated P1, P2, P4, P5, P7 and MW-11. Boring logs indicate that the subsurface soils are comprised of a silt and sand mixture grading to course basaltic and rhyolitic sand at an approximate depth of 15-feet. Below this material is a dense, gray silt of varying thickness.

Groundwater samples from both field sites were collected from wells after a purge of three well-casing volumes had been completed. A 50-L sample was collected from MW-10 at the Beatty site as a single sample in a carboy. Smaller 4-L samples were collected from each monitoring well at both sites. The samples were stored at 4 °C until analyzed.

Sediment cores were not collected at the Newberg site. A limited number of sediment cores were available from the Beatty site and were collected at the same time

the groundwater samples were collected as part of an ongoing site investigation. Samples from a variety of locations and depths were collected, cut into approximately 10 cm segments, and placed into 1 quart canning jars and stored at 4°C until analyzed.

β-Glucosidase Activity Measured on Groundwater samples. Attempts to measure β-glucosidase activity directly in groundwater with PNG as a substrate typically did not yield measurable PNP production rates. Therefore, β-glucosidase activity was measured in groundwater samples for which the microbial biomass had first been concentrated. To concentrate microorganisms, 0.25 - 3.0 L of groundwater was filtered through a sterile 47 mm 0.2 μm Nylaflo® membrane filter (Gelman Sciences) using vacuum pressure of less than 67.7 kPa. A maximum of 1.0 L was passed through a single filter; multiple filters were used for larger volumes. A portion of the filtrate was collected and set aside for use as incubation solution. The glass filtration reservoir was rinsed with three 5 mL aliquots of deionized water to ensure that all microorganisms were deposited on the filter. Filters containing the concentrated microorganisms were then placed in clean 40-mL screw-top vials with Teflon-lined lids and stored at 4 °C for no longer than 18 h prior to incubation.

Incubation solutions were prepared to contain the desired PNG concentration with the groundwater filtrate that had been collected and set aside. Filtered groundwater was used in the incubations so that the aqueous environment of the incubations more closely resembled *in situ* conditions than buffered incubation solutions, which are typically used. Incubations of biomass collected from groundwater were conducted at PNG concentrations of 16.6, 132, 266, 664, 1328, 1991, and 2655 μM. Incubations were initiated by adding 30 mL of PNG incubation solution to a 40-mL glass vial containing

filter(s) onto which biomass had been concentrated. The vial was vigorously shaken for 30 s and immediately sampled by withdrawing a 0.5-mL sample for the first sampling time point and placing the sample into a 2-mL vial containing 0.5 mL of quench solution. The aqueous quench solution consisted of 0.25 M calcium chloride and 0.20 M tris-[hydroxymethyl]-aminomethane (Tris) adjusted to pH 12 with NaOH. The quenched samples were then filtered through 13 mm 0.45 μm nylon filters into 2-mL autosampler vials and analyzed by HPLC. Subsequent sampling was conducted in a similar manner.

β-Glucosidase Activity Measured on Sediment Cores . Sediment incubations were set up in the following way. First, a small portion of the sediment sample was mixed in a clean and sterile glass jar using a sterile stainless steel spoon. Then 7.00 ± 0.02 g of sediment was weighed out and transferred to a sterile 40 mL screw top vial with a Teflon lined lid. After all sediment samples were weighed out, a 132 μM PNG solution was prepared in site groundwater that had been previously filtered through a 0.2 μm filter, collected, and stored. At time zero 30 mL of incubation solution was added to the 40 mL vial and shaken vigorously. The incubation vial was allowed to sit for 1 minute, to allow the sediment to settle, and then a 1-mL subsample was taken. Each 1.0-mL sample was mixed with 1.0 mL of quench solution, filtered through a disposable 0.2 μm nylon filter into a 2-mL autosampler vial. All filtered samples were stored at 4 °C until they were analyzed. Additional subsamples were made in the same way, the incubations vials were shaken prior to the sampling time, allowed to sit for 1 minute, and then sampled.

Push-pull test. Approximately 50-L of test solution containing 375 mM PNG and 100 mg/L Br was injected into MW-1 at the Newberg site. The solution was injected

at the bottom of the well at a rate of 0.5 L/min. The test solution was injected through braided-nylon tubing with a ¼ inch inner diameter (Grainger, Lake Forrest, IL) with a Masterflex peristaltic pump (Cole-Parmer, Vernon Hills, IL). Five samples of test solution were taken over the injection phase. The samples showed that the test solution contained 0.08 µM PNP, which was present as a contaminant.

A 27 minute rest phase followed the injection phase, after which the direction flow on the pump was reversed. During the extraction phase the test solution/ groundwater mixture was pumped from the well at a rate of 2 L every 2.5 minutes. A total volume of 103 L was extracted from the well, which is approximately two times the volume injected. Two 15-mL samples were collected every 2 L while the first 50 L was extracted, then every 3 L until a total volume of 103 L had been extracted. Extraction phase samples collected to quantify PNG and PNP concentrations were placed into pre-weighed 15-mL vials containing quench solution. Extractions phase samples collected to quantify the concentration of bromide were placed in empty 15-mL vials. Both sets of samples were stored in coolers on ice until they were transported back to the laboratory, where they were stored at 4 °C until analyzed.

Bromide concentrations were determined with a Dionex (Sunnyvale, CA) model Dx-120 ion chromatograph equipped with an electrical conductivity detector and a Dionex AS14 column.

High Performance Liquid Chromatography. A high performance liquid chromatography (HPLC) method was developed for the separation and quantitation of the substrate, PNG, and the transformation product, PNP. All separations were performed on a Waters Alliance 2690 HPLC (Waters Corp., Milford, Massachusetts) equipped with an

autosampler and a 996 Photodiode Array Detector. Absorbance measurements were made at a wavelength of 340 nm. The separation of PNG and PNP was achieved in reversed- phase mode on a Luna 5µm C18 (2) column (150 mm x 4.60 mm id; Phenomenex, Torrance, California) and guard column. The autosampler had an adjustable injection volume of that ranged from 3 to 100 µL.

Separation of the substrate and product was achieved with gradient elution using a binary solvent system of 50 mM phosphate buffer (pH 2.5) and HPLC grade methanol (Fisher Scientific). The phosphate buffer was necessary to ensure that the product, PNP, was resolved as a single peak. Without the buffer, PNP, a weak acid (pKa = 7.15 [18]) appeared as a split peak indicating the presence of the phenol and phenolate forms. During the first 5 minutes the mobile phase composition was linearly increased from the initial mobile phase composition of 10/90 (v/v) methanol to phosphate buffer to 55/45. Then from 5 to 8 minutes the composition was linearly increased to 60/40, and finally returned to the initial conditions (10/90) during the last 2 minutes. The flow rate of the mobile phase was 1 mL/min and the inlet pressure was 1200 psi. Column temperature was held constant at 30°C.

Data Analysis. The concentration of PNG and PNP, determined by HPLC, were corrected for dilution due to the addition of quench solution to the subsample. Linear regression was used to determine the rate of PNP production, the standard error in the rate, and the linear correlation coefficient (R^2). To calculate the kinetic parameters K_m and V_{max} plots of PNP production rate against substrate concentration were constructed and fit with a Michaelis-Menton rate form given by Eq. (1).

$$r_{PNP} = \frac{V_{\max} C_{PNG}}{K_m + C_{PNG}}$$ (1)

Here, r_{PNP} is the rate of PNP production, $V_{\max}$ is maximum reaction rate, K_m is Michaelis constant, and C_{PNG} is the concentration of the substrate, PNG. Note that the parameter $V_{\max}$ lumps together the influence of both the intrinsic specific reaction rate parameter and the microbial biomass

$$V_{\max} = \mu_{\max} X$$ (2)

where $\mu_{\max}$ is the effective specific rate of reaction (h^{-1}) for the subsurface organisms, and X (μM) is a measure of the active microbial biomass. The best fit of these data were determined by a nonlinear regression program (using a Marquardt-Levenberg algorithm for the minimization of errors). The standard errors of K_m and $V_{\max}$ are estimates of the uncertainties in the regression coefficients from a single set of experiments, not uncertainties from replicate experiments.

Results

The HPLC method resolved PNG and PNP as separate peaks with retention times of 4.8 and 6.7 minutes, respectively. The instrumental quantitation limits measured as 10 times the signal-to-noise ratio was 0.1 ng of PNP injected into the HPLC. The minimum concentration of PNP that was quantifiable in a 100-μL injection volume was 0.001 mg/L or 7 nM. Two calibration curves were constructed to quantify PNP and PNG by plotting the peak area versus the injected mass. The working range of the PNP curve was 0.1 to 50 ng of PNP injected, and the PNG curve was 1.3 to 2600 ng of PNG injected. Both

calibration curves were linear with R^2 of 0.999. Standards were injected at the beginning and end of sample runs and typically were within 97% of expected values. . Blank injections showed that neither PNG nor PNP was carried over from the previous injection.

Attempts to measure β-glucosidase activity directly in groundwater using PNG a as substrate typically did not yield measurable PNP production rates. Therefore, filtration was used to concentrate biomass from groundwater as described above. Biomass concentrated from 0.25 L of MW-1 groundwater gave a measurable linear increase in the concentration of PNP over a 7 h period (data not shown). The process of filtering groundwater to concentrate biomass proved reproducible as the average activity indicated by PNP production rates for triplicate 0.5 L portions of a single groundwater had a 9.0% relative standard deviation (RSD).

Substrate transformation was observed in all filtered groundwater and sediment incubations conducted. There were measurable increases in PNP concentration over the incubation period. The transformation of the substrate (PNG) was constant when expressed on a per unit time basis, as indicated by linear increase in the concentration of PNP with time (data not shown). Limited experiments with sediment demonstrated mass balance in incubations and that the rate of PNG depletion was proportional to the rate of PNP formation. The percentage of substrate converted to product typically was less than 10%.

To ensure that β-glucosidase activity, as indicated by the rate of PNP production, reflected only microbial enzymatic activity and not the abiotic hydrolysis of PNG, the stability of PNG under the conditions of the assay was investigated. Groundwater was

first filtered through a 0.2 μm filter (to remove microorganisms), and then was used to prepare a 132 μM PNG solution that was sampled over a typical incubation period. No detectable increase in the concentration of PNP was observed.

To further assure that filtration was a valid method for increasing biomass, a range of volumes (30 - 3000 mL) of a single groundwater sample were filtered and assayed for β-glucosidase activity at 132 μM PNG. Figure 2.1.a shows that the concentration of PNP increases linearly with time. Rates of PNP production were calculated as the slope of solid lines. The dashed lines show the 95% confidence interval of each PNP production rate. Figure 2.1.b shows that β-glucosidase activity increased linearly with increasing volume of filtered groundwater. A linear correlation coefficient (R^2) of 0.998 was obtained for the relation between the volume of filtered groundwater and the PNP production rate, which indicates β-glucosidase activity increased proportionally with the volume filtered over the range of volumes tested.
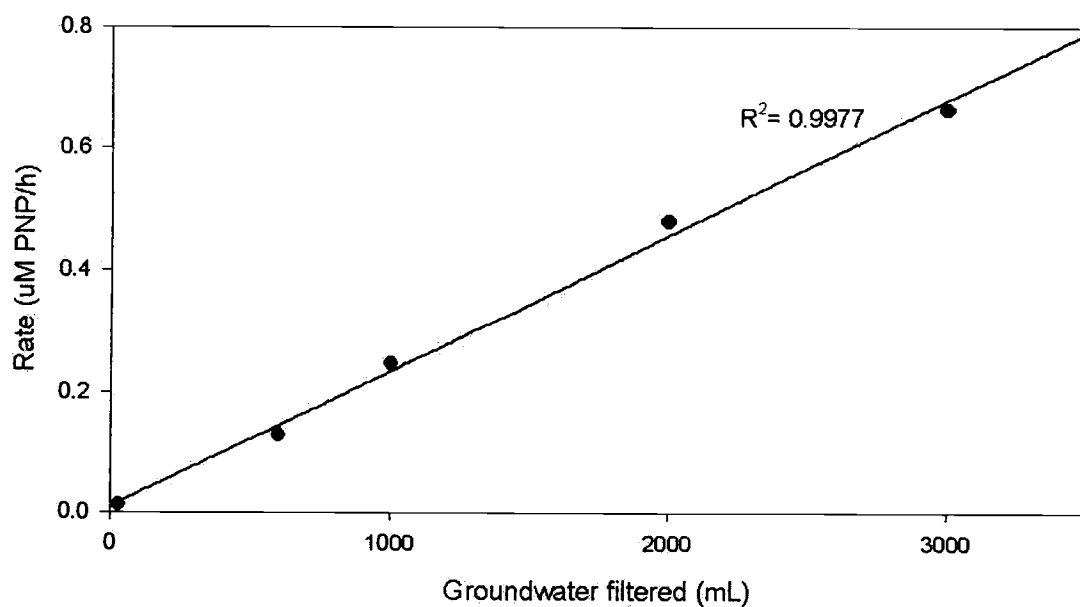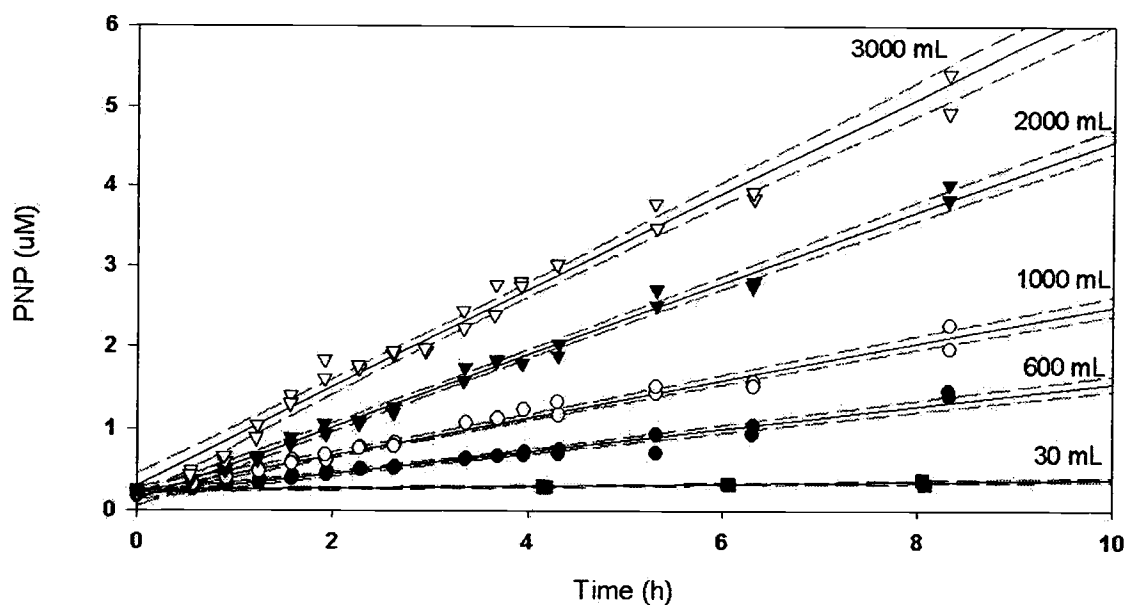
Figure 2.1. (a) Concentrations of PNP versus time for incubations conducted with biomass concentrated by filtering increasing volumes of groundwater. PNP production rates were determined by linear regression and are shown with 95% confidence interval. (b) β-glucosidase activity measured as PNP production rates versus the volume of groundwater that was filtered to concentrate biomass.
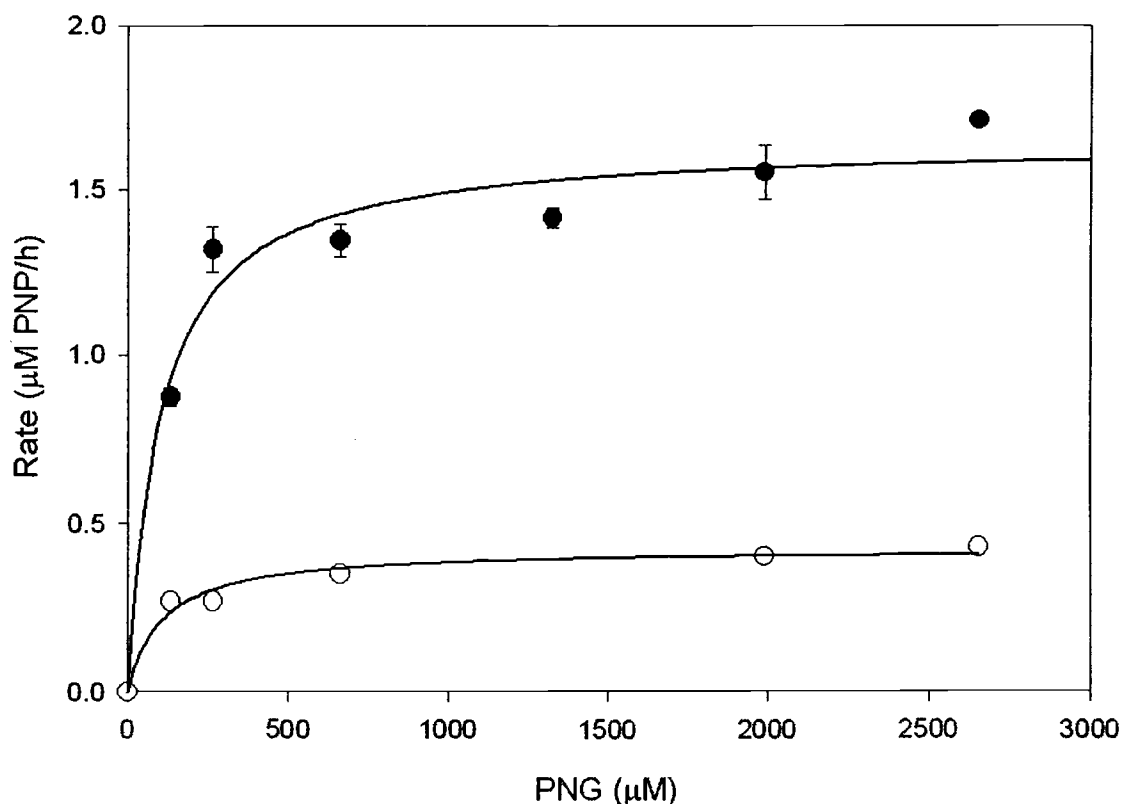
Figure 2.2. Substrate saturation curves for biomass concentrated from 500 mL (●) and 2000 mL (○) portions of a single groundwater sample.

To further investigate the reproducibility of concentrating biomass by filtering groundwater, the kinetics of b-glucosidase activity were determined. Rates were obtained for incubations conducted with biomass collected from 500 mL and 2000 mL samples of MW-1 groundwater from the Newberg site. The incubations were conducted at increasing PNG concentrations and are plotted as substrate saturation curves. The curves were fit with the Michaelis-Menten equation to obtain K_m and V_{max} (Figure 2.2). K_m values of 104 ± 29 μM PNG and 102 ± 34 μM PNG were obtained for 500 and 2000 mL of filtered groundwater, respectively. Increasing the concentration of biomass by filtering had no effect on the K_m, which was expected since K_m is a measure of the binding affinity

of the enzyme and not a function of the amount of enzyme present. V_{max} values increased approximately 4-fold (3.94) from 0.42 ± 0.02 µM PNP/h for a 500-mL of filtered groundwater to 1.66 ± 0.07 µM PNP/ h for 2000-mL of filtered groundwater. Indicating that V_{max} is proportional to the amount of enzyme present, which is consistent with the assumption listed in Eq. (2). Although V_{max} increases when the volume of groundwater filtered increases from 500 to 2000 mL, the β-glucosidase activity expressed on a per liter groundwater basis remained constant, 0.025_3 ± 0.001 and 0.024_9 ± 0.001 µM PNP/h, which were calculated by dividing the experimentally determined V_{max} values by their concentration factors, which are defined by a ratio of the volume of groundwater filtered to the incubation volume. For 500 mL the preconcentration factor is 500mL/30mL = 16.6 and 2000mL/30mL = 66.6, respectively. This demonstrates that the increase in V_{max} is consistent with the corresponding increase in microbial biomass that would be expected on the basis of the volume filtered. This finding further demonstrates that filtering is an effective method for increasing biomass over this range of volume and for obtaining reproducible measurements of β-glucosidase activity.

Table 1 shows the kinetic parameters, K_m and V_{max}, determined from incubations of biomass collected by filtering groundwater samples conducted with varying concentrations of PNG. Error estimates for K_m and V_{max} are shown along with R^2 values as a measure of the experimental fit of the data to the Michaelis-Menton. Overall groundwater samples collected from the Newberg site showed greater β-glucosidase activity as indicated by V_{max}, than samples collected from the Beatty site (Figure 2.3.a). β-glucosidase activity ranged from 0.0024 to 0.029 µM PNP/h on samples collected from the Newberg site (Figure 2.3.a). V_{max} values of groundwater samples collected from the

Beatty site ranged from 0.0029 to 0.063 µM PNP/h (Figure 2.3.b). Sediment cores collected from the Beatty site range from 0.00149 to 0.116 µmole PNP/(g·h).

Table 2.1. The kinetic parameter, K_m and V_{max}, obtained from incubations conducted with biomass concentrated from groundwater by filtration.

Well ID	V_{max} (µmole PNP/L·h)	Error	K_m (µM PNG)	Error	R^2
Newberg					
MW-1	0.025	0.0012	104	29	0.975
MW-2	0.0024	0.0002	461	121	0.998
MW-3	0.0032	0.0004	542	217	0.946
MW-4	0.0026	0.0002	114	32	0.952
MW-5	0.0086	0.0002	187	16	0.997
MW-6	0.0089	0.0004	214	40	0.948
MW-7	0.0049	0.0002	128	40	0.938
MW-8	0.0029	0.0001	98	28	0.964
MW-9	0.029	0.001	175	32	0.986
MW-10	0.0047	0.0004	368	107	0.979
Beatty					
P1	0.063	0.008	216	83	0.938
P2	0.009	0.002	485	254	0.921
P4	0.006	0.001	147	107	0.768
P5	0.0065	0.0006	16.3	10.4	0.762
P7	0.0029	0.0004	116	76	0.834
MW-11	0.009	0.001	55	42	0.724
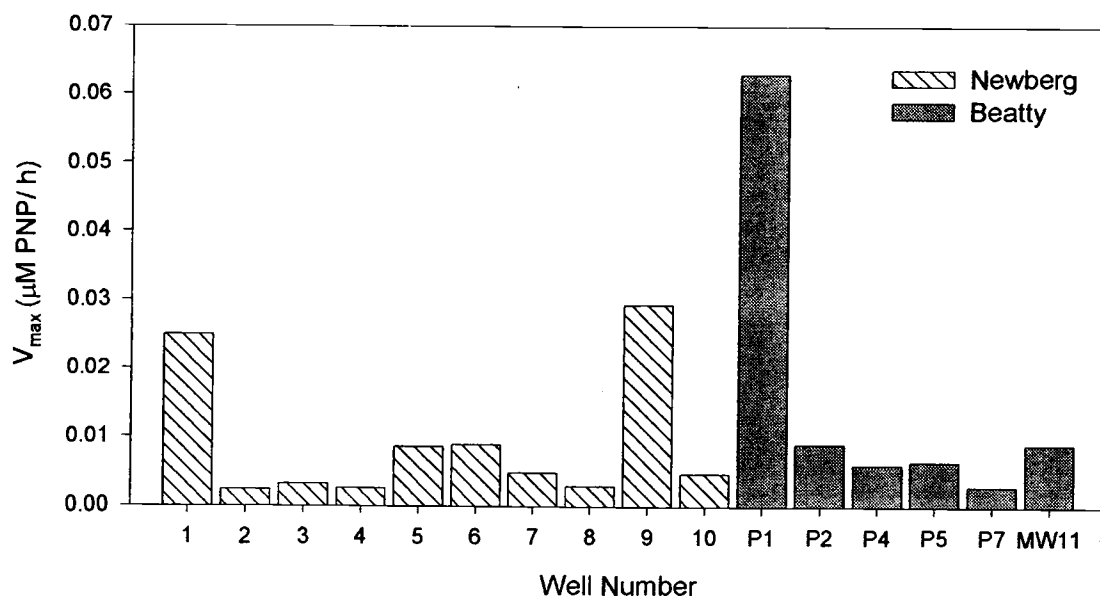
Figure 2.3. (a) Maximum reaction rates, V_{max}, for groundwater samples collected from monitoring wells at the Beatty and Newberg, Oregon sites

In the field demonstration an *in situ* β-glucosidase assay was conducted in MW-1 at the Newberg site. *In situ* conversion of PNG to PNP by native microorganisms was observed in extraction phase samples. It should be noted that a small amount of PNP was present as a contaminant in the injectate solution, so the concentration of PNP present in the injectate solution normalized to bromide to account for dilution with groundwater was subtracted from each extraction phase sample. Less than 5% of the total mass of PNP extracted during the push-pull test was injected as a contaminant. The extraction phase breakthrough curve (Figure 2.4) show that both the relative concentration (C/C_0) of bromide and PNG decline with the volume extracted. Conversely, the concentration of PNP, which starts out at 0.120 μM, increases to a maximum concentration of 0.956 μM. This increase demonstrates that PNP is produced

in the subsurface by microorganisms that transform the substrate, PNG, to PNP and glucose.
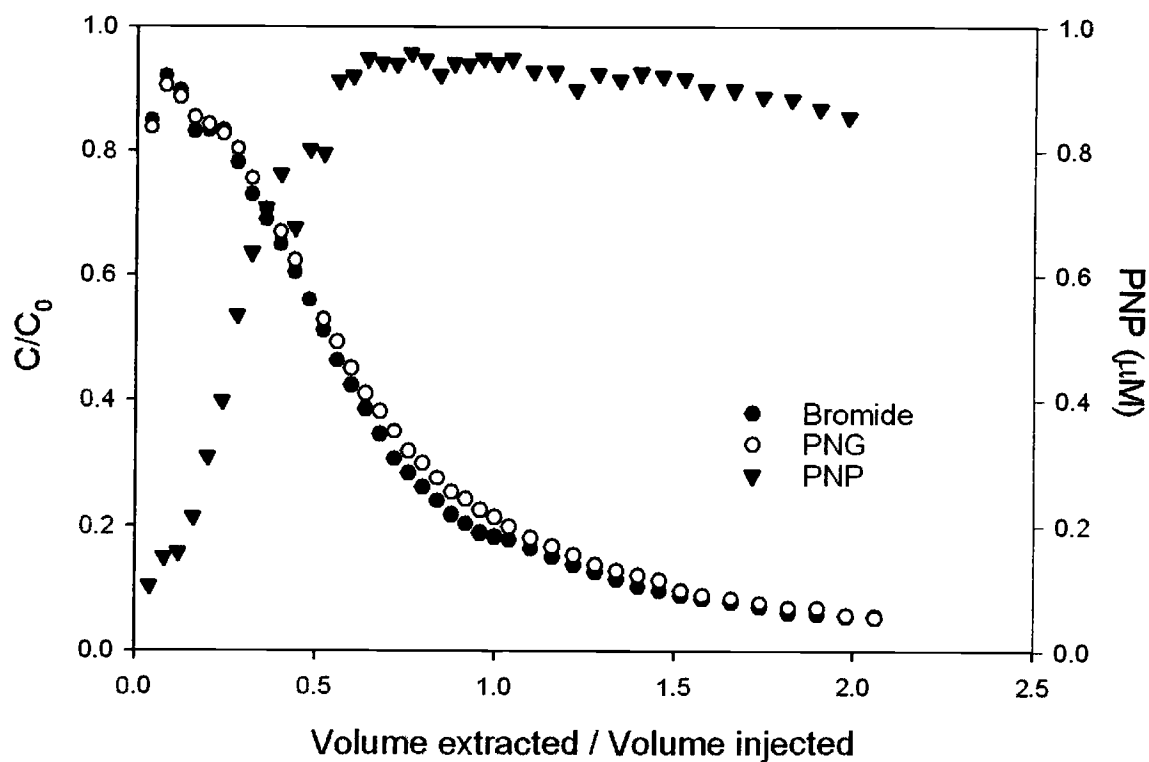
Figure 2.4. Extraction curve for the *in situ* push-pull test conducted in MW-1 at the Newberg site showing the relative concentrations of the recovered substrate (PNG) and the conservative tracer (Br) and the formation of PNP *in situ*.
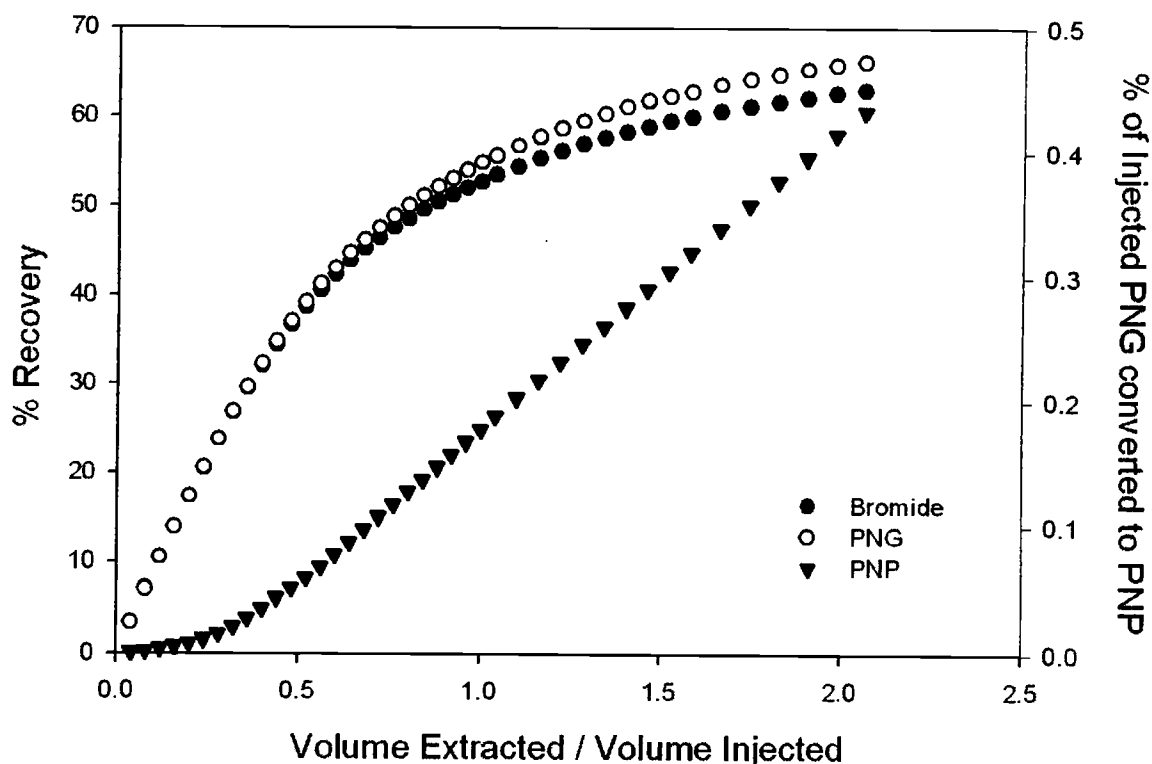
Figure 2.5. Extractions curves showing the percent mass of PNG and bromide recovered during the extraction phase of the push-pull test. The mass of PNP extracted is shown as a percent of PNG injected.

Because the injected solution mixes with native groundwater the effects of dilution and the transport properties of the substrate were evaluated by comparing the extraction curve for PNG against that of bromide. Figure 2.5 shows 62% of bromide, the conservative tracer recovered from the *in situ* test. Less than 1% of the PNG injected was converted to PNP; a total of 0.43% of the PNG injected was extracted as PNP. *In situ* reaction rates for the transformation of PNG to PNP were calculated from the concentrations of PNP in the extraction samples and estimated residence times. The residence times for the extracted test solution samples were calculated with the method of Istok [8]. This method assumes that the transport of the test solution within the

sediment pack is similar to that in a plug flow reactor. Reaction rates calculated using this method ranged from 0.27 to 1.17 μM PNP/h. For each extraction phase sample *in situ* rates were calculated and then plotted against their corresponding substrate concentration (Figure 2.6). Data points from extraction samples collected after the first 28-L of the extraction phase ($V_{extracted}/V_{injected} > 0.56$) were fit with the Michaelis-Menton equation to obtain $K_m = 49$ μM PNG, and $V_{max} = 1.47$ μM PNP/h.
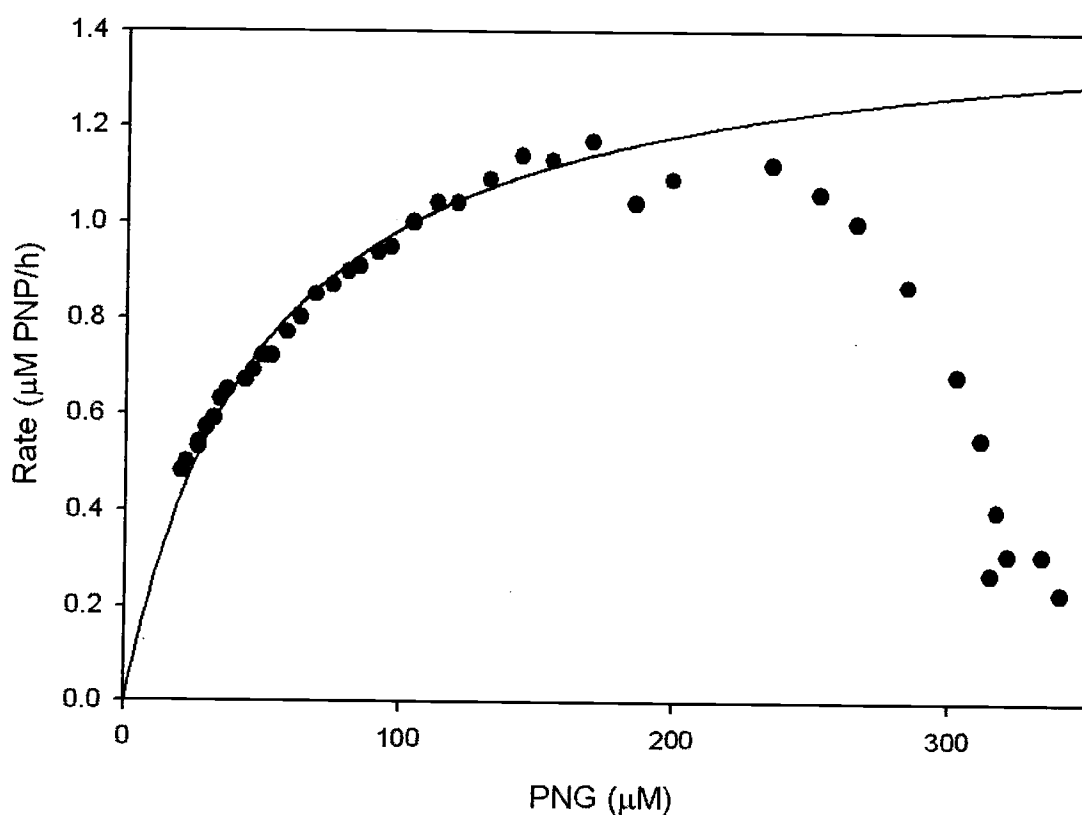
Figure 2.6. Substrate saturation curve for β-glucosidase activity determined from an in situ test conducted in MW-1 at the Newberg, Oregon site ($K_m = 49$ μM PNG and $V_{max} = 1.47$ μM PNP/h).

Discussion

The chromatographic separation of PNG and PNP allowed both substrate and product concentrations to be quantified, which is a necessary improvement to the traditional soil assay required for *in situ* applications. The method soil scientists use to prepare quantitation curves to measure the concentration of PNP [19], which is frequently referenced in soil literature, uses standards ranging from 2 to 10 μg PNP/mL (14.4 to 72 μM PNP) and a blank. The quantitation limit of the soils method was 14 μM PNP based on the lowest concentration standard. By adding chromatographic separation to our method the quantitation limit for PNP was reduced to 7 nM (0.007 μM), an improvement of three orders of magnitude. Other studies have incorporated the use of HPLC into methods for assaying enzyme activities based on the use of MUF substrates to either eliminate quench interference in fluorogenic substrate assays [20] or to simultaneously quantify multiple enzyme activities [21]. By coupling the conventional enzyme assays with an HPLC method to separate and quantify both the substrate and product, we were able to measure β-glucosidase activity in a variety of low activity samples including filtered groundwater samples and subsurface sediment cores.

β-glucosidase activities measured on groundwater samples collected in this study ranged from 0.0012 to 0.029 μM PNP/h. As a comparison, Hendel and Marxsen [22] reported β-glucosidase activities ranging from 0.00113 to 0.291 μM/h for groundwater samples using the fluorogenic substrate, MUF-β-D-glucoside, and Münster et. al. [23] measured β-glucosidase activities that ranged from 0.0012 to 0.115 μM/h in lake water samples. Our method was able to detect and quantify β-glucosidase activities at levels

previously measurable only with fluorogenic substrates. The improved quantitation limit of p-nitrophenol and the ability to independently quantify the substrate concentration was crucial for developing an assay for *in situ* applications to the subsurface. Although fluorogenic substrates still offer lower detection limits, the p-nitrophenyl substrates have much higher water solubility. This allows them to be quantitatively extracted from the subsurface during push-pull tests without having to pump prohibitively large amounts of fluid from the aquifer.

The push-pull test breakthrough curve (Figure 2.5) illustrates that the transport behavior of PNG is similar to the transport of the conservative tracer, bromide. Nearly identical percent recoveries for bromide and PNG, 63% and 64% respectively, were recovered during the extraction phase of the field test. Another indication that PNG is transported along with bromide is the tailing behavior observed toward the end of the extraction curve (Figure 2.4). The relative concentration of PNG and bromide are identical, indicating that the transport is not significantly affected by sorption in the subsurface.

In situ values of K_m and V_{max} obtained in this study ($K_m = 49$ μM PNG and $V_{max} = 1.47$ μM PNP/h) were similar to values Istok et. al. ($K_m = 115$ μM PNG and $V_{max} = 5.5$ μM PNP/h) obtained at this site. The data points taken from the first 28 L of the extraction phase ($V_{extracted}/V_{injected} > 0.56$) were not represented by the Michaelis-Menton equation and not used to determine K_m and V_{max}. These data points reflect the behavior of organisms in the well casing and sand pack surrounding the monitoring well and do not appear to be representative of the microorganisms found further out in the formation. In previous push-pull studies a clean water flush was used to ensure that any heterogeneity

of the microorganisms in the near well environment did not affect test results, and that the activities measured were those of the indigenous microorganism in the formation.

Conclusions

In summary, our study demonstrates two significant improvements to the soil science method that enabled *in situ* β-glucosidase activity to be quantified. The improvements are the decrease in the quantitation limits of PNP and the ability to quantify the substrate, PNG. With this method we were able to successfully quantify both the substrate and product concentrations on a large number of samples generated during the push-pull test. This study presents a method for quantifying *in situ* β-glucosidase activity, which can be extended to measure other *in situ* enzyme activities using additional *p*-nitrophenyl substituted compounds.

Acknowledgments

Literature Cited

[1]   Taylor, J.P., Wison, B., Mills, M.S., and Burns, R.G. Comparison of microbial numbers and enzymatic activities in surface soils and subsoils using various techniques. Soil Biol. Biochem., 2002, 34(3), p. 387-401

[2]   Stubberfield, L.C.F. and Shaw, P.J.A. A comparison of tetrazolium reduction and FDA hydrolysis with other measures of microbial activity. Journal of Microbiological Methods, 1990, 12(3), p. 151-162

[3]   Atlas, R.M. and Bartha, R. Microbial Ecology Fundamentals and Applications. 4th ed. Benjamin/Cunnings Science Publishing, Menlo Park, California, 1998,

[4]   Chróst, R.J. Microbial ectoenzymes in aquatic environments. in *Aquatic Microbial Ecology: Biochemical and Molecular Approaches*, Chróst, R.J., Editor. 1990, Springer-Verlag: New York, p. 47-78

[5]   Tabatabai, M.A. Soil Enzymes. in *Methods of Soil Analysis, Part 2. Microbiological and Biochemical Properties*. 1994: Madison, p. 775-835

[6]   Istok, J.D., Humphrey, M.D., Schroth, M.H., Hyman, M.R., and O'Reilly, K.T. Single-Well "Push-Pull" Test for In Situ Determination of Microbial Activities. Groundwater, 1997, 35(4), p. 619-631

[7]   Istok, J.D. and Humphrey, M.D. Laboratory Investigation of Buoyancy-Induced Flow (Plume Sinking) During Two-Well Tracer Tests. Groundwater, 1995, 4(33), p. 597-604

[8]   Istok, J.D., Field, J.A., and Schroth, M.H. In Situ Determination of Subsurface Microbial Enzyme Kinetics. Ground Water, 2000, 39(3), p. 348-355

[9]   Schroth, M.H., Istok, J.D., Conner, G.T., Hyman, M.R., Haggerty, R., and O'Reilly, K.T. Spatial variability in in situ aerobic respiration and denitrification rates in a petroleum-contaminated aquifer. Groundwater, 1998, 36(6), p. 924-937

[10]   Haggerty, R., Schroth, M.H., and Istok, J.D. Simplified method of "push-pull"test data analysis for determining in situ rate coeffiecients. Groundwater, 1998, 36(2), p. 314-324

[11]   Tabatabai, M.A. and Bremner, J.M. Use of p-Nitrophenyl Phosphate for Assay of Soil Phosphatase Activity. Soil Biol. Biochem., 1969, 1 p. 301-307

[12]   Eivazi, F. and Tabatabai, M.A. Phosphatase In Soils. Soil Biol. Biochem., 1977, 9 p. 167-172

[13]   Eivazi, F. and Tabatabai, M.A. Glucosidases and galactosidases in soils. Soil Biol. Biochem., 1988, **20**(5), p. 601-606

[14]   Eivazi, F. and Tabatabai, M.A. Factors affecting glucosidase and galactosidase activities in soils. Soil Biol. Biochem., 1990, **22**(7), p. 891-897

[15]   Brams, W.H. and McLaren, A.D. Phosphatase Reactions in Columns of Soil. Soil Biol. Biochem., 1974, **6** p. 183-189

[16]   Petit, N.M., Gregory, Lindsay J., Freedman, R.B., Burns, R.G. Differential stabilities of soil enzymes assay and properties of phosphatase and arylsulphatase. Biochemica et Biophysica Acta, 1977, **185** p. 357-366

[17]   Istok, J.D., Field, J.A., and Schroth, M.H. In Situ Determination of Subsurface Microbial Enzyme Kinetics. Ground Water, 2001, **39**(3), p. 348-355

[18]   Schwarzenbach, R.P., Gschwend, P.M., and Imboden, D.M. Environmental Organic Chemistry. Wiley, New York, 1993,

[19]   Browman, M.G. and Tabatabai, M.A. Phosphodiesterase activity of soils. Soil Sci. Soc. Am. J., 1978, **42**(2), p. 286-290

[20]   Freeman, C. Using HPLC to eliminate quench interference in fluorogenic substrate assays of microbial enzyme activity. Soil Biol. Biochem., 1997, **29** p. 203-205

[21]   Freeman, C. and Nevison, G.B. Simultaneous analysis of multiple enzymes in environmental samples using methylumbelliferyl substrates and HPLC. J. Environ. Qual., 1999, **28** p. 1378-1380

[22]   Hendel, B. and Marxsen, J. Measurement of low-level extracellular enzyme activity in natural waters using fluorigenic model substrates. Acta hydrochim. hydrobiol., 1997, **25**(5), p. 253-258

[23]   Munster, U., Plon, P. Einio, and Nurminen, J. Evaluation of the measurements of extracellular enzyme activities in a polyhumic lake by means of studies with 4-methylumbelliferyl-substrates. Arch. Hydrobiol., 1989, **115**(3), p. 321-337

Chapter 3

The Effects of Pore Water Velocity on Phosphatase Kinetics in Soil Columns

Karen M. Radakovich[1], Jennifer A. Field[2], and Jonathon D. Istok[3]

[1]Chemistry Department

[2]Department of Environmental and Molecular Toxicology

[3]Department of Civil, Construction, and Environmental Engineering

Oregon State University, Corvallis, OR 97331

Abstract

The effect of pore water velocity on the overall rate of phosphatase mediated reactions in soil columns is investigated. This work extends previous studies in which apparent enzyme activities were determined with a single-well push-pull test. A feature of the single-well push-pull test is the nonlinear drop in the pore water velocity of the injected solution as it moves out radially from the injection point. Sediment packed columns were operated with four different flow rates (0.4, 1.0, 2.0, and 4.0 mL/min) to achieve pore water velocities typical of the range of velocities of injected solutions in a push-pull test (41, 103, 206, and 412 μm/s). Under the conditions of this study, the concentration of the substrate was approximately constant over the length of the column and the enzyme. Phosphatase activity measured as the maximum reaction rate, V_{max}, on air-dried sediment samples increased with velocity from 167 to 1438 nmol PNP/(h·g) over the range of pore water velocities used. This increase in apparent rate with pore water velocity can be partially explained by the increased rate of removal of reaction products that inhibit the enzyme mediated reaction.

Introduction

In this paper we investigate the relationship between pore water velocity and enzyme-mediated reaction rates. Both diffusion and chemical inhibition are known to reduce the rates of enzyme mediated reactions in heterogeneous systems [1, 2]. There have been some studies that suggest diffusion effects may limit the observed phosphatase activities of environmental samples; Tabatabai and Bremner [3] found that K_m values decreased when soil incubations were shaken versus not shaken, Marxsen and Schmidt [4] observed that both K_m and V_{max} were influenced with discharge rate through sediment columns, and Brams and McLaren [5] determined that changes in K_m values indicated that phosphatase activity was catalyzed by reactions that were diffusion limited. Additionally there have been numerous studies investigating the interplay between chemical inhibition and mass transfer limitations on the reaction rates obtained from immobilized enzyme systems [6-10] . In this study we seek to investigate the potential effects of mass transfer limitations and chemical inhibition on the observed reaction rates over the range of pore water velocities achieved during a push-pull test. By representing different pore water velocities achieved during a push-pull test, we can explicitly determine (1) if pore water velocity affects the observed rates of enzyme-mediated phosphatase reactions, (2) if significant abiotic phosphatase activity measured on autoclaved sediments exists and is affected by pore water velocity, (3) if competitive inhibition by the product formed can account for changes in the observed phosphatase kinetics.

Methods to assay the activities of enzyme such as dehydrogenase, esterase, and phosphatase activity, have been used as indicators of microbial activity because they

assay large portions of the microbial community [11]. Numerous enzyme activities have been determined for water and sediment samples with a variety of methods and are reviewed by Chróst [12] and Tabatabai [13].

Recent studies have coupled an enzyme assay with an *in situ* test method, called the single well push-pull test, and demonstrated the ability to obtain enzyme activity in a subsurface ecosystem [14, 15]. In these studies, a test solution containing a nonreactive tracer and an enzyme substrate were injected into the saturated zone of an aquifer, where it mixed with groundwater as it moved outward from the well. The test solution-groundwater mixture was extracted and concentrations of the injected tracer, the substrate, and the product formed *in situ* were determined as a function of time. During this "push-pull" test, the test solution was pumped into the subsurface at a constant rate and flowed in two dimensions; as a consequence the pore water velocity ($v(r)$) decreases as a function of radial distance (r) from the well, according to the following equation,

$$v(r) = \frac{Q}{2\pi \, rh\eta} \tag{1}$$

where Q is the pumping rate (m^3 s^{-1}), h is the vertical thickness of the injection/extraction zone (m), and η is the porosity. In this study we investigate the changes in the transport properties of the solution as it moves outward from the well with laboratory studies to determine if reaction kinetics obtained from field test accurately reflect the reaction kinetics and are independent of transport limitations.

The kinetics of phosphatase-mediated reactions is described with the Michaelis-Menton equation. Although originally derived for free enzyme in homogeneous solution,

the Michaelis-Menton equation is routinely used to describe the enzyme kinetics in heterogeneous enzyme systems including environmental samples with mixed microbial populations such as soils [16], sediment [17], and lake water [18]. According to the Michaelis-Menten equation, reaction velocity (v) is a function of substrate concentration ($[S]$) and two kinetic parameters, V_{max} and K_m,

$$v = \frac{V_{max}[S]}{K_m + [S]}$$ (2)

where V_{max} is the maximum rate of reaction (mol/s) and K_m is the Michaelis constant (mol/L). The maximum reaction rate is proportional to the concentration of enzyme present in a system. The Michaelis constant is a measure of the binding affinity of the enzyme for the substrate and is a function of the specific enzyme and substrate as well as physicochemical conditions such as temperature, pH, and ionic strength. Reaction end products, which are structurally similar to the substrate, often are able to bind with free enzyme, thereby decreasing the concentration of free enzyme available to bind and transform substrate molecules; this phenomenon, known as inhibition, results in a decrease in the observed reaction rate. The effect of inhibition on the reaction velocity can be accounted for with a modified version of the Michaelis-Menten equation. The modified Michaelis-Menten equation that accounts for the effects of competitive inhibition on reaction velocity is

$$v = \frac{V_{max}[S]}{K_m(1 + \frac{[I]}{K_i}) + [S]}$$ (3)

K_i is the dissociation constant for the breakdown of the enzyme-inhibitor complex given by $K_i = [E][I]/[EI]$ where $[E]$ is the concentration of free enzyme, $[EI]$ is the

concentration of enzyme-inhibitor complex and *[I]* is the concentration of the inhibitor. Although the preceding kinetic equations were derived originally to describe the kinetics of free enzyme in a homogeneous solution, in which the concentrations of substrate and inhibitors are uniform throughout the solution, they provide a useful model for characterizing the kinetics of mixed populations [19].

Our approach is to determine reaction rates from laboratory column experiment as a function of both substrate concentration and pore water velocity. In this study we use phosphatase assay developed by Tabatabai and Bremner [20] to investigate phosphatase activity. The phosphatase assay is based on the release of *p*-nitrophenol (PNP) after being cleaved from the synthetic substrate, *p*-nitrophenyl phosphate, by phosphatase enzymes. Equation 4 shows the transformation of the $PNPO_4$ by phosphatase enzymes to *p*-nitrophenol (PNP) and phosphate (PO_4).

$$PNPO_4 \xrightarrow{\quad Phosphatase \quad} PNP + PO_4 \qquad (4)$$
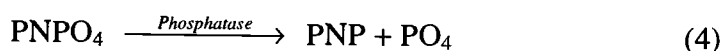
PNP and PO_4 are produced in equimolar amounts. PO_4 is the product of interest to microorganisms and PNP is a chromophore that is used to quantify the reaction.

Phosphatase activity has been shown to be competitively inhibited by both organic and inorganic forms of phosphate [4, 21] so the end product, PO_4, is expected to act as an inhibitor. Sediment-packed columns are injected at rates that result in pore water velocities typical of *in situ* push-pull tests. Only a small fraction of substrate is expected to be transformed based on reaction rates and residence time in the column. Therefore, we assume that the concentration of substrate ($PNPO_4$) is approximately constant along the length of the column. The concentrations of the products (PO_4 and PNP) along the

length of the column are expected to increase since the products are formed over the entire length of the column. However, the concentrations of both products formed in the column are taken as upper bounds and measured as the effluent concentrations.

To determine initially whether a significant fraction of the observed activity measured from air-dried sediment can be attributed to viable microorganisms, we measure the activity of air-dried sediment with and without autoclaving. As numerous processes can contribute to the breakdown of the substrate (discussed by Burns[22]), including enzymes released from or associated with viable cells, enzymes released from lysed cells, enzymes adsorbed by clays, enzymes associated with humic colloids, and hydrolysis catalyzed by mineral surfaces. Here we define biotic activity as the phosphatase activity attributed to enzymes associated with or released from but associated with viable microorganisms. We assume that by autoclaving sediment samples all viable microorganisms present in the sample are lysed and all of their phosphatase enzymes are denatured. Consequently, the phosphatase activity of air-dried sediment that has been autoclaved will be referred to as abiotic activity. This term encompasses any residual activity due to enzymes adsorbed to clays or associated with humic materials as well as hydrolysis. Biotic activity is calculated as the difference between observed activity, obtained from air-dried sediment, and abiotic activity, obtained from air-dried sediment that had been autoclaved.

Experimental

Chemicals. Disodium p-nitrophenyl phosphate hexahydrate (PNPO$_4$) of 99% purity and p-nitrophenol (PNP) of 99% purity were purchased from Aldrich Chemical Co.

(Milwaukee, WI). An aqueous quench solution of 0.25 M calcium chloride and 0.20 M tris[hydroxymethyl]aminomethane (Tris) (Fisher) was prepared in deionized water from a Millipore system and adjusted to pH 12 with NaOH. A 200 mM sodium bicarbonate buffer (pH 8) was used in all experiments to maintain the pH and ionic strength of the aqueous phase. Both incubation and injectate solutions of $PNPO_4$ were prepared in 200 mM $NaHCO_3$ solution.

Sediments. A sediment mix composed of two subsurface sediments prepared by manually mixing equal weights of the two dry sediments was used in batch and column experiments. One sediment, collected near Pasco, Washington, is from the Hanford Formation, an alluvial deposit of sands and gravels of mixed basaltic and granitic origin. The other sediment, collected from a site near Chehalis, Washington, is classified as a fine-silty soil. The sediments were collected as single batches and individually homogenized by manual mixing. Each sediment was then air-dried to a water content between 2-3% and sieved to remove particles > 2 cm in diameter. The prepared Pasco sediment was classified as a clean sand with approximately 30 % fine gravels and less than 5 % silt and clay. This sediment contains less than 0.001 wt % organic matter, and has a particle density of 2.9 g/cm^3. The prepared Chehalis soil was classified as a silty clay loam with approximately 6.2 % sand, 61.5 % silt, and 32.4 % clay. This sediment contains 7.25 wt % organic matter, and has a particle density of 2.69 g/cm^3. The mixture of the two sediments resulted in a sediment sample that had both measurable enzymatic activity and flow properties that were suitable for column experiments.

Batch incubation experiments. Batch experiments were conducted over a range of $PNPO_4$ concentrations with both air-dried and autoclaved sediment to investigate the

contribution of abiotic activity to observed phosphatase activity and determine the range of $PNPO_4$ concentrations that would be needed to characterized phosphatase kinetics. Each batch experiment consisted of 50 g of dry sediment mixed with 50 mL of buffer solution in a 250 mL Erlenmeyer flask. The mixture was allowed to equilibrate at 20 °C for 48 h then 50 mL of $PNPO_4$ was added to each flask to give ten concentrations of $PNPO_4$ ranging from 0.03 to 30 mM $PNPO_4$. The flasks were shaken vigorously for 1 min then immediately sampled by removing 1.6 mL of incubation solution to measure the initial concentrations of $PNPO_4$ and PNP. Thereafter the incubations were sampled in the same manner every hour for 6 h. Each sample was mixed with 0.3 mL of quench solution, filtered through a 0.2 μm nylon filter, and placed in a 2-mL autosampler vial. All filtered samples were stored at 4 °C until they were analyzed. All batch incubations were done in triplicate.

Control batch experiments were conducted with autoclaved sediment to measure abiotic phosphatase activity. The autoclaved sediment used in these experiments was prepared by autoclaving the air-dried sediment at 1.02 atm (15 psi) and 121 °C for 1 hour.

Column Experiments. Column experiments were conducted to investigate the effect of varying pore water velocity on the observed rates of phosphatase catalyzed reactions. Columns were constructed of polyvinyl chloride (PVC) tubing, cut in 25 cm length with an internal diameter of 2.54 cm. Both ends of the tubing were fitted with stainless steel mesh and a plug of quartz wool to prevent clogging. The columns were prepared by packing dry sediment into the columns in the following manner. Initially, approximately 20 g of sediment was added to each column and compressed with a metal rod; this process was repeated until the column was completely packed with sediment.

The columns then were oriented vertically in a 20 °C incubator, perfused with buffer from the bottom until saturated, and then allowed to equilibrate for 48 h. The packed columns had a total porosity of 0.32 based on the measured mass of the dry and saturated column and internal column volume. After the columns had equilibrated each column was connected to a single pump and flushed with four pore volumes of buffer solution. The pump was then adjusted until the desired flow rates were obtained. The flow rate of the column effluent was monitored and maintained to within ± 10% of the desired flow rate. The flow rates used in these experiments were 0.4, 1.0, 2.0, and 4.0 mL/min with corresponding pore water velocities of 41, 103, 206, and 412 μm/s. The experimental conditions used for each column are described in Table 3.1.

Table 3.1. Experimental conditions during column experiments

Column	Sediment type	Q (mL/min)	υ (μm/s)	t_R (min)[b]
1a	Air-dried	0.4	41	130
2a	Air-dried	1.0	103	47
3a	Air-dried	2.0	206	23
4a	Air-dried	4.0	412	11
1b	Autoclaved	0.4	41	130
2b	Autoclaved	1.0	103	47
3b	Autoclaved	2.0	206	23
4b	Autoclaved	4.0	412	11
4c[a]	Air-dried	4.0	412	11

[a] Table 3.3b
[b] estimated from substrate breakthrough

Column experiments were initiated by changing the influent solution from buffer to buffered $PNPO_4$ solution. Columns were injected with $PNPO_4$ solutions beginning with the lowest concentration solution and ending with the highest concentration solution. $PNPO_4$ concentrations of the injectate-solutions were selected based on the results of the

batch incubations and ranged from 0.03 mM to 28.0 mM. To eliminate column-to-column variations in the injectate solutions, a single influent solution was prepared for each concentration of $PNPO_4$. Each concentration of injectate solution was injected until constant concentrations of the substrate, $PNPO_4$, and the product, PNP, were observed in the column effluent. All of the test solutions were sampled during the experiment. Once steady-state conditions were observed the effluent was sampled every 5 minutes for 30 minutes. At the end of this sampling phase, the influent solution was switched to the next higher concentration $PNPO_4$ solution. This process continued until all four columns had been injected with each of the six $PNPO_4$ solutions.

Control column experiments were carried out as described above with autoclaved sediment to measure abiotic phosphatase activity. The sediment used in these experiments was prepared as described in the batch experiments with autoclaved sediments. The sediment was allowed to dry and then was packed into columns and equilibrated using the method described above.

Sample Analysis. All samples collected from batch and column experiments were analyzed for $PNPO_4$ and PNP. Concentrations of $PNPO_4$ and PNP were determined with a high performance liquid chromatograph (Alliance 2690, Waters Corp., Milford, Massachusetts) equipped with a Luna 5μm C18 (2) column (150 mm x 4.60 mm id; Phenomenex, Torrance, California) and a photodiode array detector. Separation of $PNPO_4$ and PNP was achieved with reversed-phase chromatography coupled with gradient elution. The mobile phase was a binary solvent of 50 mM phosphate buffer (pH 2.5) and methanol.

Phosphate concentrations were measured colorimetrically (CHEMetrics, Inc., Calverton, VA) to determine the concentration of phosphate present inhibition incubations.

Data Treatment. The concentrations of PNP and PNPO$_4$ determined from HPLC analyses were corrected for sample dilution caused by the addition of quench solution. To determine the phosphatase activity in batch incubations, the PNP production rates were determined as the slope of the line of best fit from plots of PNP concentration versus time. Phosphatase activities were calculated as

$$Activity = \frac{d[PNP]}{dt} \cdot \frac{V_{sol}}{m_{sed}}$$

(4)

where ($d[PNP]/dt$) is the rate of PNP production (mol L^{-1} s^{-1}); V_{sol} is the volume of the incubation solution (L); and m_{sed} is the mass of sediment used in the incubation (g). Activities are re-expressed as nanomoles of PNP produced per gram sediment per hour (nmol PNP/(h·g)).

To determine phosphatase activities from column experiments, elution histories were constructed to show the concentrations of PNP and PNPO$_4$ in the column effluent. Once constant concentrations of PNPO$_4$ were observed in the effluent, the average concentration of PNP was calculated. The average concentration of PNP then was used to calculate phosphatase activity for each of the columns using the method of Brams and McLaren [5]

$$Activity = \frac{[PNP] \cdot Q}{m_{sed}}$$

(5)

where *[PNP]* is the average concentration of PNP in the column effluent (mol/L); Q is the flow rate (L/min); and m_{sed} is the mass of sediment packed in the column (g). Activities are re-expressed as nanomoles PNP produced per gram of sediment per hour (nmol PNP/g·h).

The kinetic parameters, K_m and V_{max} in Michaelis-Menton equation were determined from plots of activity versus effluent PNPO$_4$ concentration with the nonlinear regression tool in the software package SigmaPlot. The standard errors of K_m and V_{max} are estimates of the uncertainties in the regression coefficients from a single set of experiments, not uncertainties from replicate experiments.

Inhibition Experiments. Three sets of batch experiments were conducted to confirm that phosphate was an inhibitor and to demonstrate that PNP was not an inhibitor. First, control incubations were conducted with PNPO$_4$ alone; next incubations were conducted with PNPO$_4$ and PNP; and finally incubations were conducted PNPO$_4$ and Na$_2$HPO$_4$. The concentrations of PNP and Na$_2$HPO$_4$ used were 0, 100, 300, 500, 700, 1000, and 1500 μM. All incubations were conducted with a single PNPO$_4$ concentration of 6.5 mM.

Once phosphate was shown to be the only end product that acted as an inhibitor, another series of incubations were conducted to determine the inhibition constant, K$_i$. This set of incubations was conducted with a range of PNPO$_4$ concentrations, selected to be near the K$_m$ value determined from batch incubation, and included concentrations of 0.7, 0.9, 1.2, 1.9, and 4.3 mM PNPO$_4$. A K$_i$ value of 2.0 mM was determined from these batch incubations (data not shown).

Results and Discussion

Batch incubation experiments. All batch incubations showed linear increases in the concentrations of PNP with time over the six-hour incubations (data not shown). Batch incubations demonstrated the dependence of PNP production rates on substrate concentration and exhibited saturation-type kinetics as seen in the substrate saturation curves shown in Figure 3.1. Error bars shown at each concentration represent error estimates of the rates obtained from the linear regressions of concentration histories. The substrate saturation curve obtained for air-dried sediment was fit to the Michaelis-Menten equation to give a K_m of 2.1 ± 0.3 mM $PNPO_4$ and a V_{max} of 132 ± 6 nmoles PNP/(h·g) (R^2 = 0.989). Greater than 98% of the total mass of substrate was accounted for in all incubations. The rates calculated from these data had an overall relative standard deviation of 12.1% from triplicate experiments (data not shown).

Incubations conducted with autoclaved sediment also showed a linear increase in the concentration of PNP formed over the 6 h incubation period. Measurable PNP production was observed on autoclaved sediment, and was attributed to abiotic phosphatase activity. Abiotic rates of PNP production also increased as a function of $PNPO_4$ concentration (Figure 3.1). Additional control experiments conducted in glass vials containing incubation solutions without sediment showed no measurable decrease in the concentration of $PNPO_4$, nor any increase in the concentration of PNP. The lack of PNP production indicates that the activity of autoclaved sediment could not be attributed to aqueous phase hydrolysis. The relationship between the activity exhibited by autoclaved sediment and $PNPO_4$ concentration is best described with saturation type kinetics (Figure 3.1). For the purpose of comparing abiotic activity to the observed

activity, the substrate saturation curve obtained for autoclaved sediment was fit to the

Michaelis-Menten equation to facilitate the comparison of biological and abiological

systems. An apparent K_m of 13 ± 3 mM $PNPO_4$ and an apparent V_{max} of 39 ± 4 nmoles

$PNP/(h \cdot g)$ ($R^2 = 0.993$) was obtained.
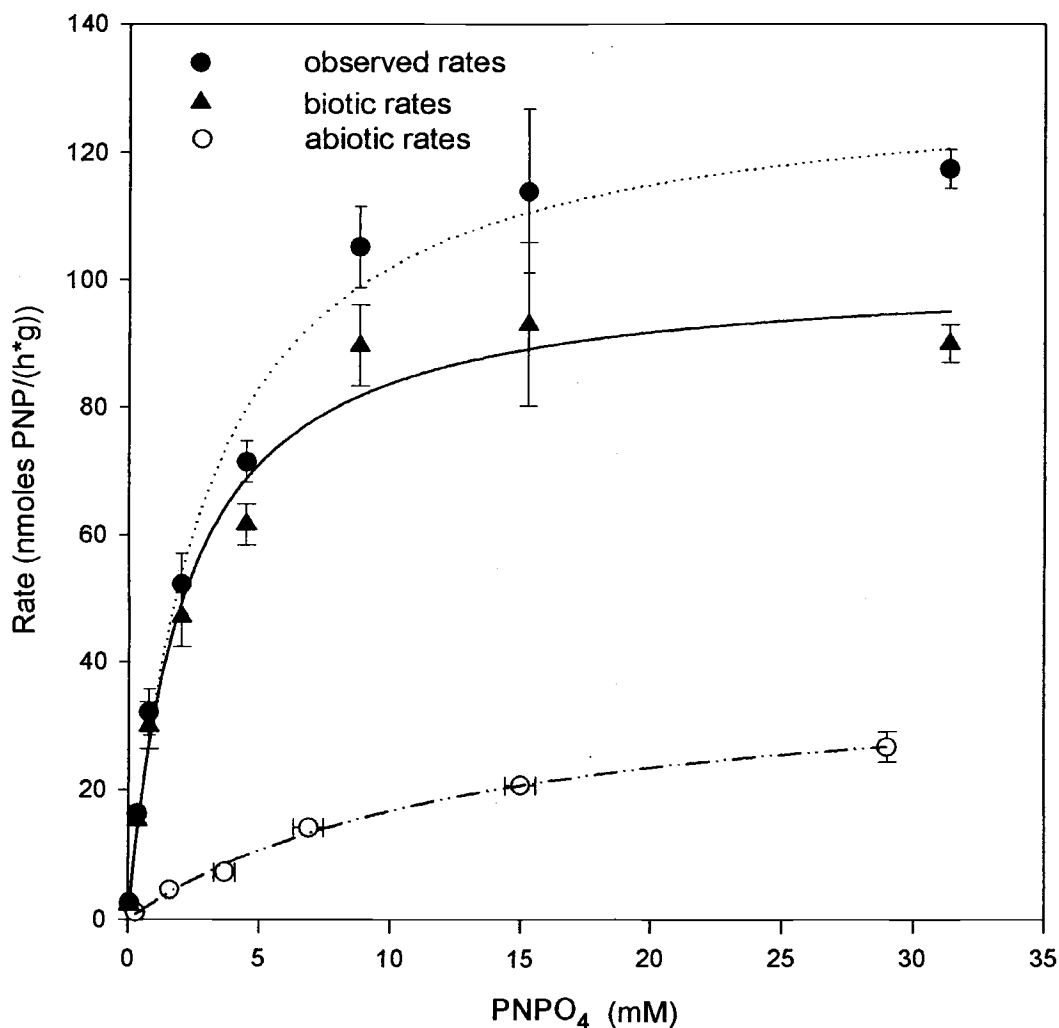
Figure 3.1. Substrate saturation curves for batch incubation conducted with air-dried sediment to obtain observed rates and air-dried sediment that was then autoclaved to obtain abiotic rates. The biotic substrate saturation curve was determined by fitting the biotic rates that were calculated as the difference between the observed rates and abiotic rates.

Biotic phosphatase activity was calculated as the difference between the phosphatase activity of air-dried and autoclaved sediment (Figure 3.1). At low substrate concentrations, biotic phosphatase activity accounted for 93 % of the total observed activity. But as substrate concentration increased and saturation conditions were achieved, biotic activity accounted for 78 % of the total observed activity (Figure 3.1) while 22 % of the total activity was due to abiotic processes. The shapes of the biotic and abiotic substrate saturation curves and their apparent K_m values indicate that biotic activity appears to reach saturation, while abiotic activity continues to increase over the experimental concentration range. The fraction of observed activity due to abiotic activity for this sediment mix changes over the concentration range of interest. Consequently, abiotic phosphatase activity should be explicitly considered, especially at higher substrate concentration where biological activity becomes constant and abiotic activity continues to increase.

From the batch incubation shown in Figure 3.1, the range of $PNPO_4$ concentrations selected to represent the substrate saturation curve for subsequent column experiments was 0.03 to 28.0 mM. It was, however, desirable to use fewer than the ten original batch-incubation concentrations of $PNPO_4$ in order to limit the length of subsequent column experiments. Therefore, six concentrations of $PNPO_4$ (0.03, 0.7, 4.0, 8.0, 14.0, and 28.0 mM) were selected to détermine the kinetics of the sediment mix in subsequent column experiments.

Column Experiments. Concentration histories of a column packed with air-dried sediment and a column packed with autoclaved sediment are shown in Figure 3.2. In each plot six distinct $PNPO_4$ concentration steps are visible. The stepped

concentration profiles are expected because six injectate solutions containing successively higher concentrations of $PNPO_4$ were injected sequentially. Idealized concentration histories of $PNPO_4$ based on conservative, non-retarded plug-flow behavior are shown as dashed lines and are intended to provide a reference for evaluating the breakthrough of $PNPO_4$. The actual breakthrough curves show that effluent $PNPO_4$ concentrations increase sharply and then appear to reach steady state (Figure 3.2). The concentrations of PNP of the column effluent also increase and then levels off. Influent samples collected during the experiment and analyzed for PNP concentrations verified that PNP was formed in the column and not present in the injectate solution. Mass balance calculations indicated that greater than 95% of the injected substrate, $PNPO_4$, was recovered as a combination of substrate and product.
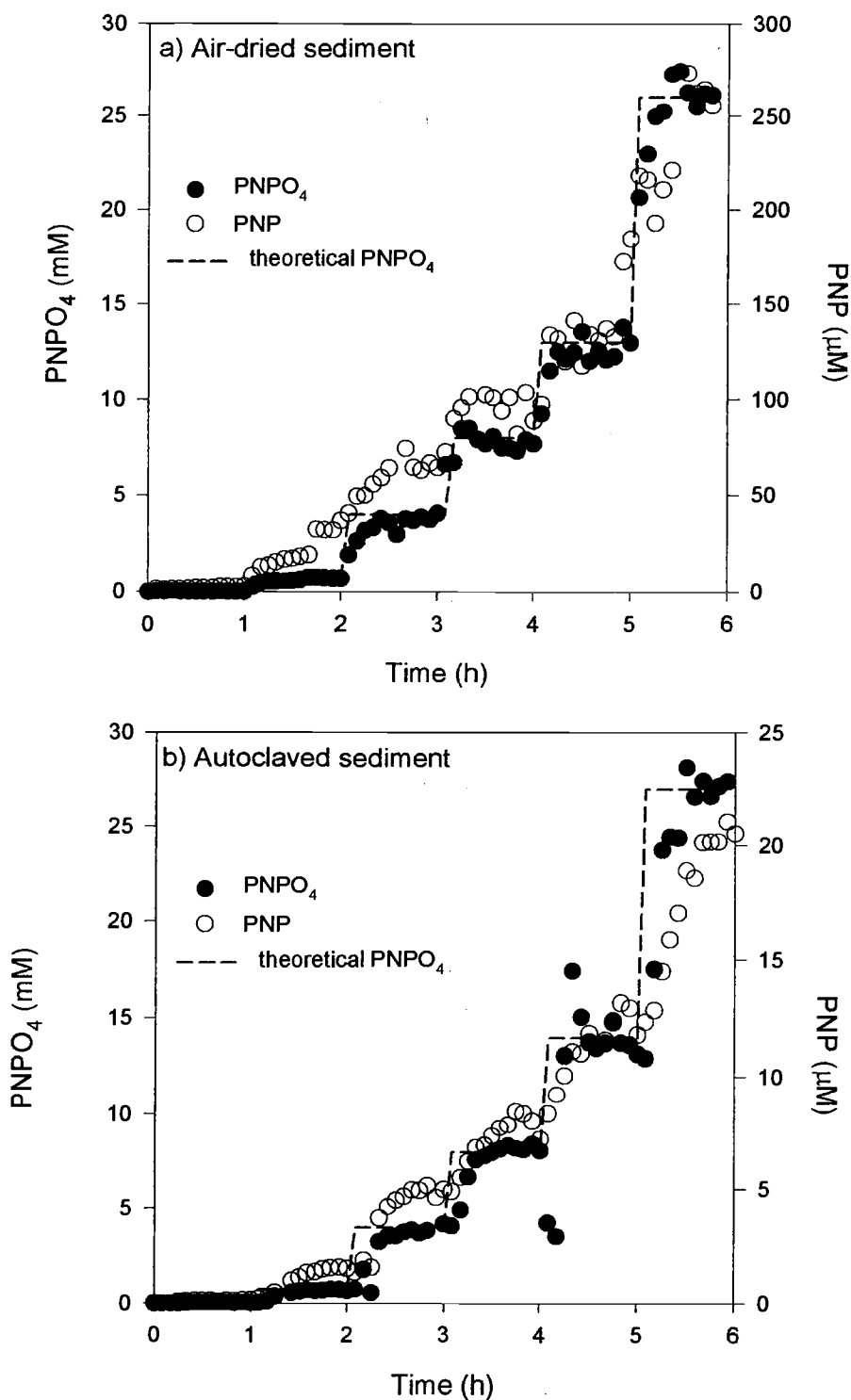
Figure 3.2. Concentration histories for PNPO₄ during column experiments conducted with (a) air-dried sediment and (b) air-dried sediment that was autoclaved. The flow rate and corresponding pore water velocity for both columns are 4.0 mL/min and 412 μm/s, respectively.

Steady-state effluent concentrations of PNP and $PNPO_4$ were calculated as the average concentration during the last 30 minutes of injection for each of the six injectate solutions. PNP production rates were calculated from steady state PNP concentrations, flow rate, and the mass of sediment in the column with equation 4. The resulting rates were plotted versus their corresponding $PNPO_4$ concentrations to yield substrate saturation curves shown in Figure 3.3. The observed PNP production rates increased not only as a function of substrate concentration but also as a function of flow rate. The error bars shown on both PNP production rates and $PNPO_4$ concentrations represent standard deviations in their respective average values during each sampling period. The substrate saturation curves determined for each flow rate are distinct from one another as indicated by the error bars for the rates.
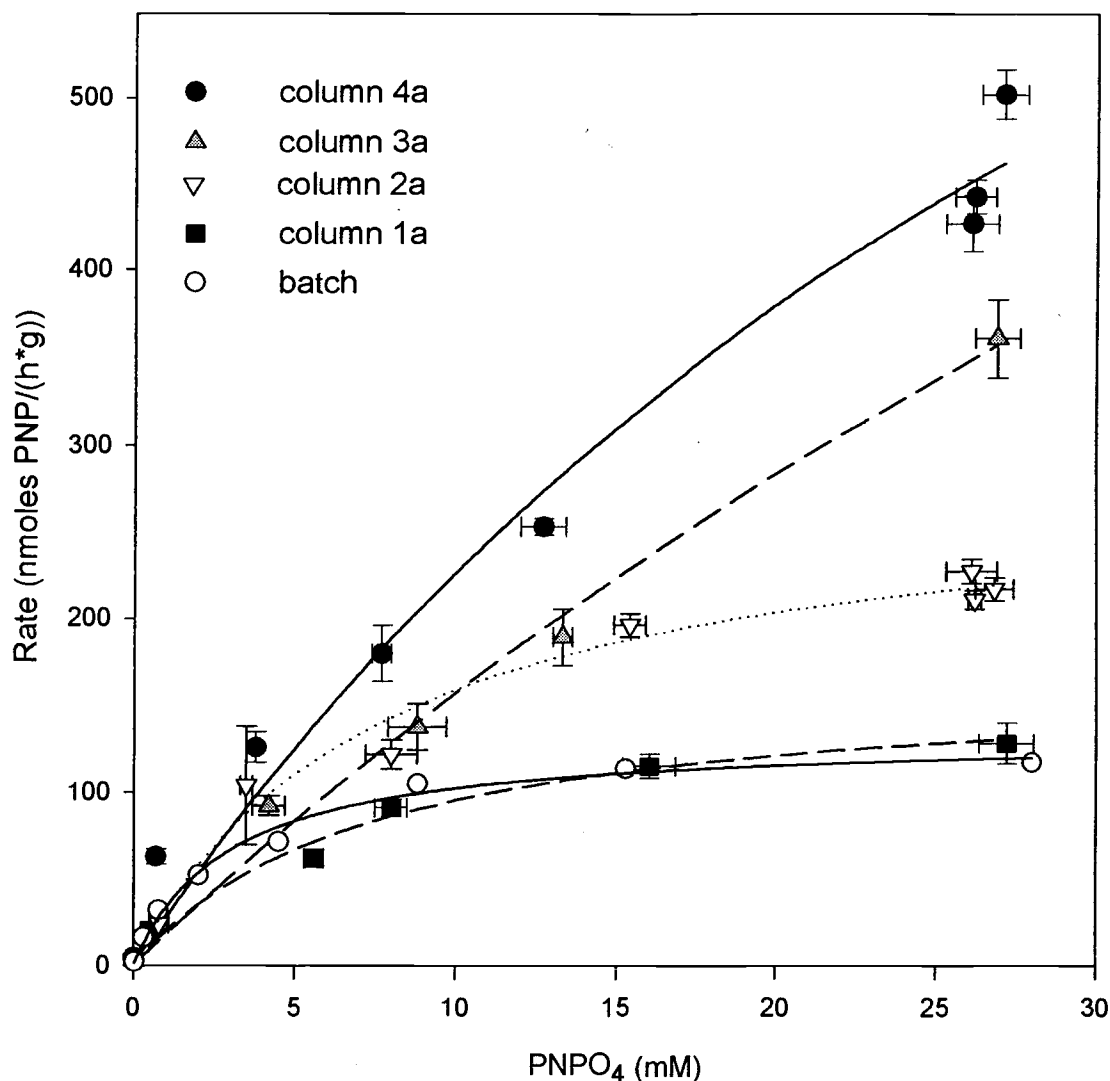
Figure 3.3. Substrate saturation curves for observed phosphatase activity from column experiments conducted with air-dried sediment. The columns 1a (0.4mL/min), 2a (1.0 mL/min), 3a (2.0 mL/min) and 4a (4.0 mL/min) had pore water velocities of 41, 103, 206, and 412 μm/s, respectively.

To test the reproducibility of PNP production rates measured from flow through columns, four additional columns were injected with the highest $PNPO_4$ concentration (40 mM) at two flow rates (1.0 and 4.0mL/min). Rates determined from the triplicate column experiments were 218 ± 8 nmoles PNP/(h·g) (RSD = 3.8%) and 457 ± 40 nmoles PNP/(h·g) (RSD = 8.7%) at 1.0 and 4.0 mL/min respectively. Differences in rates

measured on columns with varying flow rate greatly exceed the relative standard deviations of replicate column tests. These results indicate that phosphatase activity depends on flow rate, or more importantly pore water velocity within the columns. A similar relationship between phosphatase activity and flow rate was observed in a study conducted by Marxsen and Schmidt [4] using stream sediments.
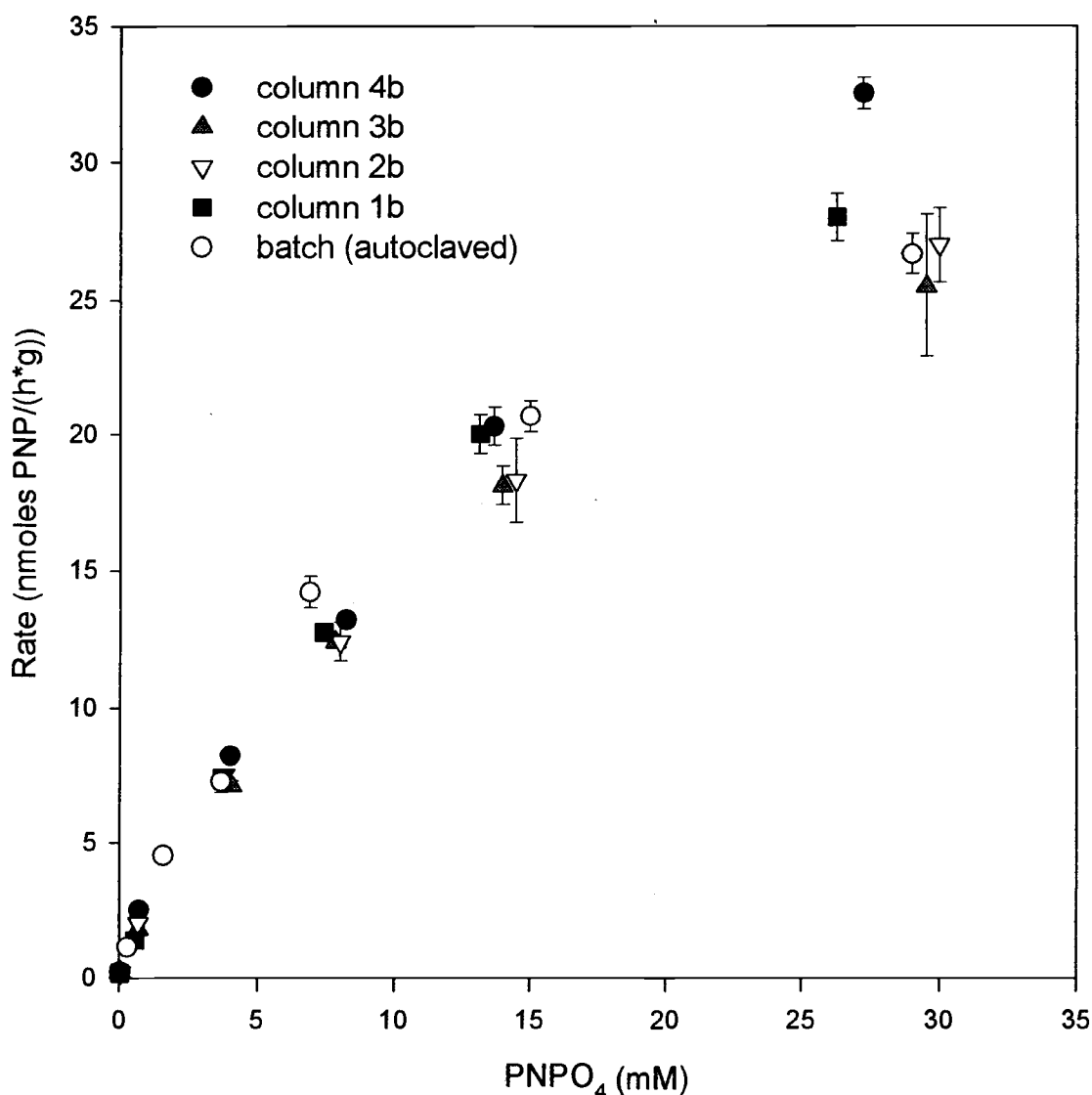
Figure 3.4. Substrate saturation curves for the abiotic component of phosphatase activity from column experiments conducted with air-dried sediment that was autoclaved. The columns 1b (0.4mL/min), 2b (1.0 mL/min), 3b (2.0 mL/min) and 4b (4.0 mL/min) had pore water velocities of 41, 103, 206, and 412 μm/s, respectively.

Columns experiments were conducted with autoclaved sediment at each of the four flow rates to investigate the effect of flow rate on abiotic hydrolysis. Autoclaved sediments yielded measurable PNP production rates that appear to follow saturation type kinetics (Figure 3.4). In contrast to the results obtained from air-dried sediments (Figure 3.3), abiotic phosphatase activity showed no dependence on pore water velocity. Additionally, batch experiments conducted with autoclaved sediment produced a substrate saturation curve that mimicked those from column experiments, which suggests that in both batch and column systems the same abiotic process for the conversion of $PNPO_4$ to PNP is present and that the process is independent of flow rate. For these reasons, abiotic kinetics appears to be defined by a property of the sediment and not controlled by the delivery of substrate to active sites within the sediment.

To investigate the effect of flow rate on biotic phosphatase activity, the abiotic contributions to phosphatase activity were subtracted from the observed activity. The resulting data was then fit with the Michaelis-Menton equation. The abiotic substrate saturation curve (Figure 3.4) was subtracted from the substrate saturation curve obtained from air-dried sediment (Figure 3.3) to obtain biotic activity curves shown in Figure 3.5 and labeled as columns 1-4. Once corrected for abiotic activity the substrate saturation curves obtained at each flow rate were fit with the Michaelis-Menten equation to obtain apparent values of K_m and V_{max} (Table 3.2). Substrate saturation curves obtained from columns 1 and 2 as well as those from batch incubations exhibit zero-order kinetics at higher $PNPO_4$ concentrations (Figures 3.1 and 3.5). These curves are well represented by the Michaelis-Menten equation, with estimated errors of K_m and V_{max} ranging from 15-32% and 4-12%, respectively (Table 3.2, Figures 3.1 and 3.5). However, the substrate

saturation curves for columns 3 and 4 show that saturation was not achieved at higher

PNPO$_4$ concentrations; instead, phosphatase activity appears to increase linearly with

PNPO$_4$ concentration (Figure 3.5). Error estimates associated with the V$_{max}$ and K$_m$

values also increased in column 3 and 4 over those obtained from lower flow rate

columns. For the substrate saturation curves obtained for columns 3 and 4 the Michaelis-

Menten equation did not provide a good fit to the data. This departure from Michaelis-

Menton kinetics are unlike the results reported by Marxsen and Schmidt, where an

increase in the pore water velocity lead to an increase in the rates but the substrate

saturation curves were still well represented by the Michaelis-Menton equation [4].

Furthermore, they found that a small change in the rate of hydrolysis occurred at limiting

substrate concentrations while the greatest change in rates was observed at or near

substrate saturation levels. Unlike the results of Marxsen and Schmidt, an earlier study

conducted by Brams and McLaren [5] showed some variation in K$_m$ or V$_{max}$ with flow

rate but no clear correlation was established.

Table 3.2. Values of K$_m$ and V$_{max}$ Obtained from Batch and Column Experiments.

	Q (mL/min)				
	0[d]	0.4	1.0	2.0	4.0
V$_{max}$ (nmoles PNP/h·g)					
Observed[a]	132±6	167±20	273±28	1421±545	1400±500
Abiotic[b]	39±4	52±3	46±2	42±1	79±9
Biotic[c]	102±5	118±5	247±29	900±300	1216±59
K$_m$ (mM PNPO$_4$)					
Observed[a]	2.1±0.3	8±2	8±2	80±39	50±24
Abiotic[b]	13±3	22±2	21±2	19±1	38±7
Biotic[c]	2.1±0.4	3.8±0.6	7±2	54±24	51±34

[a] measured on air-dried sediment
[b] measured on air-dried sediment that was autoclaved
[c] calculated as the difference between observed and abiotic activity
[d] batch incubations
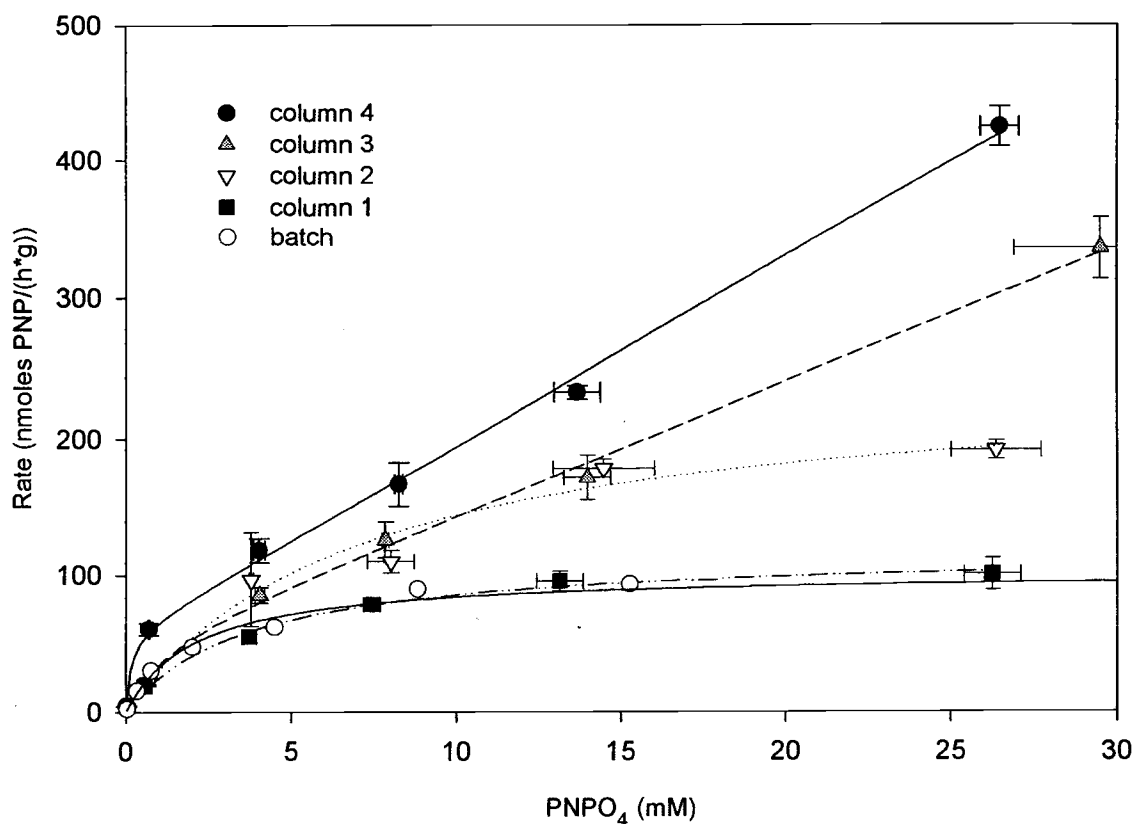
Figure 3.5. Substrate saturation curves for the biotic component of phosphatase activity, calculated as the difference between observed and abiotic rates and then fit with the Michaelis-Menten equation. The columns 1 (0.4 mL/min), 2 (1.0 mL/min), 3 (2.0 mL/min) and 4 (4.0 mL/min) had pore water velocities of 41, 103, 206, and 412 mm/s, respectively.

Pore water velocity has been shown to influence the rates of phosphatase-mediated reactions but the specific processes that control phosphatase reactions catalyzed by sediments in dynamic systems are unclear. Several factors including the effects of inhibition and mass transport limitations due to diffusion have been investigated as likely causes of the change in reaction rate with pore water velocity [23]. The observed reaction

rates of sediment bound microorganism have the potential to be limited by diffusion from bulk solution across a stagnant layer to the catalytic site on the sediment bound microorganism. In a heterogeneous system the hydraulic properties such as pore water velocity are known to influence the thickness of stagnant layer. To elucidate the previously observed effects of pore water on phosphatase activity the combined effects of inhibition and diffusion must be considered. In this paper, we begin by investigating the role of inhibition and recognize that additional research is needed to determine the effect of mass transfer limitation.

Inhibition of phosphatase activity by phosphate. To evaluate inhibition effects we consider the changes in the concentration of product along the length of the column. It should be stated explicitly that we assume that there are no mass transfer limitations from bulk solution to the active site, to determine if inhibition alone is responsible for the reduction in rates with decreasing pore water velocity. Our earlier assumption that the concentration of substrate was constant over the length of the column appears to be valid, because only a small percentage (typically less than 10%) of the substrate, $PNPO_4$, was transformed in the column experiments (Table 3.3a). $PNPO_4$ is transformed to PNP and PO_4 throughout the column, and the concentration of PNP and PO_4 increase in the test solution as it moves through the column. The test solutions injected into columns with the lower pore water velocities experience longer residence time, and subsequently have the greatest build up in the concentration of PO_4 over the length column. Table 3.3a shows that the concentration of PO_4 is higher in column 1a ($\upsilon = 41$ μm/s) than that in column 4a ($\upsilon = 412$ μm/s). We hypothesize that decreasing pore water velocities lead to increasing PO_4 concentrations that cause the observed reduction in PNP production rates.

Table 3.3a. Concentrations of Substrate Used in the Injectate Solutions of Column 1a and 4a along with the Resulting Phosphatase Activities.

Q (mL/min)	Effluent Concentration		PNP production rates (nmoles PNP/h·g)
	PNPO$_4$ (mM)	PO$_4$ (μM)[a]	
4.0 (column 4a)	0.03	2.4	4.6 ± 0.4
	0.7	33.3	63 ± 4
	4.0	66.8	126 ± 9
	8.0	95.1	180 ± 16
	14.0	143.8	281 ± 44
	28.0	265.7	502 ± 15
0.4 (column 1a)	0.03	--	--
	0.7	121.0	20 ± 1
	4.0	370.4	62 ± 5
	8.0	544.7	91 ± 5
	14.0	690.6	115 ± 7
	28.0	768.8	128 ± 12

Table 3.3b. Concentrations of Substrate and Product in the Injectate Solutions of Column 1c and the Resulting Phosphatase Activities.

Q (mL/min)	Injectate Solution Concentration		PNP production rates (nmoles PNP/h·g)
	PNPO$_4$ (mM)	PO$_4$ (μM)[a]	
4.0 (column 1c)	0.03	23	6 ± 1
	0.7	122	50 ± 5
	4.0	423	140 ± 5
	8.0	570	149 ± 38
	14.0	690	232 ± 45
	28.0	826	262 ± 46

[a] indicated by the measured concentrations of PNP

To test this hypothesis experimentally, an additional column experiment was conducted. Column 4a was injected with solutions prepared to contain PNPO$_4$ as well as PO$_4$, at concentrations consistent with the effluent from the column 1a, which had the highest PO$_4$ effluent concentrations. The effluent concentrations of column 1a can be

found in Table 3a along with the concentrations of $PNPO_4$, PNP, and PO_4 in the solutions injected into column 4c. Effluent product concentrations were selected as an upper bound to ensure that the effects of inhibition would not be under estimated. The injectate solution then was pumped into the column with the highest pore water velocity, 412 μm/s.

Figure 3.6 shows the substrate-saturation curve obtained from column 1c along with those of columns 1a and 4a comparison. The resulting substrate-saturation curve (Figure 3.6) was fit with the Michaelis-Menten equation to obtain a K_m value of 6 ± 2 mM and a V_{max} value of 310 ± 40 nmoles PNP/(h·g). Both column 4a and 4c had the same flow rate; the difference between these two columns was the composition of the injected test solution. Column 4c was injected with both $PNPO_4$ and PNP, and column 4a was injected with $PNPO_4$ alone. The addition of PO_4 to the injected test solution reduced both K_m and V_{max}. A comparison the substrate saturation curves from column 1a and 4c shows that the Michaelis constants are similar, but V_{max} was doubled. These results demonstrate that inhibition by phosphate depresses the observed rates of phosphatase-mediated reactions. But only a fraction of the reduction in phosphatase activity with declining pore water velocity can be explained by inhibition. The differences in the V_{max} values obtained from each of the three columns cannot be the result of competitive inhibition. By inspecting Equation 3 it is clear that a competitive inhibitor can only increase the K_m value, and has not effect on the value of V_{max}.
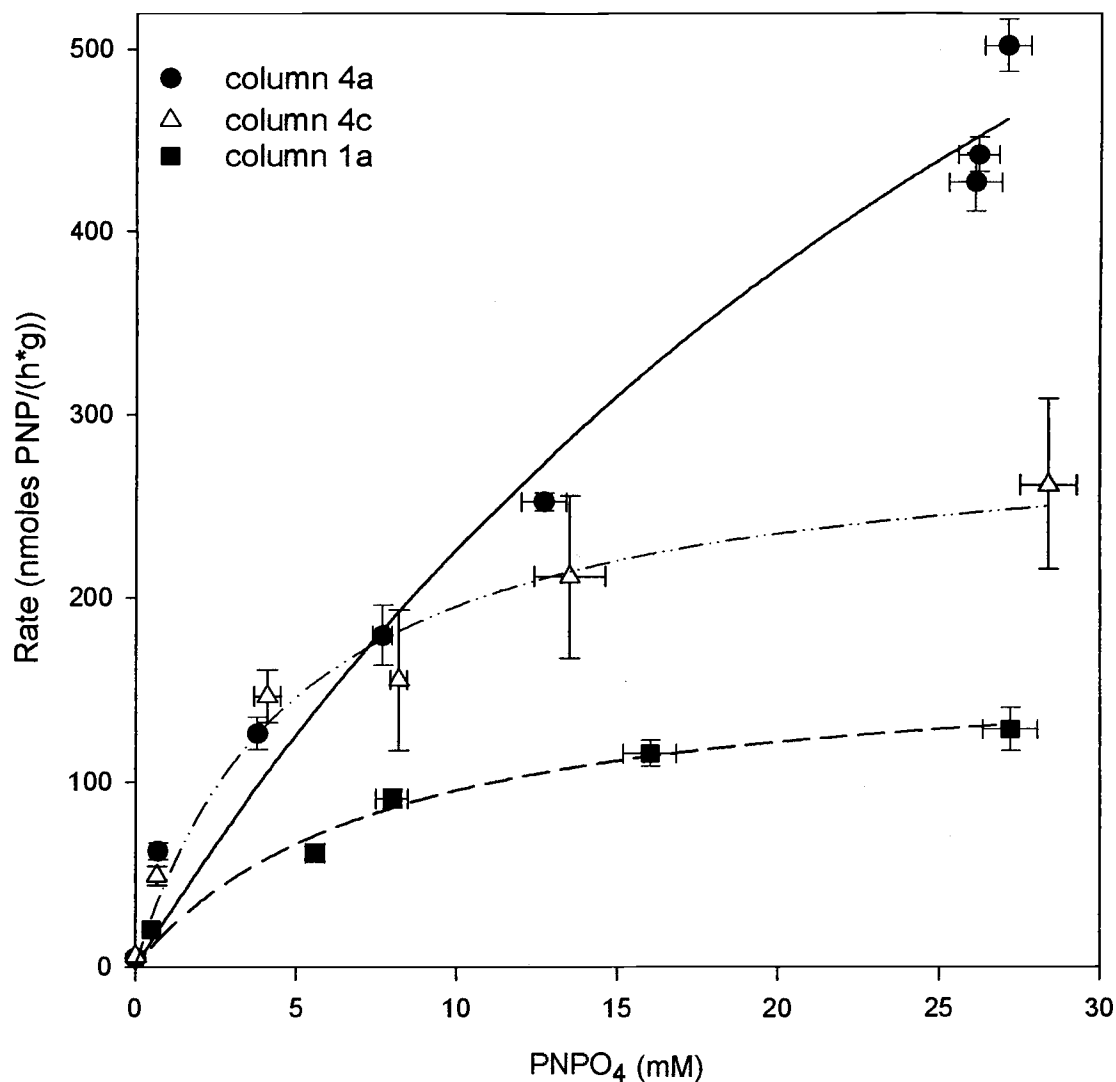
Figure 3.6. The substrate saturation curve for the observed PNP production rates of column 1c, in which injectate solutions included both the substrate ($PNPO_4$) and the product (PNP). The concentrations of $PNPO_4$ and PNP are listed in Table 3b. Shown for reference are the substrate saturation curves with the observed phosphatase activity for column 1a (0.4 mL/min, 41 $\mu m/s$), which had the highest phosphate concentrations in the column effluent, and column 4a (4.0 mL/min, 412 $\mu m/s$), which had the lowest phosphate concentrations in the column effluent (Table 3a).

To determine if the modified Michaelis-Menten equation (Equation 3), which accounts for competitive inhibition, provided a satisfactory representation of the experimental data a model was constructed by holding K_m and V_{max} constant. The

concentration of PO_4 was allowed to vary according to the experimentally measured values made from column 1a. Recall that the concentrations of phosphate produced in column 1a, which had the lowest pore water velocity, ranged from 121 to 769 μM PO_4 and were the same concentrations of phosphate used in the inhibition column experiment (Table 3.3a). A Ki value of 2 mM was determined from batch experiments conducted with this mixed sediment. In this model K_i was allowed to vary from an upper value of 4.0 mM to a lower value of 0.05mM. The values of K_m and V_{max} used in this model are are 50 mM and 1400 nmoles PNP/h·g, which are the kinetic parameters determined from column 4a.
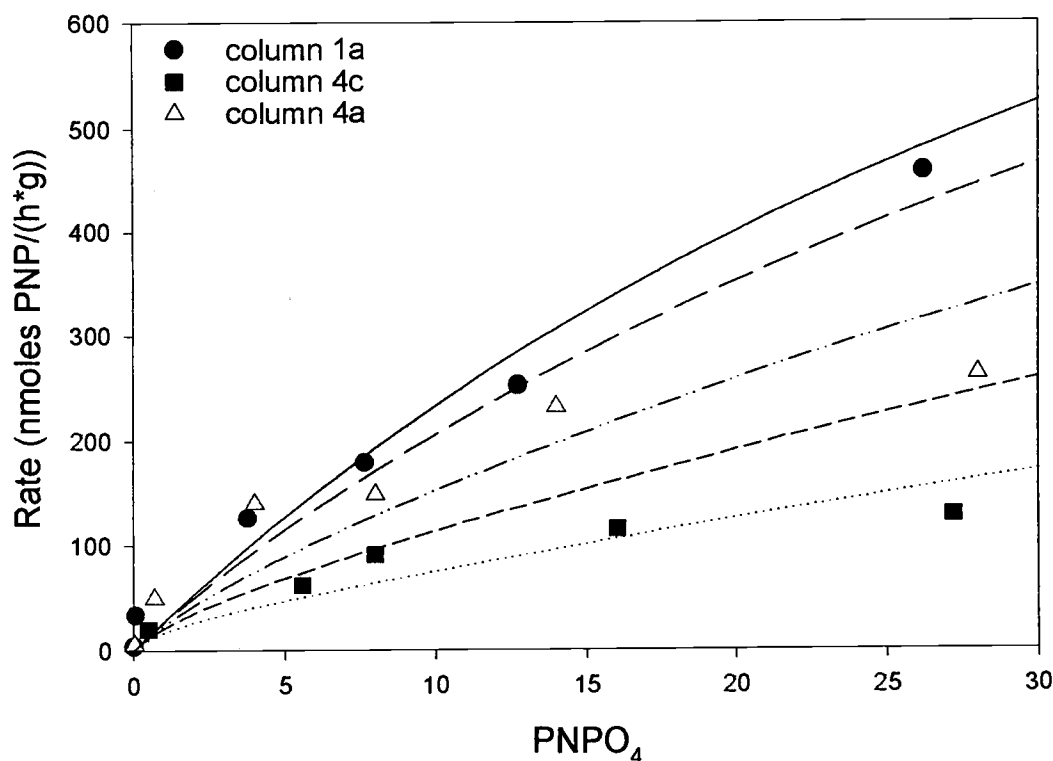
Figure 3.7. Substrate saturation curves obtained from columns experiments are shown as data points for columns 1a, 4a, and 4c (Tables 1, 3a, and 3b). The fit lines represent the Michaelis-Menten equation modified to include competitive inhibition (Equation 3). In this model the concentrations of the substrate and inhibitor were set at the concentrations measured in column 1a, and the inhibition constant (K_i) was varied . The K_i used to calculated the fit lines are 0.15, 0.25, 0.5, 1 and 4 mM, from bottom to top. The upper solid line is the Michaelis-Menton fit for column 4a with no inhibition.

Figure 3.7 shows rates measured from column experiments 1a (41 μm/s), 4a (412 μm/s), and 4c (412 μm/s) as data points. The fit lines show the rates calculated with Equation 3 and the above parameters, labeled with their corresponding K_i values. As the K_i values decrease, the observed kinetics is more sensitive to the concentration of PO_4. By including the effect of the inhibitor at the experimental concentrations present in the columns a decrease in the observed rates is observed, but the calculated rates shown as lines do not fit the experimental data, shown as data points. The Michaelis-Menton

equation for competitive inhibition does not provide a good fit to the data. At this point we hypothesize that the changes in pore water velocity lead to a reduction in activity due to the combined effects of chemical inhibition and mass transfer limitation. An additional model is needed to evaluate the effects of substrate diffusion from bulk solution to the enzyme, and to determine the extent to which mass transfer limitation and inhibition act together to reduce the observed phosphatase activity.

Conclusions

This study has demonstrated the influence of pore water velocity on the phosphatase reaction rates with flow through sediment packed columns as simple models. Substrate saturation curves plotted as reaction rate against substrate concentration further demonstrated the effect pore water velocity has on the phosphatase reaction. The apparent Michaelis-Menten kinetic parameters, K_m and V_{max}, determined by fitting the substrate saturation curves increased with pore water velocity. A positive linear relationship exists between the apparent maximum reaction velocity, V_{max}, and pore water velocity. Phosphate, a known inhibitor, has been shown to diminish phosphatase activity to varying degrees over a range of pore water velocities used. The changes in substrate saturation curves at varying pore water velocities could not be attributed solely to inhibition. A model was constructed to account for the effects of inhibition and attempt to fit experimentally determined substrate saturation curves. The inhibition constant, K_i, which was determined from batch experiments, was used in this model. Experiments conducted to investigate the effects of inhibition by the phosphate as well as the substrate saturation curves obtained from the model, both indicate the inhibition contributes but is

not solely responsible for the reduction in phosphatase activity that is observed with increasing phosphate concentrations.

To increase our understanding of the effects of pore velocity on reaction kinetics obtained from column experiments advection, dispersion, and inhibition have been addressed. But further investigation of the effects diffusion are needed to determine if the observed phosphatase reaction rates are due to a coupling of true reaction rates and diffusion rates and to determine which of the two processes is limiting.

Literature Cited

[1]   Bailey, J.E. and Ollis, D.F. Biochemical Engineering Fundamentals. 2nd ed.
        McGraw-Hill Book Company, New York, 1986, 202-223

[2]   Engasser, J.-M. and Horvath, C. Applied Biochemistry and Bioengineering. in
        Immobilized Enzyme Principles, Goldstein, L., Editor. 1976, Academic Press:
        New York, p. 144-167

[3]   Tabatabai, M.A. and Bremner, J.M. Michaelis Constants of Soil Enzymes. Soil
        Biology and Biochemistry, 1971, **3** p. 317-323

[4]   Marxsen, J. and Schmidt, H. Extracellular phosphatase activity in sediments of the
        Breitenbach, a Central European mountain stream. Hydrobiologia, 1993, **253** p.
        207-216

[5]   Brams, W.H. and McLaren, A.D. Phosphatase Reactions in Columns of Soil. Soil
        Biol. Biochem., 1974, **6** p. 183-189

[6]   Engasser, J.M. and Horvath, C. Inhibition of bound enzymes. II. Characterization
        of product inhibition and accumulation. Biochemistry, 1974, **13**(19), p. 3849-54.

[7]   Gomez, J.L., Bodalo, A., Gomez, E., Bastida, J., and Maximo, M.F. Two-
        parameter model for evaluating effectiveness factor for immobilized enzymes
        with reversible Michaelis-Menten kinetics. Chemical Engineering Science, 2003,
        58 p. 4287-4290

[8]   Horvath, C. and Engasser, J.-M. External and Internal Diffusion in Heterogeneous
        Enzymes Systems. Biotechnology and Bioengineering, 1974, **16** p. 909-923

[9]   Goldstein, L. Kinetic Behavior of Immobillized Enzyme Systems. in *Kinetics of
        Immobilzed Enzymes*. 1980, Academic Press: New York, p. 397443

[10]   Laidler, K.J. and Bunting, P.S. The Kinetics of Immobilized Enzyme Systems. in
        Immobilized Enzyme Kinetics. 1980, Academic Press: New York

[11]   Atlas, R.M. and Bartha, R. Microbial Ecology Fundamentals and Applications.
        4th ed. Benjamin/Cunnings Science Publishing, Menlo Park, California, 1998,

[12]   Chróst, R.J. Microbial ectoenzymes in aquatic environments. in *Aquatic
        Microbial Ecology: Biochemical and Molecular Approaches*, Chróst, R.J., Editor.
        1990, Springer-Verlag: New York, p. 47-78

[13]   Tabatabai, M.A. Soil Enzymes. in *Methods of Soil Analysis, Part 2.
        Microbiological and Biochemical Properties*. 1994: Madison, p. 775-835

[14]   Istok, J.D., Field, J.A., and Schroth, M.H. In Situ Determination of Subsurface
       Microbial Enzyme Kinetics. Ground Water, 2000, **39**(3), p. 348-355

[15]   Radakovich, K.M., Field, J.A., Istok, J.D., and Wood, B.D. Demonstration of an
       Analytical Method to Support the Measurement of Enzyme Activity In Situ.
       Enzyme and Microbial Technology, 2005,

[16]   Eivazi, F. and Tabatabai, M.A. Glucosidases and galactosidases in soils. Soil Biol.
       Biochem., 1988, **20**(5), p. 601-606

[17]   King, G.M. Characterization of b-glucosidase activity in intertidal marine
       sediments. Applied and Environmental Microbiology, 1986, **51**(2), p. 373-380

[18]   Chróst, R.J. Characterization and significance of β-glucosidase activity in lake
       water. Limnol. Oceanogr., 1989, **34**(4), p. 660-672

[19]   Williams, P.J. The validity of the application of simple kinetic analysis to
       heterogeneous microbial populations. Limnol. Oceanogr., 1973, **18**(1), p. 159-165

[20]   Tabatabai, M.A. and Bremner, J.M. Use of p-Nitrophenyl Phosphate for Assay of
       Soil Phosphatase Activity. Soil Biol. Biochem., 1969, **1** p. 301-307

[21]   Kiss, S., Dragan-Sularda, M., and Radulescu, D. Biological significance of
       enzymes accumulated in soil. Advances in Agromony, 1975, **27** p. 25-87

[22]   Burns, R.G. Enzyme Activity in Soil: Location and a Possible Role in Microbial
       Ecology. Soil Biol. Biochem., 1982, **14** p. 423-427

[23]   Skujins, J.J. Enzymes in soil. in *Soil Biochemistry*, Peterson, G.H., Editor. 1967,
       Marcel Dekker: New York, p. 371-414

Chapter 4

Theoretical and Numerical Investigation of Limiting Mechanisms of Phosphatase Activity

Karen M. Radakovich[1], Brian Wood[2], Fabrice Golfier[3]

[1]Department of Chemistry

[2] Department of Civil, Construction, and Environmental Engineering

Oregon State University, Corvallis, OR 97331

[3] LAEGO, Ecole de Géologie de Nancy

Introduction

In this study we investigate the role of mass transfer and its affect on observed enzyme-mediated reaction rates, which we model as a surface-mediated process. Recently, the measurement of kinetic rate parameters for enzyme reactions occurring in the subsurface was demonstrated with an *in situ* testing method know as a 'single-well push pull test' [1]. We recently reported results that examined the potential for measuring enzyme reactions in natural porous media in more carefully controlled laboratory experiments with sediment-packed columns [2]. Results from that work lead to two significant observations: (1) there was both a biotic and abiotic component of the total phosphatase activity (however, the abiotic component was only a small fraction of the total), (2) the observed biologically-mediated phosphatase activity tended to increase with increasing pore water velocity, and (3) inhibition of the enzyme mediated reaction by the build up of product concentrations at low pore water velocity could only partially explain the decrease in the observed reaction rates. In this paper we seek to determine if mass transport of substrate to the enzyme due to diffusion is the rate-limiting step in the transformation of the substrate, p-nitrophenyl phosphate (PNPO$_4$), to its product, p-nitrophenol (PNP), within the range of pore water velocities experienced by the test solution during an *in situ* push-pull test.

Enzyme assays in natural porous media. A variety of enzyme assays including assays of dehydrogenase, esterase, and phosphatase activity are used as measures of microbial metabolic activity in soil science because these enzymes measure general activities of a large portion of the microbial community [3-5]. These measurements are conducted as batch incubations or flow through columns with intact sediment cores.

Although some studies have described anecdotal evidence suggesting that enzyme-mediated reaction rates measured from soil batch incubations and flow through soil packed column experiments are diffusion-limited. Few studies have investigated the effects of transport on reaction rates measured from natural porous media. Tabatabai and Bremner [6] reported that shaking the soil-substrate mixture decreased K_m values and increased V_{max} values for phosphatase and sulfatase activity [6]. Marxsen and Schmidt [8] found that both V_{max} and K_m increased with increased flow rate through sediment cores. Brams and McLaren [7] used flow through columns packed with artificially formed soil crumbs (1 mm in diameter) to investigate the effect of flow rate on the observed K_m and V_{max} values. In this study no clear correlation between flow rate and K_m or V_{max} was established. But K_m values obtained from column experiments decreased to those obtained from batch incubations when soil crumbs were crushed to a powder suggesting that the reactions catalyzed by the soil crumb were diffusion-limited. In this study we investigate the effects of pore water velocity on phosphatase activity. Phosphatases are a large group of enzymes that catalyze the hydrolysis of both esters and anhydrides of phosphoric acid [9]. We assume that measured activities resulted from reactions catalyzed by the ectoenzymes of sediment bound microorganism and investigate the role that diffusion plays in transporting substrate to the enzyme.

The reaction rate kinetics that describes enzyme-mediated reactions were developed for well mixed solution, where the concentrations of reactants and products were uniform throughout the system. This however is not necessarily the case when reactions take place in heterogeneous environments, such as at the surface of a solid [10-15]. The concentrations of the reactants and products in bulk solution can differ greatly

from those at the surface of the solid due to mass transport limitations. To begin describing the effects of diffusion we introduce the Nernst diffusion layer model as a simple representation of the enzyme-mediated reaction of sediment-bound microorganisms [16]. We assume a stagnant layer exist near the surface of the sediment. Outside of this layer the concentration of substrates and product are uniform and referred to as bulk solution. In this layer mass transport occurs by diffusion alone. Because substrate is consumed by the enzyme and converted to product, a simultaneous depletion of substrate and accumulation of product occurs at the enzyme, resulting in concentration gradients being established across the stagnant layer. For enzyme-mediated reactions that take place in heterogeneous systems there are three potential rate-limiting steps that must be considered: first, the substrate must be transported from bulk solution to the enzyme; second, the reaction occurs and the substrate is transformed into product at the surface; and third, the product is transported from the surface to bulk solution. Because the reaction takes place at the surface the actual concentration of substrate and product are lower and higher than in bulk solution, respectively. The concentrations of the substrate and product at the surface depend on the rate of the reaction and the transport characteristic of the solution. To understand the potential interplay between the enzyme-mediated reaction and mass transfer, pore scale processes must be considered to determine if these processes will likely affect the observed or macroscale reaction kinetics measured from concentration changes in bulk solution.

Diffusion limited reactions. Diffusion-limited reactions are reactions in which the mass transport step is the slowest step. Reaction rates fundamentally depend on the frequency of the substrates coming near enough each other in order to be able to react

[17]. We describe our experimental system as a packed-bed reactor with the enzyme-mediated reaction taking place at the surface of the particle pores. Figure 4.1 levels I, II, and III show the sub-pore view of the porous solid, the Darcy scale of the porous solid, and the experimental scale of the sediment packed columns. To investigate the potential effects of mass transfer limitation made as observation at the experimental scale (Figure 4.1, Level III) we investigate processes that occur at the sub-pore scale (Figure 4.1, Level I). We assume that the microorganisms are distributed sparsely on the surface of the solid and the reaction takes place at the surface of the microorganism. As a reaction occurs, the reactant is depleted near the surface of the pore, and subsequently is replenished by some process of diffusion that takes place across the interfacial region shown in Figure 4.1 Level I. The rates of reaction depend on the competition between reactivity at the pore surface and diffusive flow to the pore surface. Early studies conducted by Thiele, Zeldovitch, and Damköhler all presented mathematical analysis of the interaction between reaction and diffusive flow in porous catalysts to determine where and when diffusion is considered relevant and influential.

In this paper we examine the importance of transport limitations for describing the influence of transport processes on the effective rate of reaction. For this analysis, we will adopt the perspective that the reactions occur at the fluid-solid interface. Although in reality the reactions may take place at the surfaces and within microbial cell mass associated with the sediments, this idealization is reasonable, and is consistent with our interest in providing a concrete yet necessarily qualitative explanation for the experimental data reported previously [2]. Our theoretical investigation will be conducted by formally upscaling the proposed sub-pore-scale processes to develop a

macroscale (or Darcy scale) description of the transport of the reactive chemical species. Our particular goals in this work are: (1) determine the macroscale reaction rate parameters and their dependence upon transport of the reacting chemical species, and (2) to determine if the experimentally observed dependence of the kinetic parameters K_m and V_{max} can be reasonably explained by a diffusive mass transfer limitation in the previously reported laboratory studies [2].

Theory

For our analysis, we are considering the transport and reaction processes to characterized by three discrete length scales. In Figure 4.1. we have indicated these by (1) the *microscale*, with characteristic length ℓ_β, (2) the volume averaging scale, with characteristic length r_0, and (3) the *macrosale*, with characteristic length L. Our goal for the upscaling portion of this work is to generate a macroscale description of reactive transport beginning with the relevant microscale transport and reaction phenomena. This will be accomplished by conducting an average of the microscale processes using an averaging volume with characteristic length r_0, as indicated in Figure 4.1. At the pore-scale, the solid-phase and the fluid-phase are identified as the σ-phase and the β-phase, respectively. In the following equations, $A_{\beta\sigma}$ represents the area of the interface between the two phases and $\mathbf{n}_{\beta\sigma}$ represents the unit normal vector directed from β-phase towards the σ-phase. We denote the mass concentration of the substrate in the β-phase as $c_{A\beta}$. In this model we make two approximations about the reactive phase. First, we treat the enzyme-mediated reaction as if it were a surface reaction and assume that there are no

mass transfer limitations within the cells. In reality, the enzyme-mediated reaction may be taking place on the surface of and inside of microbial cells. However, if the cells are distributed sparsely on the solid surfaces (as opposed to being distributed in biofilms), then it is reasonable to approximate the enzyme-mediated reaction as occurring at the surface of the cell phase [18-22]. Second, we treat the reactive surface as being spatially homogeneous. Figure 4.1 (Level I) illustrates a spatially heterogeneous distribution of cells on the solid surface. However, Wood et al. [23] have provided a method for smoothing such spatially heterogeneous reactions sites, and we assume that such a pre-averaged representation can be adopted here. In the material that follows, we will treat the enzyme-mediated reactions as if they were uniformly distributed on the solid surface.

IIIa. Field Scale (subsurface)
(10's of cm to 100's of meters)

IIIb. Field Scale (reactor)
(10's of cm to meters)

Recycle

Product +
Byproducts +

L

Reactants

II. Darcy Scale
(10's of mm to 10's of cm)

fluid
(β-*phase*)

solid
(σ-*phase*)

ℓ_β

$\mathscr{V}$

r_o

fluid

*Interfacial
Reaction*

I. Sub-Pore /
Interfacial Scale
(μm to 10's of mm)

solid
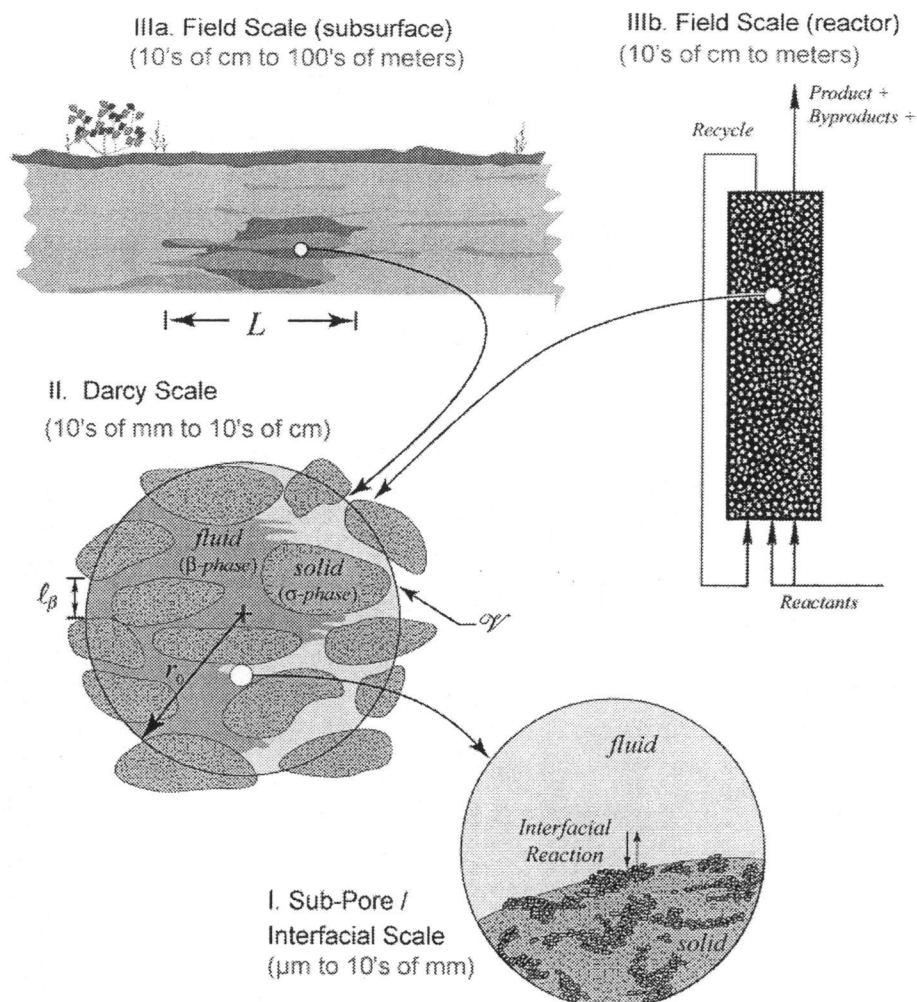
Figure 4.1. One example of a sequence of length scales associated with interfacial reactions in porous media.

Microscale description. Our approach will be to conduct a theoretical evaluation with the purpose of testing our hypothesis rather than attempting to model quantitatively the processes occurring at the pore scale. Our hypothesis is that the increase in the apparent K_m and V_{max} are the result of diffusional effects within the system. Competitive inhibition of phosphatase-mediated reaction by the end product, phosphate, has been documented in the literature and the effects of inhibition were considered in an earlier

investigation of this system [2]. Inhibition effects are not taken into account in this model. Here, we focus on the impact of mass transfer limitations of the substrate alone.

There are two different approaches to modeling this reactive transport problem, the direct simulation and the up-scaling method. The direct simulation solves the problem at the pore-scale to determine the pore water velocities and substrate concentration throughout the domain. Once the velocities and concentrations within the domain are known the pore scale reaction term is solved through iteration. Once the pore scale reaction term is determined it can be integrated to obtain the macroscopic reaction term. The direct simulation method solves the reaction rate under a given set of experimental condition but does not determine the important parameters that control the rates and requires specific knowledge of the system. Conversely, the upscaling method averages the concentration over the domain. Then the concentration within a unit cell or representative volume element of the domain is integrated with respect to volume to obtain the macroscopic reaction term. The up-scaling method results in a description of the large scale reaction coefficient defined in terms of the important small and large scale parameters. Our goal is to use volume averaging to identify the sub-pore and pore scale processes that control the experimentally measured rates obtained from observations made at the large scale. We validate the up-scaling method by comparing the results generated from up-scaling method with the empirical results obtained from the direct simulation for a defined set of conditions.

Given all the assumptions presented before, the pore-scale description of the problem can be written as follows:

Sub-pore-scale process description

$$\underbrace{\frac{\partial c_{A\beta}}{\partial t}}_{\text{Accumulation}} + \underbrace{\nabla \cdot \left(\mathbf{v}_\beta c_{A\beta} \right)}_{\text{Convection}} = \underbrace{\nabla \cdot (D_{A\beta} \nabla c_{A\beta})}_{\text{Diffusion}}, \quad \text{in the } \beta\text{-phase} \tag{1}$$

BC 1: $$\underbrace{-D_{A\beta} \nabla c_{A\beta} \cdot \mathbf{n}_{\beta\sigma}}_{\substack{\text{Diffusive flux to} \\ \text{the surface}}} = \underbrace{R_A}_{\text{Surface Reaction}}, \quad \text{at } A_{\beta\sigma} \tag{2}$$

$$R_A = \underbrace{\frac{k_{\max} c_{A\beta}}{K_m + c_{A\beta}}}_{\text{Surface Reaction}} \tag{3}$$

(Definitions and units for all variables are given in the notation section.) The terms $k_{\max}$ and K_m represent the maximum reaction velocity and the half-saturation constant, respectively. It should be noted that here $k_{\max}$ represents the combination of an intrinsic rate parameter and a surface concentration of enzyme, i.e., $k_{\max} = k' a_v X$, where k' is the intrinsic surface reaction rate parameter (s^{-1}), a_v is the surface area per unit volume given by $a_v = A_{\beta\sigma} / V$ (m^2/m^3), and X is the surface concentration of enzyme (kg/m^2). The velocity field, $\mathbf{v}_\beta$, that appears in Eq. (1.2) is determined by the Stokes flow equation and a mass balance for the fluid phase; these are given by Eqs. (4) and (5), respectively,

$$\nabla p_\beta = \rho_\beta \mathbf{g} + \mu_\beta \nabla^2 \mathbf{v}_\beta \tag{4}$$

$$\nabla \cdot \mathbf{v}_\beta = 0 \tag{5}$$

These equations, plus initial and external boundary conditions, fully specify the conservation of mass and momentum at the sub-pore scale.

Upscaling. Upscaling transport problems with heterogeneous reactions has been the focus of a number of studies (e.g., [23-35]). The principle idea is to average the microscale transport and reaction processes (that applies to processes at a length scale

substantially less than ℓ_β) over a representative support volume to produce a macroscopic model of the reactive transport (that applies to processes viewed at the Darcy scale, with characteristic length r_0). For the case of the nonlinear kinetics that apply to enzyme reactions, upscaling to the Darcy-scale is not straightforward. The nonlinear form of the reaction kinetics makes it impossible to express the average of the reaction term in terms of only the average concentrations. Therefore, we consider the two limiting cases representing two extremes (low and high concentration) observed for Michaelis-Menton type kinetics: (1) first-order reactions and (2) zero-order reactions.

It is beyond the scope of this paper to present a complete derivation of the Darcy-scale equations from the pore-scale problem. Below we briefly discuss the most important steps that lead to such a development. Additional detail regarding this development can be found in the paper by Quintard and Whitaker [36].

In the developments that follow, we make use of two kinds of averages, the superficial average and the intrinsic average. These two averages differ only by a factor of the volume fraction of the fluid phase. For example the superficial average of a field quantity, say $c_{A\beta}$, is given by

$$\langle c_{A\beta} \rangle = \frac{1}{V} \int_{V_\beta} c_{A\beta} \, dV \tag{6}$$

where V_β represents the volume of the phase contained within the averaging volume, V, represented Figure 4.1. This average represents an average over a volume of porous media. The intrinsic average is similarly defined, but in this case it represents an average taken only over the fluid-filled pore space in the porous media. As an example, the intrinsic average concentration is defined by

$$\langle c_{A\beta} \rangle^{\beta} = \frac{1}{V_{\beta}} \int_{V_{\beta}} c_{A\beta} \, dV \tag{7}$$

Note that the two averages are related through the volume fraction of the fluid phase V_{β} / V, which is the porosity, ε_{β}

$$\varepsilon_{\beta} = \frac{V_{\beta}}{V} \tag{8}$$

Through this definition the superficial and intrinsic averages are related by $\langle c_{A\beta} \rangle^{\beta} = \varepsilon_{\beta} \langle c_{A\beta} \rangle$. These averages can be defined similarly for the velocity vector field $\mathbf{v}_{\beta}$. In our analysis it will become necessary to take the average of the gradient of the concentration. Because ultimately we need an expression that depends only on the average of the concentration, $\langle c_{A\beta} \rangle^{\beta}$, rather than the average of the gradient of the concentration, $\langle \nabla c_{A\beta} \rangle^{\beta}$, we need to be able to interchange the averaging and differentiation operations. This is accomplished by the spatial averaging theorem [37-42]

$$\langle \nabla c_{A\beta} \rangle^{\beta} = \nabla \langle c_{A\beta} \rangle^{\beta} + \int_{A_{\beta\sigma}} \mathbf{n}_{\beta\sigma} c_{A\beta} \, dA \tag{9}$$

One can think of this as the three-dimensional analogue to the Leibniz rule for integration.

Averaging the sub-pore scale. We begin the upscaling process by forming the superficial average, defined by Eq. (6), to the sub-pore scale conservation equation given by Eq. (1):

$$\frac{\partial \langle c_{A\beta} \rangle}{\partial t} + \langle \mathbf{v}_{\beta} \cdot \nabla c_{A\beta} \rangle = \langle \nabla \cdot (D_{A\beta} \nabla c_{A\beta}) \rangle \tag{10}$$

Equation (10) can be simplified somewhat by application of the spatial averaging theorem, and use of the relationship between intrinsic and superficial averages. After simplification, this leads to [36],

$$
\varepsilon_\beta \frac{\partial \langle c_{A\beta} \rangle^\beta}{\partial t} + \nabla \cdot \langle \mathbf{v}_\beta c_{A\beta} \rangle = \nabla \cdot (\varepsilon_\beta \mathbf{D}_{A\beta} \nabla \langle c_{A\beta} \rangle^\beta) + \nabla \cdot \left(\frac{\mathbf{D}_{A\beta}}{V} \int_{A_{\beta\sigma}} \mathbf{n}_{\beta\sigma} c_{A\beta} dA \right)
$$
$$
+ \frac{1}{V} \int_{A_{\beta\sigma}} \mathbf{n}_{\beta\sigma} \cdot (\mathbf{D}_{A\beta} \nabla c_{A\beta}) dA
$$

(11)

where we have assumed explicitly that variations in the porosity, ε_β, can be neglected. This assumption generally requires that the radius of the averaging volume is sufficiently larger than the characteristic length of the geometrical structure of the porous media, i.e.,

$$
\ell \ll r_0
$$

(12)

At this point, we introduce the following decompositions [43] which allow us to eliminate the appearance of the sub-pore scale concentration, $c_{A\beta}$, and velocity, $\mathbf{v}_\beta$, at the expense of generating a dependence upon deviations.

$$
c_{A\beta} = \langle c_{A\beta} \rangle^\beta + \tilde{c}_{A\beta}
$$

(13)

$$
\mathbf{v}_\beta = \langle \mathbf{v}_\beta \rangle^\beta + \tilde{\mathbf{v}}_\beta
$$

(14)

Here $\tilde{c}_{A\beta}$ and $\tilde{\mathbf{v}}_\beta$ represent the spatial concentration and velocity deviations, respectively. Use of these spatial decomposition in Eq. (11) yields [44]

$$
\underbrace{\frac{\partial \langle c_{A\beta} \rangle^\beta}{\partial t}}_{\text{accumulation}} + \underbrace{\langle \mathbf{v}_\beta \rangle^\beta \cdot \nabla \langle c_{A\beta} \rangle^\beta}_{\text{convection}} = \underbrace{\nabla \cdot (\mathbf{D}_{A\beta} \nabla \langle c_{A\beta} \rangle^\beta)}_{\text{diffusion}} + \underbrace{\varepsilon_\beta^{-1} \nabla \cdot \mathbf{f}_\beta}_{\text{macrodiffusion}}
$$
$$
- \underbrace{\varepsilon_\beta^{-1} \nabla \cdot \langle \tilde{\mathbf{v}}_\beta \tilde{c}_{A\beta} \rangle}_{\substack{\text{hydrodynamic} \\ \text{dispersion}}} + \underbrace{\frac{\varepsilon_\beta^{-1}}{V} \int_{A_{\beta\sigma}} \mathbf{n}_{\beta\sigma} \cdot (\mathbf{D}_{A\beta} \nabla c_{A\beta}) dA}_{\text{interfacial flux}}
$$

(15)

In this expression, the macrodiffusive flux, $\mathbf{f}_\beta$, is given by

$$\mathbf{f}_\beta = \frac{D_{A\beta}}{V} \int_{A_{\beta\sigma}} \mathbf{n}_{\beta\sigma} \tilde{c}_{A\beta} dA \tag{16}$$

In the development of Eq. (15) we have neglected the area integral of the averaged concentration arising from the decomposition of the concentration in the first integral on the right hand side of Eq. (11). This approximation is valid under the conditions [45]

$$r_0 \ll L \tag{17}$$

which has been assumed from the beginning of the analysis. We can make a final simplification to Eq. (15) by using the reaction boundary condition given by Eq. (2) to eliminate the interfacial flux term. Introducing the area per unit volume, $a_v = A_{\beta\sigma}/V$, the interfacial flux term leads to the definition of a macroscale reaction term as follows

$$\underbrace{\frac{\partial \langle c_{A\beta} \rangle^\beta}{\partial t}}_{\text{accumulation}} + \underbrace{\langle \mathbf{v}_\beta \rangle^\beta \cdot \nabla \langle c_{A\beta} \rangle^\beta}_{\text{convection}} = \underbrace{\nabla \cdot (D_{A\beta} \nabla \langle c_{A\beta} \rangle^\beta)}_{\text{diffusion}} + \underbrace{\varepsilon_\beta^{-1} \nabla \cdot \mathbf{f}_\beta}_{\text{macrodiffusion}}$$
$$\underbrace{- \varepsilon_\beta^{-1} \nabla \cdot \langle \tilde{\mathbf{v}}_\beta \tilde{c}_{A\beta} \rangle}_{\substack{\text{hydrodynamic} \\ \text{dispersion}}} - R_{\text{eff}} \tag{18}$$

$$\text{where,} \quad R_{\text{eff}} = \varepsilon_\beta^{-1} a_v \underbrace{\frac{1}{A_{\beta\sigma}} \int_{A_{\beta\sigma}} R_A \, dA}_{\substack{\text{macroscale} \\ \text{heterogeneous reaction}}}$$

Closure. Our analysis is almost complete at this point. Equation (18) represents a macroscale transport equation that provides a continuum representation of the reactive transport process at the Darcy scale with support volume V (Figure 4.1, Level II), and it is valid under the constraint given by Eq. (17). However, this expression is not yet in a form that is particularly useful in applications because of the dependence of the

macrodiffusion, hydrodynamic dispersion, and heterogeneous reaction terms on averages of the concentration deviations (which are sub-pore scale quantities). In order to eliminate this dependence, one generally seeks to model the behavior of these deviation terms over a representative volume of porous media. For applications to dispersion, the geometrical structure of the representative volume can dramatically influence the results that are observed, even in isotropic media. Appropriate representation of the potentially complex geometrical structure is central to obtaining reasonable predictions of the hydrodynamic dispersion term (see ref. [46], section 3.4.1). Conversely, for the macrodiffusion term, the dependence upon the geometrical structure of the representative region is very weak for isotropic media, and it is primarily the volume fraction of the fluid phase that controls this term [47]. The focus of our work is the macroscale reaction term, and we will adopt simple and structured two-dimensional representations to examine the behavior of the macroscale rate of reaction. An example of a simple two-dimensional unit cell that is used for the geometry of the closure problem is illustrated in Figure 4.2.
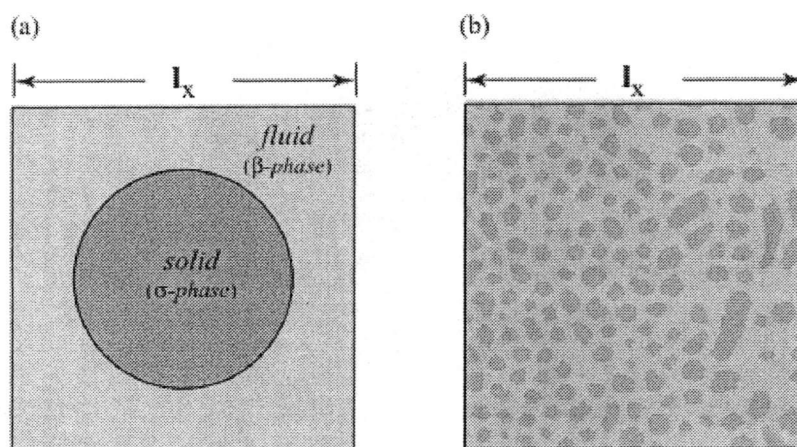
Figure 4.2. (a) A simiple unit cell. (b) A complex unit cell.

In order to develop an equation for the spatial deviation concentration, we develop a conservation equation for $\tilde{c}_{A\beta}$ using the definition of the decomposition. From Eq. (13) it is clear that the deviation is defined by

$$\tilde{c}_{A\beta} = c_{A\beta} - \langle c_{A\beta} \rangle^{\beta} \tag{19}$$

and this suggests that a conservation equation for $\tilde{c}_{A\beta}$ can be developed by subtracting the averaged conservation equation (Eq. (18)) from the sub-pore scale equation (Eq. (1)). The result is

$$\frac{\partial \tilde{c}_{A\beta}}{\partial t} + \mathbf{v}_{\beta} \cdot \nabla \tilde{c}_{A\beta} + \tilde{\mathbf{v}}_{\beta} \cdot \nabla \langle c_{A\beta} \rangle^{\beta} = \nabla \cdot \left(D_{A\beta} \nabla \tilde{c}_{A\beta} \right) - \underbrace{\varepsilon_{\beta}^{-1} \nabla \cdot \mathbf{f}_{\beta}}_{\text{macrodiffusion}}$$
$$+ \underbrace{\varepsilon_{\beta}^{-1} \nabla \cdot \langle \tilde{\mathbf{v}}_{\beta} \tilde{c}_{A\beta} \rangle}_{\substack{\text{hydrodynamic} \\ \text{dispersion}}} + \varepsilon_{\beta}^{-1} a_v \frac{1}{A_{\beta\sigma}} \int_{A_{\beta\sigma}} R_A \, dA \tag{20}$$

We neglect the macrodiffusion and hydrodynamic dispersion terms in Eq. (20), and consider a quasi-steady form for the closure problem. Although the accumulation, macrodiffusion, and hydrodynamic dispersion terms are very important in the macroscopic conservation equation (Eq. (18)), these terms can generally be neglected in the closure problem on the basis of the restrictions

$$\nabla \cdot \left(D_{A\beta} \nabla \tilde{c}_{A\beta} \right) \quad \gg \quad \underbrace{\varepsilon_{\beta}^{-1} \nabla \cdot \mathbf{f}_{\beta}}_{\text{macrodiffusion}} \tag{21}$$

$$\nabla \cdot \left(D_{A\beta} \nabla \tilde{c}_{A\beta} \right) \quad \gg \quad \underbrace{\varepsilon_{\beta}^{-1} \nabla \cdot \langle \tilde{\mathbf{v}}_{\beta} \tilde{c}_{A\beta} \rangle}_{\substack{\text{hydrodynamic} \\ \text{dispersion}}} \tag{22}$$

$$\nabla \cdot \left(D_{A\beta} \nabla \tilde{c}_{A\beta} \right) \quad \gg \quad \underbrace{\frac{\partial \tilde{c}_{A\beta}}{\partial t}}_{\substack{\text{accumulation} \\ \text{(deviation)}}} \tag{23}$$

This simplification is discussed further in chapter 3 of ref. [46]; the associated restrictions for these constraints are essentially the separation of length scales, given by Eq. (12) and (17), and the additional constraint

$$\frac{D_{A\beta}t^*}{\ell_\beta^2} \gg 1 \qquad (24)$$

where t^* is a characteristic time for diffusion. With these simplifications the conservation equation for $\tilde{c}_{A\beta}$ can now be stated as

$$\mathbf{v}_\beta \cdot \nabla \tilde{c}_{A\beta} + \tilde{\mathbf{v}}_\beta \cdot \nabla \langle c_{A\beta} \rangle^\beta = \nabla \cdot \left(D_{A\beta} \nabla \tilde{c}_{A\beta} \right) + \varepsilon_\beta^{-1} a_v \frac{1}{A_{\beta\sigma}} \int\limits_{A_{\beta\sigma}} R_A \, dA \qquad (25)$$

Using Eq. (25) as a starting point, we now turn to examining simplifications to the reaction term in the zero-order and first-order extremes.

The First-order case. At low substrate concentrations, relative to the half-saturation constant, the reaction rate R_A depends linearly on the concentration. In other words, for $c_A \ll K_m$, the reaction rate given by Eq. (3) reduces to the first-order form

$$R_A = \frac{k_{max}}{K_m} c_A \qquad (26)$$

Adopting this representation in the conservation for $\tilde{c}_{A\beta}$ and in the reactive boundary condition given by Eq. (2), we have the following completely specified closure problem for the zero order reaction case

First order reaction closure problem

$$\mathbf{v}_\beta \cdot \nabla \tilde{c}_{A\beta} + \underbrace{\tilde{\mathbf{v}}_\beta \cdot \nabla \langle c_{A\beta} \rangle^\beta}_{\substack{\text{convective source} \\ \text{term}}} = \nabla \cdot \left(\mathbf{D}_{A\beta} \nabla \tilde{c}_{A\beta} \right)$$

$$+ \underbrace{\varepsilon_\beta^{-1} a_v k_{\max} \langle c_{A\beta} \rangle^\beta}_{\substack{\text{reactive source} \\ \text{term}}} + \varepsilon_\beta^{-1} a_v \frac{k_{\max}}{K_m} \frac{1}{A_{\beta\sigma}} \int_{A_{\beta\sigma}} \tilde{c}_{A\beta} \, dA \tag{27}$$

$$\text{BC 1:} -\mathbf{D}_{A\beta} \nabla \tilde{c}_{A\beta} \cdot \mathbf{n}_{\beta\sigma} - k_{\max} \tilde{c}_{A\beta} = \underbrace{\mathbf{D}_{A\beta} \nabla \langle c_{A\beta} \rangle^\beta \cdot \mathbf{n}_{\beta\sigma}}_{\substack{\text{diffusive source} \\ \text{term}}} + \underbrace{\frac{k_{\max}}{K_m} \langle c_{A\beta} \rangle^\beta}_{\substack{\text{reactive source} \\ \text{term}}}, \quad \text{at } A_{\beta\sigma} \tag{28}$$

Periodicity: $\qquad\qquad \tilde{c}_{A\beta} \left(\mathbf{r} + \mathbf{l}_i \right) = \tilde{c}_{A\beta} \left(\mathbf{r} \right)$ \hfill (29)

Constraint: $\qquad\qquad \langle \tilde{c}_{A\beta} \rangle^\beta = 0$ \hfill (30)

$$\nabla p_\beta = \rho_\beta \mathbf{g} + \mu_\beta \nabla^2 \mathbf{v}_\beta \tag{31}$$

$$\nabla \cdot \mathbf{v}_\beta = 0 \tag{32}$$

Periodicity: $\qquad\qquad \tilde{\mathbf{v}}_\beta \left(\mathbf{r} + \mathbf{l}_i \right) = \tilde{\mathbf{v}}_\beta \left(\mathbf{r} \right)$ \hfill (33)

Constraint $\qquad\qquad \langle \mathbf{v}_\beta \rangle^\beta = \mathbf{v}_0$ \hfill (34)

Note that here we have used Eq. (13) to decompose the reaction rate term in the conservation equation and in the boundary condition. Through Eqs. (29) and (33) we have imposed periodic conditions for the concentration and velocity deviations at the edges of the cell. The use of periodic conditions at the cell boundaries is only a device to make the solution soluble; it does not imply that porous media itself is conceived of as being periodic. The use of periodic boundary conditions has been discussed extensively in the literature, and interested readers can find additional details the relevant references [48-50]. Finally, note that two constraints have been specified so that the problem will be soluble. Equations (31)-(34) are entirely independent of the concentration, and from here

on the velocity will be treated as a independently known parameter field from the perspective of solving Eqs. (27)-(30).

Under the constraints that we have imposed on this analysis (Eqs. (12) and (17)) it is possible to show that the solution to the closure problem can be represented in terms of linear functions of the source terms identified above [46, 50]. A general form for the deviation concentration, then, can be stated as

$$\tilde{c}_{A\beta} = \mathbf{b}_\beta \cdot \nabla \langle c_{A\beta} \rangle^\beta + s_\beta \langle c_{A\beta} \rangle \tag{35}$$

where $\mathbf{b}_\beta$ and s_β are the mapping variables of the associated closure problems. Substituting Eq. (35) into the closure problem specified by Eqs. (27)-(30) gives two separate ancillary problems; these ancillary problems are detailed in the Appendix.

Returning to the 'unclosed' version of the averaged conservation of mass equation (Eq. (18)), the use of the closure relation given by Eq. (35) allows the problem to be expressed in the final form

$$\underbrace{\frac{\partial \langle c_{A\beta} \rangle^\beta}{\partial t}}_{\text{accumulation}} + \underbrace{\mathbf{v}_{\text{eff}} \cdot \nabla \langle c_{A\beta} \rangle^\beta}_{\text{convection}} = \underbrace{\nabla \cdot (\mathbf{D}_\beta^* \nabla \langle c_{A\beta} \rangle^\beta)}_{\text{diffusion}} - \underbrace{k_{\text{eff},1} \langle c_{A\beta} \rangle^\beta}_{\substack{\text{macroscale} \\ \text{heterogeneous reaction}}} \tag{36}$$

where the effective parameters $\mathbf{v}_{\text{eff}}$, $\mathbf{D}_\beta^*$, and $k_{\text{eff},1}$ are defined in terms of the small scale parameters and geometry as described in the Appendix. The important point about each of these effective parameters is that they are each dependent on sub-pore scale diffusion coefficient, reaction rate parameters, and hydrodynamics.

To determine the value of the effective reaction rate parameter, $k_{\text{eff},1}$, equations (27)-(34) were decomposed using Eq. (36), and solved using a commercial numerical

PDE solution package (FEMLAB). The decomposition is described in the Appendix. Upon solving the closure problem, the effective reaction rate parameter is given by

$$k_{eff,1} = \varepsilon_\beta^{-1} a_v \frac{k_{max}}{K_m} + \varepsilon_\beta^{-1} a_v \frac{k_{max}}{K_m} \frac{1}{A_{\beta\sigma}} \int_{A_{\beta\sigma}} s_\beta \, dA \tag{37}$$

where the variable s_β comes from the solution to the decomposed version of Eqs. (27)-(34). For these calculations, a simple unit cell of the form illustrated in Figure 4.2a was adopted. Parameters used for the simulations are summarized in Table 1.

Table 4.1. Parameters Used in the Simulations for the Closure Problem.

Parameter	Value	Description
ε_β	0.37	Porosity
ℓ_β	1×10^{-3} m	Characteristic length of the microscale
r_0	4.45×10^{-4} m	Characteristic length of the volume averaging scale
a_v	2800 m^2/m^3	Surface area per unit volume
ρ	1000 kg/m^3	Density
μ	1×10^{-3} N's/m^2	Viscosity
$D_{A\beta}$	1×10^{-9} m^2/s	Diffusion coefficient

Results from the simulations are presented in Figure 4.3 in the form of the effectiveness factor (which measures the effective reaction rate relative to the maximum reaction rate that would be observed if there were no diffusion limitations) as a function of a Thiele modulus (a ratio of reaction to diffusion) for two different Péclet numbers (a

ratio of convection to diffusion). The effectiveness factor (η), Thiele modulus (ϕ), and

Péclet (*Pe*) numbers are given by

Effectiveness factor:

$$\eta = \frac{k_{eff,1}}{\varepsilon_\beta^{-1} a_v (k_{max} K_m^{-1})} \qquad (38)$$

Thiele modulus:

$$\phi = \sqrt{\frac{\ell_\beta^2 (k_{max} K_m^{-1})}{D_{A\beta}}} \qquad (39)$$

Péclet number:

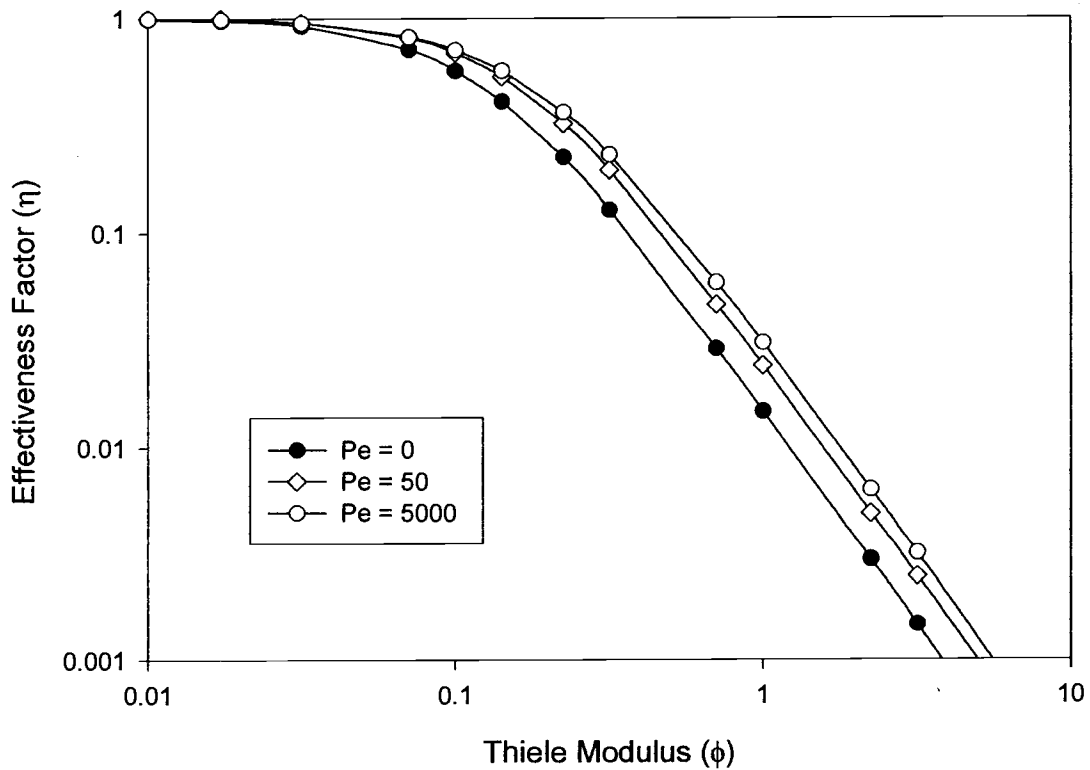$$Pe = \frac{\ell_\beta v_{ave}}{D_{A\beta}} \qquad (40)$$

Figure 4.3. The effectiveness factor as a function of the Thiele modulus for three Péclet numbers.

In Figure 4.3, one can see that for small Péclet numbers (*Pe* = 0), a classical

correspondence between the effectiveness factor and Thiele modulus is observed, where

at a Thiele modulus of near 1, the curve sharply decreases as the reaction becomes diffusion-controlled. However, these results also show a distinct dependence upon the fluid velocity, as indicated by the change in the effectiveness factor behavior for the larger ($Pe = 100$). In this case, the increase in velocity actually increases the effective rate parameter by decreasing the diffusive resistance. Although this kind of behavior has been discussed previously [51], it is still not widely recognized by the hydrology community that the rate of reaction measured in the field can be significantly lower than the rate that can be observed in the laboratory, especially where mixing is used to eliminate diffusion limitations.

Zero order case. At high substrate concentrations, relative to the half-saturation constant, the reaction rate R_A is essentially independent of concentration. In other words, for $c_A \gg K_m$, the reaction rate given by Eq. (3) reduces to the zero-order form

$$R_A = k_{max} \tag{41}$$

Adopting this representation in the conservation for $\tilde{c}_{A\beta}$ and in the reactive boundary condition given by Eq. (2), we have the following completely specified closure problem for the zero order reaction case

Zero order reaction closure problem

$$\mathbf{v}_\beta \cdot \nabla \tilde{c}_{A\beta} + \underbrace{\tilde{\mathbf{v}}_\beta \cdot \nabla \langle c_{A\beta} \rangle^\beta}_{\substack{\text{convective source} \\ \text{term}}} = \nabla \cdot \left(D_{A\beta} \nabla \tilde{c}_{A\beta} \right) + \underbrace{\varepsilon_\beta^{-1} a_v k_{max}}_{\substack{\text{reactive source} \\ \text{term}}} \tag{42}$$

$$\text{BC 1: } -D_{A\beta} \nabla \tilde{c}_{A\beta} \cdot \mathbf{n}_{\beta\sigma} = \underbrace{D_{A\beta} \nabla \langle c_{A\beta} \rangle^\beta \cdot \mathbf{n}_{\beta\sigma}}_{\substack{\text{diffusive source} \\ \text{term}}} + \underbrace{k_{max}}_{\substack{\text{reactive source} \\ \text{term}}} , \quad \text{at } A_{\beta\sigma} \tag{43}$$

$$\text{Periodicity: } \tilde{c}_{A\beta}\left(\mathbf{r} + \mathbf{l}_i\right) = \tilde{c}_{A\beta}\left(\mathbf{r}\right) \tag{44}$$

In analogy to the previous case, the general solution to the closure problem can be specified in terms of the sources.

$$\tilde{c}_{A\beta} = \mathbf{b}_\beta \cdot \nabla \langle c_{A\beta} \rangle^\beta + \psi_\beta k_{\max} \tag{45}$$

Using this representation in the closure problem (see the Appendix), the volume averaged conservation equation can be written

$$\underbrace{\frac{\partial \langle c_{A\beta} \rangle^\beta}{\partial t}}_{\text{accumulation}} + \underbrace{\mathbf{v}_{\textit{eff}} \cdot \nabla \langle c_{A\beta} \rangle^\beta}_{\text{convection}} = \underbrace{\nabla \cdot (\mathbf{D}_\beta^* \nabla \langle c_{A\beta} \rangle^\beta)}_{\text{diffusion}} - \underbrace{k_{\textit{eff},0}}_{\substack{\text{macroscale} \\ \text{heterogeneous} \\ \text{reaction}}} \tag{46}$$

In this case, the effective reaction rate coefficient does not depend on the closure variables, and, hence, does not depend upon the microscale transport properties. The effective reaction rate coefficient is given analytically by the simple expression

$$k_{\textit{eff},0} = \varepsilon_\beta^{-1} a_v k_{\max} \tag{47}$$

Results and Discussion

To evaluate the validity of the models presented above we compared results obtained by (1) direct simulation of reactive transport at the pore scale, and (2) the upscaled results obtained by volume averaging. Agreement between these models is important to demonstrate because the large scale averaged result is an approximate representation and the direct simulations are exact. Agreement between these two methods tells us that the averaging keeps the important details. For the two approaches, we adopted the same two dimensional porous medium and the same set of data. The data set is given in Table 4.2.

Table 4.2. Numerical data

k_{max}	$3.9 \cdot 10^{-9}$ kg.m^{-3}.s^{-1}
K_m	$3 \cdot 10^{-3}$ kg.m^{-3}
D_A	10^{-9} m^2.s^{-1}
ε_β	0.65

In addition to the data shown in Table 4.2, both models require a representation of the porous medium structure. A physical representation of the pore scale of the porous medium used in our experiments was needed to perform the simulations. Because information about the pore-scale geometry of our experimental porous medium was lacking, a random two dimensional porous medium, illustrated in Figure 4.2(b), was selected for use in the simulations. The random porous medium is complex enough to capture features of a real system. Flow rates used in the simulations 0.43 and 43 cm^3.h^{-1} represent pore water velocities of 0.15 and 15 μm.s^{-1}, respectively. These pore water velocities are lower than the pore water velocities from earlier column experiments. As stated earlier, our purpose is to develop a qualitative description of the phenomenon, and not to replicate our results in a quantitative manner.
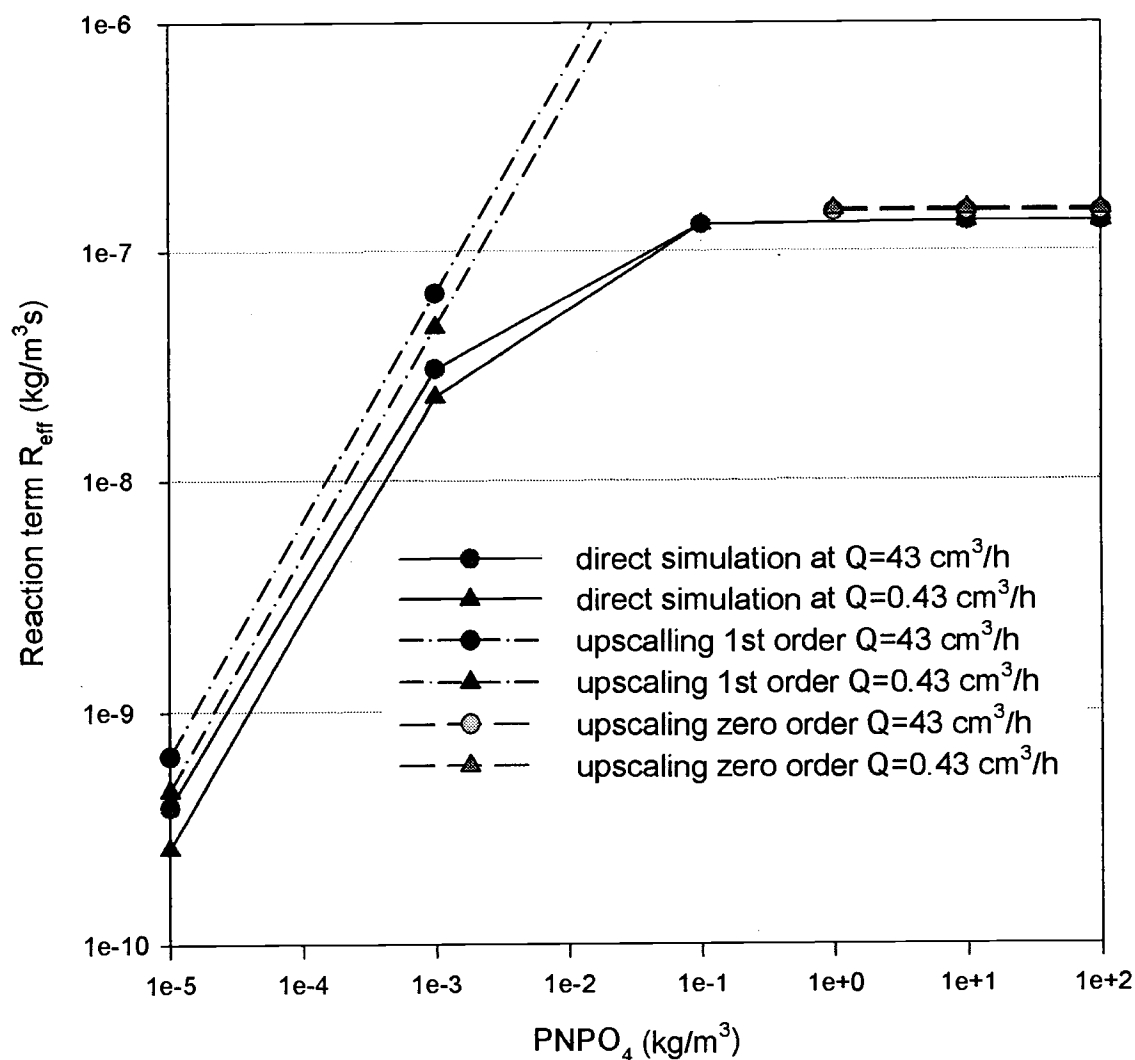
Figure 4.4. (a). Comparison of the pore-scale and Darcy-scale simulations showing the reaction rate (R_{eff}) as a function of the concentration of substrate at the inlet.

Results obtained from simulations performed with the both models are shown in Figure 4.4. The value of the macroscopic reaction term, R_{eff}, is represented as a function of the mass concentration of the substrate injected at the inlet, for two different flow rates, $Q = 0.43\,cm^3.h^{-1}$ and $Q = 43\,cm^3.h^{-1}$. The simulations show good agreement in both the zero-order and first-order region. In the first-order region the reaction term increases

as a function of flow rate in both the upscaling and direct simulation. The increase in R_{eff} with flow rate demonstrates the mass transfer effects at the pore scale are observed in the first order region. In contrast, both simulations show that R_{eff} is independent of flow rate in the zero-order region. At high concentration values (zero-order region), we recover the analytical solution described for k_{eff} in Eq. (48).

Application to the experimental results. The effective first-order and zero-order reaction rates defined in Eq. (37) represent the small concentration $\left(\left\langle c_{A\beta}\right\rangle^{\beta} \ll K_{m,eff}\right)$ and large concentration $\left(\left\langle c_{A\beta}\right\rangle^{\beta} \ll K_{m,eff}\right)$ endpoints to the more general Michaelis-Menten reaction rate kinetics. Ultimately, we would like to have a hyperbolic form for the effective reaction rate so that the upscaled and microscale reactions have the same form. It has been shown previously with a few restrictions that it is possible to average the limiting cases of Michaelis-Menten kinetics [20,52]. We can extrapolate from the results of the numerical models shown in Figure 4.3 the form of the macroscopic reaction term that we are looking for. Results from the upscaling and direct simulations both suggest that a Michealis-Menten kinetics form can be kept at the Darcy-scale and the macroscopic reaction term is

$$R_{eff} = \frac{k_{0,eff} \left\langle c_{A\beta} \right\rangle^{\beta}}{K_{m,eff} + \left\langle c_{A\beta} \right\rangle^{\beta}} \tag{48}$$

where the effective half-saturation constant is defined by

$$K_{m,eff} = \frac{k_{0,eff}}{k_{1,eff}} \tag{49}$$

where $A_{\beta\sigma}$ is the area of the solid fluid interface and V is the volume.

Now, we can test our theoretical expression by applying the results from the simulations to our experimental results. For this purpose, we have fitted Eq. (48) to the experimental curves by holding $k_{0,eff}$ constant and varying the value of $K_{m,eff}$ as a function of the injection velocity. The flow rates used in an earlier study conducted with sediment packed columns are listed in Table 4.2 along with the values of $k_{0,eff}$ and $K_{m,eff}$ that were measured at each flow rate.

Table 4.3. Values of Macroscopic Reaction Coefficients Used in the Comparison of Experimental Data and the Theoretical Curves.

Flow rate		$K_{m,eff}$ (kg.m^{-3})	$k_{0,eff}$ (kg.m^{-3}.s^{-1})
(cm^3.h^{-1})	(mL.min^{-1})		
Experimental values obtained from column experiments			
24	0.4	1.7	$1.67 \cdot 10^{-6}$
240	4.0	1.28	$4.31 \cdot 10^{-5}$
Values used in the theoretical evaluation			
24	0.4	4.4	$4.31 \cdot 10^{-5}$
240	4.0	1.1	$4.31 \cdot 10^{-5}$
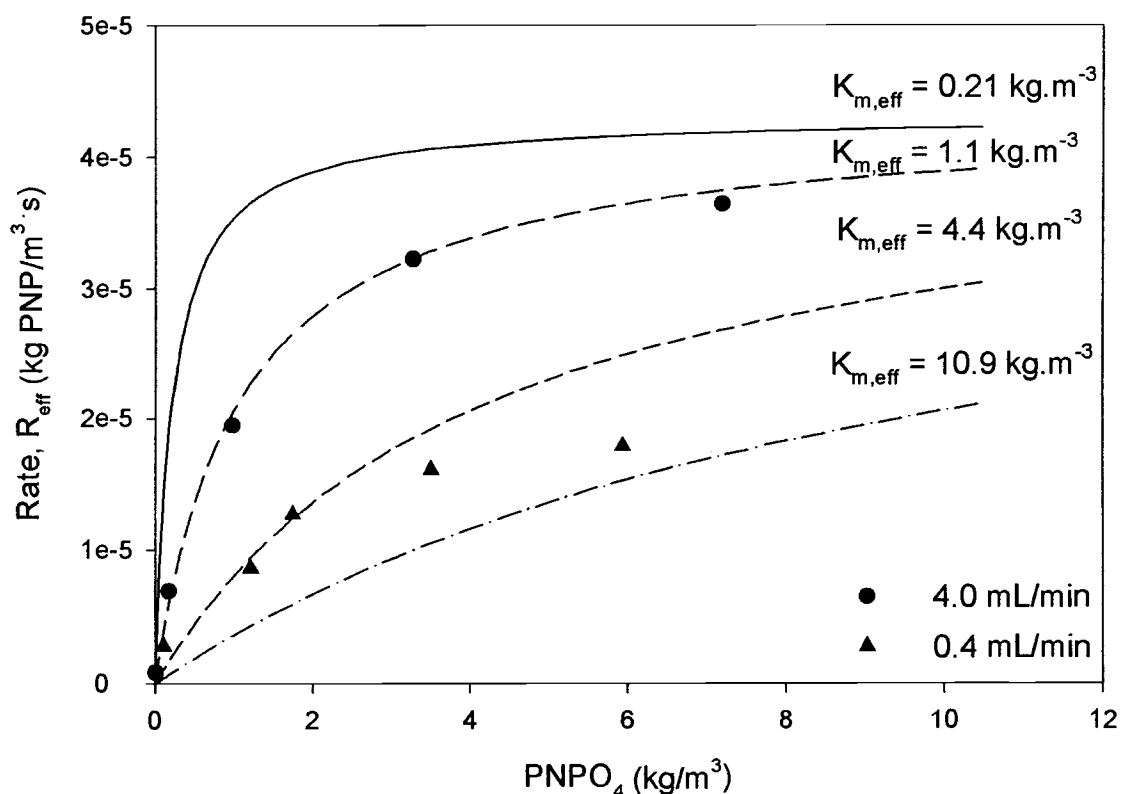
Figure 4.5. Comparison between behavior of the experimental data and theoretical expression

Figure 4.5 shows the experimentally determined rates as data points and theoretical values are shown as lines. The theoretical values were calculated by holding the value of $k_{0,eff}$ constant at the maximum experimentally obtained value, which was obtained in the 4.0 mL/min column. Values of $K_{m,eff}$ were allowed to varied over the range of values that was observed experimentally in the column experiments. A comparison between the theoretical and experiment results illustrated in Figure 4.5 demonstrates agreement between the behavior of the theoretical and experimental rates at low substrate concentrations, both increase as a function of flow rate in the first order

region. But at higher substrate concentrations the experimental results are not well represented by the theoretical results. The agreement in the first-order region of the Figure 4.5 demonstrates that mass transfer limitations of the substrate to the enzyme are only evident at low substrate concentrations, and the decline in $k_{0,eff}$ is due to another process.

Conclusion

This investigation leads us to two important results. First, from a qualitative point of view at least, it is possible to explain the kinetic variations of $K_{m,eff}$ observed experimentally by the mass transfer limitations. Second, the variation in $k_{0,eff}$ cannot be attributed to such a mechanism. Our hypothesis that diffusion effects were responsible for the changes in the observed reaction rates appears to be valid only in the first-order region at low substrate concentrations.

As an extension to this study, it would be interesting, in a second step, to improve the modeling of phosphatase activity in order to estimate the quantitative contributions to the variations in the kinetics of both the mass transfer limitation and the inhibition effect of the phosphate. In this way, we could verify if the inhibition effect *at the pore-scale* can explain the variation of $k_{0,eff}$ which is observed *at the macro-scale* with increasing phosphate concentrations.

Appendix.

The development of the closure problem. Substituting the generic solution for the deviation concentration (Eq. (35)) into the closure problem (Eqs. (27)-(30)) and collecting terms that involve $\nabla \langle c_{A\beta} \rangle^{\beta}$ and $\langle c_{A\beta} \rangle^{\beta}$ respectively.

First order reactions

For the case of first-order reactions, two separate closure problems can be identified that allow one to compute the fields $\mathbf{b}_{\beta}$ and s_{β} respectively. Recall that he deviation equation was given by

$$\tilde{c}_{A\beta} = \mathbf{b}_{\beta} \cdot \nabla \langle c_{A\beta} \rangle^{\beta} + s_{\beta} \langle c_{A\beta} \rangle \tag{50}$$

Substituting this into Eqs. (27)-(30) yields the following two closure problems.

Problem I

$$\mathbf{v}_{\beta} \cdot \nabla \mathbf{b}_{\beta} + \underbrace{\tilde{\mathbf{v}}_{\beta}}_{\substack{\text{convective source} \\ \text{term}}} = \mathrm{D}_{A\beta} \nabla^2 \mathbf{b}_{\beta} + \varepsilon_{\beta}^{-1} a_v \frac{k_{\max}}{K_m} \frac{1}{A_{\beta\sigma}} \int_{A_{\beta\sigma}} \mathbf{b}_{\beta} dA \tag{51}$$

BC 1: $\qquad -\mathrm{D}_{A\beta} \nabla \mathbf{b}_{\beta} \cdot \mathbf{n}_{\beta\sigma} - k_{\max} \mathbf{b}_{\beta} = \underbrace{\mathrm{D}_{A\beta} \mathbf{I} \cdot \mathbf{n}_{\beta\sigma}}_{\substack{\text{diffusive source} \\ \text{term}}} \qquad \text{at } A_{\beta\sigma} \tag{52}$

Periodicity: $\qquad\qquad \mathbf{b}_{\beta}(\mathbf{r}+\mathbf{l}_i) = \mathbf{b}_{\beta}(\mathbf{r}) \tag{53}$

Constraint: $\qquad\qquad \langle \mathbf{b}_{\beta} \rangle^{\beta} = 0 \tag{54}$

Problem II

$$\mathbf{v}_{\beta} \cdot \nabla s_{\beta} = \mathrm{D}_{A\beta} \nabla^2 s_{\beta} + \underbrace{\varepsilon_{\beta}^{-1} a_v \frac{k_{\max}}{K_m}}_{\substack{\text{reactive source} \\ \text{term}}} + \varepsilon_{\beta}^{-1} a_v \frac{k_{\max}}{K_m} \frac{1}{A_{\beta\sigma}} \int_{A_{\beta\sigma}} s_{\beta} dA \tag{55}$$

$$\text{BC 1:} \qquad -\mathbf{D}_{A\beta}\nabla s_\beta \cdot \mathbf{n}_{\beta\sigma} - \frac{k_{max}}{K_m}s_\beta \;=\; \underbrace{\frac{k_{max}}{K_m}}_{\substack{\text{reactive source} \\ \text{term}}}, \qquad \text{at } A_{\beta\sigma} \tag{56}$$

$$\text{Periodicity:} \qquad s_\beta\left(\mathbf{r}+\mathbf{l}_i\right) = s_\beta\left(\mathbf{r}\right) \tag{57}$$

$$\text{Constraint:} \qquad \langle s_\beta \rangle^\beta \;=\; 0 \tag{58}$$

One interesting feature to note here; the source terms relating to hydrodynamics appear only in Problem I, whereas the source terms applying to reaction appear only in Problem II. This is because the sources that appear in Problem I arise strictly from the sources that involve the gradient of the average concentration; the sources that appear in Problem II arise from terms that involve the average concentration itself. Note that linearly combining Problems I and II as indicated by Eq. (35) recovers the original closure problem specified by Eqs. (27)-(30).

Once the general form of the closure relation is know, this expression can be substituted into the averaged equation to close it (i.e., all terms involving the unknown concentration deviation $\tilde{c}_{A\beta}$ have been replaced by a form that involves only $\nabla\langle c_{A\beta}\rangle^\beta$ and $\langle c_{A\beta}\rangle^\beta$). Substituting Eq. (50) into Eq. (18) allows the averaged conservation equation to be specified by

$$\underbrace{\frac{\partial\langle c_{A\beta}\rangle^\beta}{\partial t}}_{\text{accumulation}} + \underbrace{\mathbf{v}_{eff}\cdot\nabla\langle c_{A\beta}\rangle^\beta}_{\text{convection}} \;=\; \underbrace{\nabla\cdot(\mathbf{D}^*_\beta\nabla\langle c_{A\beta}\rangle^\beta)}_{\text{diffusion}} - \underbrace{k_{eff,1}\langle c_{A\beta}\rangle^\beta}_{\substack{\text{macroscale} \\ \text{heterogeneous reaction}}} \tag{59}$$

where the effective parameters are given by

$$\mathbf{v}_{eff} = \langle\mathbf{v}_\beta\rangle^\beta - \frac{\mathbf{D}_{A\beta}}{V_\beta}\int_{A_{\beta\sigma}}\mathbf{n}_{\beta\sigma}s_\beta dA + \varepsilon_\beta^{-1}a_v\frac{k_{max}}{K_m}\frac{1}{A_{\beta\sigma}}\int_{A_{\beta\sigma}}\mathbf{b}_\beta\,dA \tag{60}$$

$$\mathbf{D}_\beta^* = \mathrm{D}_{A\beta}\left(\mathbf{I} + \frac{1}{V_\beta} \int_{A_{\beta\sigma}} \mathbf{n}_{\beta\sigma}\mathbf{b}_\beta dA\right) - \langle \tilde{\mathbf{v}}_\beta \mathbf{b}_\beta \rangle^\beta \tag{61}$$

$$k_{eff,1} = \varepsilon_\beta^{-1} a_v \frac{k_{\max}}{K_m} + \varepsilon_\beta^{-1} a_v \frac{k_{\max}}{K_m} \frac{1}{A_{\beta\sigma}} \int_{A_{\beta\sigma}} s_\beta\, dA \tag{62}$$

In this analysis, we have assumed that all averaged properties can be assumed to be spatially stationary (i.e., constants in space). It is interesting to note that for this case, each of the effective parameters depend on the sub-pore scale diffusion coefficient, reaction rate parameters, and hydrodynamics.

Because the focus of this work is on the effective reaction rate, it is useful to put closure problem II into an alternative, dimensionless form.

$$Pe \cdot \frac{\mathbf{v}_\beta}{v_{ave}} \cdot \nabla s_\beta = \nabla^2 s_\beta + \varepsilon_\beta^{-1}\alpha\phi\left(1 + \frac{1}{A_{\beta\sigma}} \int_{A_{\beta\sigma}} s_\beta\, dA\right) \tag{63}$$

BC 1: $\qquad -\nabla s_\beta \cdot \mathbf{n}_{\beta\sigma} - \phi s_\beta = \phi, \quad \text{at } A_{\beta\sigma}$ (64)

Periodicity: $\qquad s_\beta(\mathbf{r} + \mathbf{l}_i) = s_\beta(\mathbf{r})$ (65)

Constraint: $\qquad \langle s_\beta \rangle^\beta = 0$ (66)

Where the parameters in Eq. (63) and (64) are defined by

$$v_{ave} = \sqrt{\mathbf{v}_\beta \cdot \mathbf{v}_\beta} \tag{67}$$

Péclet number: $\qquad Pe = \dfrac{\ell_\beta v_{ave}}{\mathrm{D}_{A\beta}}$ (68)

Thiele modulus: $\qquad \phi = \sqrt{\dfrac{\ell_\beta^2\, (k_{\max} K_m^{-1})}{\mathrm{D}_{A\beta}}}$ (69)

$$\alpha = a_v \ell_\beta \tag{70}$$

Zero order reactions

The case of zero order reactions is actually more difficult than would appear at first, because the reaction rate term is actually nonlinear near $c_A = 0$. However, for the case we are considering, the high-concentration extreme for Michaelis-Menton kinetics, we must by definition have $c_A > 0$. Recall that for this case the deviation concentration was given by

$$\tilde{c}_{A\beta} = \mathbf{b}_\beta \cdot \nabla \langle c_{A\beta} \rangle^\beta + \psi_\beta k_{max} \tag{71}$$

Substituting this into Eqs. (42)-(44) yields the following two closure problems.

Problem I

$$\mathbf{v}_\beta \cdot \nabla \mathbf{b}_\beta + \underbrace{\tilde{\mathbf{v}}_\beta}_{\substack{\text{convective source} \\ \text{term}}} = D_{A\beta} \nabla^2 \mathbf{b}_\beta \tag{72}$$

BC 1:
$$-D_{A\beta} \nabla \mathbf{b}_\beta \cdot \mathbf{n}_{\beta\sigma} = \underbrace{D_{A\beta} \mathbf{n}_{\beta\sigma}}_{\substack{\text{diffusive source} \\ \text{term}}}, \quad \text{at } A_{\beta\sigma} \tag{73}$$

Periodicity:
$$\mathbf{b}_\beta (\mathbf{r} + \mathbf{l}_i) = \mathbf{b}_\beta (\mathbf{r}) \tag{74}$$

Problem II

$$\mathbf{v}_\beta \cdot \nabla \psi_\beta = D_{A\beta} \nabla^2 \psi_\beta + \underbrace{\varepsilon_\beta^{-1} a_v}_{\substack{\text{reactive source} \\ \text{term}}} \tag{75}$$

BC 1:
$$-D_{A\beta} \nabla \psi_\beta \cdot \mathbf{n}_{\beta\sigma} = \underbrace{1}_{\substack{\text{reactive source} \\ \text{term}}}, \quad \text{at } A_{\beta\sigma} \tag{76}$$

Periodicity:
$$\psi_\beta (\mathbf{r} + \mathbf{l}_i) = \psi_\beta (\mathbf{r}) \tag{77}$$

The closed form of the macroscale equation is found, as before, by substituting the decomposition (Eq. (71)) into the unclosed form of the averaged equation (Eq. (18)). This allows the averaged conservation equation to be specified by

$$\underbrace{\frac{\partial \langle c_{A\beta} \rangle^{\beta}}{\partial t}}_{\text{accumulation}} + \underbrace{\mathbf{v}_{e\!f\!f} \cdot \nabla \langle c_{A\beta} \rangle^{\beta}}_{\text{convection}} = \underbrace{\nabla \cdot (\mathbf{D}_{\beta}^{*} \nabla \langle c_{A\beta} \rangle^{\beta})}_{\text{diffusion}} - \underbrace{k_{e\!f\!f,0}}_{\substack{\text{macroscale} \\ \text{heterogeneous reaction}}} \tag{78}$$

where the effective parameters are given by

$$\mathbf{v}_{e\!f\!f} = \langle \mathbf{v}_{\beta} \rangle^{\beta} \tag{79}$$

$$\mathbf{D}_{\beta}^{*} = \mathrm{D}_{A\beta}\!\left(\mathbf{I} + \frac{1}{V_{\beta}} \int_{A_{\beta\sigma}} \mathbf{n}_{\beta\sigma} \mathbf{b}_{\beta} dA \right) - \langle \tilde{\mathbf{v}}_{\beta} \mathbf{b}_{\beta} \rangle^{\beta} \tag{80}$$

$$k_{e\!f\!f,0} = \varepsilon_{\beta}^{-1} a_{v} k_{\max} \tag{81}$$

Interestingly, for this case, the effective reaction rate coefficient is not a function of any closure variables. This suggests that the zero order effective reaction rate is independent of the transport processes.

Direct Simulations

Typically, this approach is solved with a series of iterative computations. The equations are discretized on a two-dimensional uniform Cartesian mesh. A staggered grid for pressure and velocity is used to obtain a non-oscillating pressure field with respect to the space variables.

The first step is to compute the velocity field inside the domain. Once the steady velocity field is defined, the concentration field is determined. A time-splitting method [22] and the SSO algorithm (sequential split-operator) is used, which splits the equation into a hyperbolic part and a diffusive part (including the reaction term). A first order explicit Euler scheme in time and a second order total variation diminishing (TVD) scheme in space [23], is used for the hyperbolic part in order to have sufficient accuracy

[24]. The dispersive and reactive part is discretized with a classical implicit discretization.

At each time step, a convergence criterion is imposed to ensure the steady solution for the concentration field is obtained such as,

$$\left\| c_{A\beta}^{n+1} - c_{A\beta}^{n} \right\|_{L^2} \leq \varepsilon_0 \tag{0.82}$$

Otherwise, a new time step is solved for the transport equation.

The macroscopic reaction term R^* is calculated by using the following relation:

$$R^* = \frac{1}{V_\beta} \int_{A_{\beta\sigma}} D\nabla c_{A\beta} \cdot \mathbf{n}_{A\beta} \, dA \tag{0.83}$$

In this way, we can express the macroscopic reaction term as a function of the concentration of the substrate in the fluid-phase and the injection velocity for a given geometry of the porous medium: $R^* = f\left(c_{A\beta}, \mathbf{v}_\beta\right)$.

Nomenclature

Roman Letters

$A_{\beta\sigma}$	interfacial area of the solid-fluid ($\beta-\sigma$) interface in an averaging volume (m^2)
a_v	area of the solid-fluid interface per unit volume of bulk porous media ($1/m$)
$c_{A\beta}$	the concentration of chemical species A in the fluid phase (m^2/s)
$D_{A\beta}$	diffusion coefficient for chemical species A in the fluid phase (m^2/s)
$D_{A\beta}\nabla c_{A\beta}\cdot\mathbf{n}_{\beta\sigma}$	diffusive flux normal to the fluid-solid interface
g	acceleration due to gravity (m/s^2)
$k_{0,eff}$	$= \varepsilon_\beta^{-1}a_v k_{max}$, the zero-order macroscale heterogeneous reaction term ($kg/(m^3\cdot s)$)
$k_{1,eff}$	the first-order macroscale heterogeneous reaction term defined in Eq. (37) ($kg/(m^3\cdot s)$)
k_{max}	maximum substrate conversion rate parameter ($kg/(m^2\cdot s)$)
K_m	the half-saturation constant (kg/m^3)
$K_{m,eff}$	the effective half-saturation constant
$\mathbf{n}_{\beta\sigma}$	unit normal vector directed from the fluid phase to the solid surface
p_β	total pressure in the fluid phase (Pa)
Pe	$= \ell_\beta v_{ave}/D_{A\beta}$, a Péclet number defined in Eq. (40) (-)
R_{eff}	the effective reaction rate
s_β	closure mapping variable defined by Eq. (35) (-)
v_{ave}	closure mapping variable defined by Eq. (35) (-)
$\mathbf{v}_\beta$	velocity in the fluid phase (m/s)

Greek Letters

α	$= a_v\ell_\beta$, a ratio of length scales from the first-order reaction closure problem (-)
ε_β	volume fraction of the fluid phase defined by Eq. (9) (-)
η	effectiveness factor defined by Eq. (39) (-)
μ_β	viscosity of the fluid phase ($Pa\cdot s$)
ρ_β	density of the fluid phase (kg/m^3)
ϕ	Thiele modulus defined by Eq. (40) (-)

Literature Cited

[1]   Istok, J.D., J.A. Field, and M.H. Schroth, *In Situ Determination of Subsurface Microbial Enzyme Kinetics.* Ground Water, 2000. **39**(3): p. 348-355.

[2]   Radakovich, K.M., J.A. Field, and J.D. Istok, *The Effects of Pore Water Velocity on Phosphatase Kinetics in Soil Columns.* planned for submission to Environ. Sci. Technol., 2005.

[3]   Taylor, J.P., et al., *Comparison of microbial numbers and enzymatic activities in surface soils and subsoils using various techniques.* Soil Biol. Biochem., 2002. **34**(3): p. 387-401.

[4]   Stubberfield, L.C.F. and P.J.A. Shaw, *A comparison of tetrazolium reduction and FDA hydrolysis with other measures of microbial activity.* Journal of Microbiological Methods, 1990. **12**(3): p. 151-162.

[5]   Atlas, R.M. and R. Bartha, *Microbial Ecology Fundamentals and Applications.* 4th ed. 1998, Menlo Park, California: Benjamin/Cunnings Science Publishing.

[6]   Tabatabai, M.A. and J.M. Bremner, *Michaelis Constants of Soil Enzymes.* Soil Biology and Biochemistry, 1971. **3**: p. 317-323.

[7]   Brams, W.H. and A.D. McLaren, *Phosphatase Reactions in Columns of Soil.* Soil Biol. Biochem., 1974. **6**: p. 183-189.

[8]   Marxsen, J. and H. Schmidt, *Extracellular phosphatase activity in sediments of the Breitenbach, a Central European mountain stream.* Hydrobiologia, 1993. **253**: p. 207-216.

[9]   Tabatabai, M.A., *Soil Enzymes*, in *Methods of Soil Analysis, Part 2. Microbiological and Biochemical Properties.* 1994: Madison. p. 775-835.

[10]   Engasser, J.-M. and C. Horvath, *Applied Biochemistry and Bioengineering*, in *Immobilized Enzyme Principles*, L.B. Wingard Jr., E. Katchalski-Katzir, and L. Goldstein, Editors. 1976, Academic Press: New York. p. 144-167.

[11]   Horvath, C. and J.-M. Engasser, *External and Internal Diffusion in Heterogeneous Enzymes Systems.* Biotechnology and Bioengineering, 1974. **16**: p. 909-923.

[12]   Goldstein, L., *Kinetic Behavior of Immobillized Enzyme Systems*, in *Kinetics of Immobilzed Enzymes.* 1980, Academic Press: New York. p. 397443.

[13]   Laidler, K.J. and P.S. Bunting, *The Kinetics of Immobilized Enzyme Systems*, in *Immobilized Enzyme Kinetics*. 1980, Academic Press: New York.

[14]   Marrazzo, W.N., R.L. Merson, and B.J. McCoy, *Enzyme Immobilized in a Packed-Bed Reactor: Kinetic Parameters and Mass Transfer Effects*. Biotechnol. Bioeng., 1975. **17**(10): p. 1515-28.

[15]   Gomez, J.L., et al., *Two-parameter model for evaluating effectiveness factor for immobilized enzymes with reversible Michaelis-Menten kinetics*. Chemical Engineering Science, 2003. **58**: p. 4287-4290.

[16]   Bailey, J.E. and D.F. Ollis, *Biochemical Engineering Fundamentals*. 2nd ed. 1986, New York: McGraw-Hill Book Company. 202-223.

[17]   Debye, P., *Reaction rates in ionic solutions*. Trans. Electrochem. Soc., 1942: p. 265-272.

[18]   Parker, J.C. and A.J. Valocchi, *Constraints on the validity of equilibrium and first-order kinetic transport models in structured soils*. Water Resour Res, 1986. **22**(3): p. 399-407.

[19]   Valocchi, A.J., *Theoretical analysis of deviations from local equilibrium during sorbing solute transport through idealized stratified aquifers*. J Contam Hydrol, 1988. **2**: p. 191-207.

[20]   Wood, B.D. and S. Whitaker, *Diffusion and reaction in biofilms*. Chemical Engineering Science, 1998. **53**: p. 397-425.

[21]   Wood, B.D. and S. Whitaker, *Erratum to "Diffusion and reaction in biofilms" [Chemical Engineering Science 53 (1998) 397-425]*. Chemical Engineering Science, 2000. **55**: p. 2349.

[22]   Wood, B.D. and S. Whitaker, *Multi-species diffusion and reaction in biofilms*. Chemical Engineering Science, 2000. **55**: p. 3397-3418.

[23]   Wood, B.D., M. Quintard, and S. Whitaker, *Jump conditions at non-uniform boundaries: The catalytic surface*. Chemical Engineering Science, 2000. **Submitted**.

[24]   Edwards, D.A. and A.M.J. Davis, *Diffusion and convective dispersion through arrays of spheres with surface-adsorption, diffusion, and unequal solute partitioning*. Chemical Engineering Science, 1995. **50**(9): p. 1441-1454.

[25]   Edwards, D.A., M. Shapiro, and H. Brenner, *Dispersion And Reaction In 2-Dimensional Model Porous-Media.* Physics Of Fluids A-Fluid Dynamics, 1993. **5**(4): p. 837-848.

[26]   Kechagia, P.E., et al., *On the upscaling of reaction-transport processes in porous media with fast or finite kinetics.* Chemical Engineering Science, 2002. **57**(13): p. 2565-2577.

[27]   Mauri, R., *Dispersion, Convection, And Reaction In Porous-Media.* Physics Of Fluids A-Fluid Dynamics, 1991. **3**(5): p. 743-756.

[28]   Mojaradi, R. and M. Sahimi, *Diffusion-Controlled Reactions In Disordered Porous-Media.2. Nonuniform Distribution Of Reactants.* Chemical Engineering Science, 1988. **43**(11): p. 2995-3004.

[29]   Pagitsas, M., A. Nadim, and H. Brenner, *Macrotransport Processes In The Presence Of Bulk And Surface Chemical-Reactions.* Journal Of Chemical Physics, 1986. **85**(7): p. 4038-4044.

[30]   Quintard, M. and S. Whitaker, *Aerosol filtration: An analysis using the method of volume averaging.* Journal Of Aerosol Science, 1995. **26**(8): p. 1227-1255.

[31]   Ryan, D., R.G. Carbonell, and S. Whitaker, *Effective Diffusivities For Catalyst Pellets Under Reactive Conditions.* Chemical Engineering Science, 1980. **35**(1-2): p. 10-16.

[32]   Sahimi, M., *Diffusion-Controlled Reactions In Disordered Porous-Media.1. Uniform-Distribution Of Reactants.* Chemical Engineering Science, 1988. **43**(11): p. 2981-2993.

[33]   Shapiro, M. and H. Brenner, *Taylor dispersion of chemically reactive species: irreversible first-order reactions in bulk and on boundaries.* Chem. Engng. Sci., 1986. **41**: p. 1417-1433.

[34]   Shapiro, M. and H. Brenner, *Chemically reactive generalized Taylor dispersion phenomena.* AIChE Journal, 1987. **33**: p. 1155-1167.

[35]   Shapiro, M. and H. Brenner, *Dispersion of a chemically reactive solute in a spatially periodic model of a porous medium.* Chemical Engineering Science, 1988. **43**: p. 551-571.

[36]   Quintard, M. and S. Whitaker, *Dissolution of an immobile phase during flow in porous media.* Ind. and Engng Chem. Res., 1999. **38**(3): p. 833-844.

[37]   Anderson, T.B. and R. Jackson, *A fluid mechanical description of fluidized beds.* Ind. Engng Chem. Fundam., 1967. **6**(527-538).

[38]   Cushman, J.H., *Volume averaging, probabilistic averaging, and ergodicity.*
         Advances in Water Resources, 1983. **6**: p. 182-184.

[39]   Gray, W.G., et al., *Mathematical Tools for Changing Spatial Scales in the
         Analysis of Physical Systems.* 1993, Boca Raton, Florida.: CRC Press.

[40]   Howes, F. and S. Whitaker, *The spatial averaging theorem revisited.* Chem.
         Engng Sci., 1985. **40**(8): p. 1387-1392.

[41]   Slattery, J.C., *Flow of Viscoelastic Fluids Through Porous Media.* AIChE J.,
         1967. **13**: p. 1066-1071.

[42]   Whitaker, S., *Diffusion and dispersion in porous media.* A.I.Ch.E. J., 1967. **13**: p.
         420-427.

[43]   Gray, W.G., *A derivation of the equations for multiphase transport.* Chem. Engng
         Sci., 1975. **30**: p. 229-233.

[44]   Carbonell, R. and S. Whitaker, *Dispersion in pulsed systems II: Theoretical
         developments for passive dispersion in porous media.* Chem. Engng Sci., 1983.
         38: p. 1795-1802.

[45]   Quintard, M. and S. Whitaker, *Transport in ordered and disordered porous media
         II: Generalized volume averaging.* Transport in Porous Media, 1994. **14**: p. 179-
         206.

[46]   Whitaker, S., *The Method of Volume Averaging.* Theory and Applications of
         Transport in Porous Media, ed. J. Bear. 1999, Dordrecht: Kluwer.

[47]   Quintard, M., *Diffusion in isotropic and anisotropic porous systems.* Transport in
         Porous Media, 1993. **11**: p. 187-199.

[48]   Pickup, G.E., et al., *Permeability tensors for sedimentary structures.* Math. Geol.,
         1994. **26**: p. 227-250.

[49]   Renard, P. and G. de Marsily, *Calculating equivalent permeability: A review.*
         Advances in Water Resources, 1997. **20**: p. 253-278.

[50]   Wood, B.D., et al., *Comparison of Volume and Ensemble Averaging: Solute
         Transport in Porous Media.* Water Resour. Res., 2003. **39**: p.
         {doi:10.1029/2002WR001723}.

[51]   Cherblanc, F., *Etude du Transport Miscible en Milieux Poreux Heterogenes:
         Prise en Compte du Non-Equilibre.* 1999, Universite Bordeaux I.

[52] Quintard, M. and S. Whitaker, *Convection, dispersion and interfacial transport of contaminants: Homogeneous porous media.* Adv. Water Resour., 1994. **17**: p. 221-239.

[53] Kaney, J.F., C.T. Miller, and C.T. Kelley, *Convergence of iterative split-operator approaches for approximating nonlinear reactive transport problems.* Adv. Water Resour., 2003. **26**(247-261).

[54] Takacs, L., *A two-step scheme for the advection equation with minimised dissipation and dispersion errors.* Mon. Weather Rev., 1985. **113**(6).

[55] Bruneau, C.H., P. Fabrie, and P. Rasetarinera, *An accurate finite difference scheme for solving convection-dominated diffusion equations.* Intl J. Num. Meth. Fluids, 1997. **24**(169-183).

Chapter 5

Summary

The β-glucosidase and phosphatase activities of groundwater and sediment samples were investigated both ex situ in laboratory experiments and in situ with a single well push-pull test. A method for quantifying these enzyme activities was develop that extended the soil science methods based on the use of *p*-nitrophenyl substituted substrates by chromatographically separating and quantifying both substrate and product concentrations with high performance liquid chromatography. Laboratory experiments were conducted on groundwater samples to develop and validate the method. β-Glucosidase activities measured on groundwater samples collected from two sites ranged from 0.0024 to 0.063 µmole PNP/h·L. An *in situ* demonstration of this method was carried out in a petroleum-contaminated aquifer near Newberg, Oregon. From the extraction-phase data of this test the Michaelis-Menton parameters were determined to be $K_m = 49$ µM PNG and $V_{max} = 1.47$ µM PNP/h.

The effect of pore water velocity on the overall rate of phosphatase-mediated reactions in soil columns is investigated. A feature of the *in situ* single-well push-pull test is the nonlinear drop in the pore water velocity of the injected solution as it moves out radially from the injection point. The effects of pore water velocity on observed reaction rates were investigated with sediment packed columns that were operated at four different flow rates (0.4, 1.0, 2.0, and 4.0 mL/min) to achieve pore water velocities typical of injected solutions in a push-pull test (41, 103, 206, and 412 µm/s). The

apparent Michaelis-Menten kinetic parameters, K_m and V_{max}, determined by fitting the substrate saturation curves increased with pore water velocity. V_{max} increased from 167 to 1438 nmol PNP/(h·g) over the range of pore water velocities used. Demonstrating that under typical push-pull test conditions the observed rates of phosphatase-mediated reactions increased with pore water velocity; this apparent increase in rate with pore water velocity can be explained only in part by inhibition.

The role of mass transfer and its effect on observed enzyme-mediated reaction rates were modeled as a surface-mediated process to develop a qualitative explanation for the results obtained from column experiments. Our hypothesis was that the dependence both K_m and V_{max} showed on pore water velocity could be explained by diffusive mass transfer limitations. Our numerical result showed that from a qualitative view it is possible to explain the kinetic variations of K_m observed experimentally by mass transfer limitation due to diffusion. But diffusion effects were limiting only in the first-order region at low substrate concentrations. Therefore, the variation in V_{max} could not be explained by mass transfer limitations.

Bibliography

Anderson, T.B. and R. Jackson, *A fluid mechanical description of fluidized beds.* Ind. Engng Chem. Fundam., 1967. **6**(527-538).

Atlas, R. M. and R. Bartha (1998). Microbial Ecology Fundamentals and Applications. Menlo Park, California, Benjamin/Cunnings Science Publishing.

Bailey, J. E. and D. F. Ollis (1986). Biochemical Engineering Fundamentals. New York, McGraw-Hill Book Company.

Brams, W. H. and A. D. McLaren (1974). "Phosphatase Reactions in Columns of Soil." Soil Biol. Biochem. **6**: 183-189.

Browman, M. G. and M. A. Tabatabai (1978). "Phosphodiesterase activity of soils." Soil Sci. Soc. Am. J. **42**(2): 286-290.

Bruneau, C.H., P. Fabrie, and P. Rasetarinera, *An accurate finite difference scheme for solving convection-dominated diffusion equations.* Intl J. Num. Meth. Fluids, 1997. **24**(169-183).

Burns, R. G. (1982). "Enzyme Activity in Soil: Location and a Possible Role in Microbial Ecology." Soil Biol. Biochem. **14**: 423-427.

Carbonell, R. and S. Whitaker, *Dispersion in pulsed systems II: Theoretical developments for passive dispersion in porous media.* Chem. Engng Sci., 1983. **38**: p. 1795-1802.

Chapelle, F. H. (1993). Ground-Water Microbiology and Geochemistry. Englewood Cliffs, NJ., John Wiley and Sons, Inc.

Cherblanc, F., *Etude du Transport Miscible en Milieux Poreux Heterogenes: Prise en Compte du Non-Equilibre.* 1999, Universite Bordeaux I.

Christian, J. R. and D. M. Karl (1995). "Bacterial ectoenzymes in marine waters: activity ratios and temperature responses in three oceanographic provinces." Limnol. Oceanogr. **40**(6): 1042-1049.

Chróst, R. J. (1989). "Characterization and significance of β-glucosidase activity in lake water." Limnol. Oceanogr. **34**(4): 660-672.

Chróst, R. J., Ed. (1990). Microbial ectoenzymes in aquatic environments. Aquatic Microbial Ecology: Biochemical and Molecular Approaches. New York, Springer-Verlag.

Chróst, R. J. (1991). "Ectoenzymes in aquatic environments: Microbial strategy for substrate supply." Verh. Internat. Verein. Limnol. **24**: 2597-2600.

Chróst, R. J. (1991). Environmental Control of Microbial Ectoenzymes. Microbial Enzymes in Aquatic Environmentsl. R. J. Chròst. New York, Speinger-Verlag: 30-59.

Costura, R. K. and P. J. J. Alvarez (2000). "Expression and longevity of toluene dioxygenase in Pseudomonas putida F1 induced at different dissolved oxygen concentrations." Water Research **34**(11): 3014-3018.

Cotner, J. B. and R. G. Wetzel (1991). Bacterial Phosphatases from Different Habitats in a Small, Hardwater Lake. Microbial Enzymes in Aquatic Environments. R. J. Chròst. New York, Springer-Verlag: 187-205.

Cushman, J.H., *Volume averaging, probabilistic averaging, and ergodicity.* Advances in Water Resources, 1983. **6**: p. 182-184.

Debye, P., *Reaction rates in ionic solutions.* Trans. Electrochem. Soc., 1942: p. 265-272.

Deeb, R. A., K. M. Scow, et al. (2000). "Aerobic MTBE biodegradation: an examination of past studies, current challenges, and future research directions." Biodegradation **11**(2-3): 171-186.

Edwards, D.A. and A.M.J. Davis, *Diffusion and convective dispersion through arrays of spheres with surface-adsorption, diffusion, and unequal solute partitioning.* Chemical Engineering Science, 1995. **50**(9): p. 1441-1454.

Edwards, D.A., M. Shapiro, and H. Brenner, *Dispersion And Reaction In 2-Dimensional Model Porous-Media.* Physics Of Fluids A-Fluid Dynamics, 1993. **5**(4): p. 837-848.

Eivazi, F. and M. A. Tabatabai (1976). "Phosphatases in Soils."

ivazi, F. and M. A. Tabatabai (1977). "Phosphatase In Soils." Soil Biol. Biochem. **9**: 167-172.

Eivazi, F. and M. A. Tabatabai (1988). "Glucosidases and galactosidases in soils." Soil Biol. Biochem. **20**(5): 601-606.

Eivazi, F. and M. A. Tabatabai (1990). "Factors affecting glucosidase and galactosidase activities in soils." Soil Biol. Biochem. **22**(7): 891-897.

Engasser, J. M. and C. Horvath (1974). "Inhibition of bound enzymes. II. Characterization of product inhibition and accumulation." Biochemistry 13(19): 3849-54.

Engasser, J.-M. and C. Horvath (1976). Applied Biochemistry and Bioengineering. Immobilized Enzyme Principles. L. B. Wingard Jr., E. Katchalski-Katzir and L. Goldstein. New York, Academic Press. 1: 144-167.

F ayolle, F., J. P. Vandecasteele, et al. (2001). "Microbial degradation and fate in the environment of methyl tert-butyl ether and related fuel oxygenates." Applied Microbiology and Biotechnology 56(3-4): 339-349.

Freeman, C. (1997). "Using HPLC to eliminate quench interference in fluorogenic substrate assays of microbial enzyme activity." Soil Biol. Biochem. 29: 203-205.

Freeman, C. and G. B. Nevison (1999). "Simultaneous analysis of multiple enzymes in environmental samples using methylumbelliferyl substrates and HPLC." J. Environ. Qual. 28: 1378-1380.

Gomez, J. L., A. Bodalo, et al. (2003). "Two-parameter model for evaluating effectiveness factor for immobilized enzymes with reversible Michaelis-Menten kinetics." Chemical Engineering Science 58: 4287-4290.

Goldstein, L. (1980). Kinetic Behavior of Immobillized Enzyme Systems. Kinetics of Immobilzed Enzymes. New York, Academic Press. 44: 397443.

Gray, W.G., A derivation of the equations for multiphase transport. Chem. Engng Sci., 1975. 30: p. 229-233.

Gray, W.G., et al., Mathematical Tools for Changing Spatial Scales in the Analysis of Physical Systems. 1993, Boca Raton, Florida.: CRC Press.

Haggerty, R., M. H. Schroth, et al. (1998). "Simplified method of "push-pull"test data analysis for determining in situ rate coeffiecients." Groundwater 36(2): 314-324.

Hendel, B. and J. Marxsen (1997). "Measurement of low-level extracellular enzyme activity in natural waters using fluorigenic model substrates." Acta hydrochim. hydrobiol. 25(5): 253-258.

Horvath, C. and J.-M. Engasser (1974). "External and Internal Diffusion in Heterogeneous Enzymes Systems." Biotechnology and Bioengineering 16: 909-923.

Howes, F. and S. Whitaker, *The spatial averaging theorem revisited.* Chem. Engng Sci., 1985. **40**(8): p. 1387-1392.

Istok, J. D. and M. D. Humphrey (1995). "Laboratory Investigation of Buoyancy-Induced Flow (Plume Sinking) During Two-Well Tracer Tests." Groundwater **4**(33): 597-604.

Istok, J. D., M. D. Humphrey, et al. (1997). "Single-Well "Push-Pull" Test for In Situ Determination of Microbial Activities." Groundwater **35**(4): 619-631.

Istok, J. D., J. A. Field, et al. (2001). "In Situ Determination of Subsurface Microbial Enzyme Kinetics." Ground Water **39**(3): 348-355.

Kaney, J.F., C.T. Miller, and C.T. Kelley, *Convergence of iterative split-operator approaches for approximating nonlinear reactive transport problems.* Adv. Water Resour., 2003. **26**(247-261).

Kechagia, P.E., et al., *On the upscaling of reaction-transport processes in porous media with fast or finite kinetics.* Chemical Engineering Science, 2002. **57**(13): p. 2565-2577.

King, G. M. (1986). "Characterization of b-glucosidase activity in intertidal marine sediments." Applied and Environmental Microbiology **51**(2): 373-380.

Kiss, S., M. Dragan-Sularda, et al. (1975). "Biological significance of enzymes accumulated in soil." Advances in Agromony **27**: 25-87.

Laidler, K. J. and P. S. Bunting (1980). The Kinetics of Immobilized Enzyme Systems. Immobilized Enzyme Kinetics. New York, Academic Press. **64**.

Leahy, J. G., A. M. Byrne, et al. (1996). "Comparison of factors influencing trichloroethylene degradation by toluene-oxidizing bacteria." Applied and Environmental Microbiology **62**(3): 825-833.

Madsen, E. L. (1998). "Epistemology of Environmental Microbiology." Environ. Sci. Technol. **32**(4): 429-439.

Magnuson, J. K., M. F. Romine, et al. (2000). "Trichloroethene reductive dehalogenase from Dehalococcoides ethenogenes: Sequence of tceA and substrate range characterization." Applied and Environmental Microbiology **66**(12): 5141-5147.

Magnuson, J. K., R. V. Stern, et al. (1998). "Reductive dechlorination of tetrachloroethene to ethene by two-component enzyme pathway." Applied and Environmental Microbiology **64**(4): 1270-1275.

Marrazzo, W. N., R. L. Merson, et al. (1975). "Enzyme Immobilized in a Packed-Bed Reactor: Kinetic Parameters and Mass Transfer Effects." Biotechnol. Bioeng. **17**(10): 1515-28.

Marxsen, J. and H. Schmidt (1993). "Extracellular phosphatase activity in sediments of the Breitenbach, a Central European mountain stream." Hydrobiologia **253**: 207-216.

Mauri, R., *Dispersion, Convection, And Reaction In Porous-Media.* Physics Of Fluids A-Fluid Dynamics, 1991. **3**(5): p. 743-756.

Mojaradi, R. and M. Sahimi, *Diffusion-Controlled Reactions In Disordered Porous-Media.2. Nonuniform Distribution Of Reactants.* Chemical Engineering Science, 1988. **43**(11): p. 2995-3004.

Munster, U., Plon, P. Einio, and Nurminen, J. (1989). "Evaluation of the measurements of extracellular enzyme activities in a polyhumic lake by means of studies with 4-methylumbelliferyl-substrates." Arch. Hydrobiol. **115**(3): 321-337.

Nelsestuen, G. L. and M. B. Martinez (1997). "Steady State Enzyme Velocities That Are Independent of [Enzyme]: An Important Behavior in Many Membrane and Particle-Bound States." Biochemistry **36**(30): 9081-9086.

Parker, J.C. and A.J. Valocchi, *Constraints on the validity of equilibrium and first-order kinetic transport models in structured soils.* Water Resour Res, 1986. **22**(3): p. 399-407.

Pagitsas, M., A. Nadim, and H. Brenner, *Macrotransport Processes In The Presence Of Bulk And Surface Chemical-Reactions.* Journal Of Chemical Physics, 1986. **85**(7): p. 4038-4044.

Patwardhan, V. S. and N. G. Karanth (1982). "Film diffusional influences on the kinetic parameters in packed-bed immobilized enzyme reactors." Biotechnol. Bioeng. **24**(4): 763-80.

Petit, N. M., Gregory, Lindsay J., Freedman, R.B., Burns, R.G (1977). "Differential stabilities of soil enzymes assay and properties of phosphatase and arylsulphatase." Biochemica et Biophysica Acta **185**: 357-366.

Pickup, G.E., et al., *Permeability tensors for sedimentary structures.* Math. Geol., 1994. **26**: p. 227-250.

Prenafeta-Boldu, F. X., J. Vervoort, et al. (2002). "Substrate interactions during the biodegradation of benzene, toluene, ethylbenzene, and xylene (BTEX)

hydrocarbons by the fungus Cladophialophora sp strain T1." Applied and Environmental Microbiology 68(6): 2660-2665.

Quintard, M. and S. Whitaker, *Dissolution of an immobile phase during flow in porous media*. Ind. and Engng Chem. Res., 1999. **38**(3): p. 833-844.

Quintard, M. and S. Whitaker, *Transport in ordered and disordered porous media II: Generalized volume averaging*. Transport in Porous Media, 1994. **14**: p. 179-206.

Quintard, M., *Diffusion in isotropic and anisotropic porous systems*. Transport in Porous Media, 1993. **11**: p. 187-199.

Quintard, M. and S. Whitaker, *Convection, dispersion and interfacial transport of contaminants: Homogeneous porous media*. Adv. Water Resour., 1994. **17**: p. 221-239.

Radakovich, K. M., J. A. Field, et al. (2005). "Quantifying in situ b-glucosidase activity in groundwater." Enzyme and Microbial Technology, manuscript in preparation.

Radakovich, K.M., J.A. Field, and J.D. Istok, *The Effects of Pore Water Velocity on Phosphatase Kinetics in Soil Columns*. planned for submission to Environ. Sci. Technol., 2005.

Renard, P. and G. de Marsily, *Calculating equivalent permeability: A review*. Advances in Water Resources, 1997. **20**: p. 253-278.

Ryan, D., R.G. Carbonell, and S. Whitaker, *Effective Diffusivities For Catalyst Pellets Under Reactive Conditions*. Chemical Engineering Science, 1980. **35**(1-2): p. 10-16.

Sahimi, M., *Diffusion-Controlled Reactions In Disordered Porous-Media.1. Uniform-Distribution Of Reactants*. Chemical Engineering Science, 1988. **43**(11): p. 2981-2993.

Scholz, O. and J. Marxsen (1996). "Sediment phosphatases of the Breitenbach, a first-order Central European stream." Arch. Hydrobiol. **135**(4): 433-450.

Schroth, M. H., J. D. Istok, et al. (1998). "Spatial variability in in situ aerobic respiration and denitrification rates in a petroleum-contaminated aquifer." Groundwater **36**(6): 924-937.

Schwarzenbach, R. P., P. M. Gschwend, et al. (1993). Environmental Organic Chemistry. New York, Wiley.

Shapiro, M. and H. Brenner, *Taylor dispersion of chemically reactive species: irreversible first-order reactions in bulk and on boundaries.* Chem. Engng. Sci., 1986. **41**: p. 1417-1433.

Shapiro, M. and H. Brenner, *Chemically reactive generalized Taylor dispersion phenomena.* AIChE Journal, 1987. **33**: p. 1155-1167.

Shapiro, M. and H. Brenner, *Dispersion of a chemically reactive solute in a spatially periodic model of a porous medium.* Chemical Engineering Science, 1988. **43**: p. 551-571.

Slattery, J.C., *Flow of Viscoelastic Fluids Through Porous Media.* AIChE J., 1967. **13**: p. 1066-1071.

Somville, M. (1984). "Measurement and Study of Substrate Specificity of Exoglucosidase Activity in Eutrophic Water." Applied and Environmental Microbiology **48**(6): 1181-1185.

Stubberfield, L. C. F. and P. J. A. Shaw (1990). "A comparison of tetrazolium reduction and FDA hydrolysis with other measures of microbial activity." Journal of Microbiological Methods **12**(3): 151-162.

Tabatabai, M. A. (1994). Soil Enzymes. Methods of Soil Analysis, Part 2. Microbiological and Biochemical Properties. Madison: 775-835.

Tabatabai, M. A. and J. M. Bremner (1969). "Use of p-Nitrophenyl Phosphate for Assay of Soil Phosphatase Activity." Soil Biol. Biochem. **1**: 301-307.

Tabatabai, M. A. and J. M. Bremner (1971). "Michaelis Constants of Soil Enzymes." Soil Biology and Biochemistry **3**: 317-323.

Takacs, L., *A two-step scheme for the advection equation with minimised dissipation and dispersion errors.* Mon. Weather Rev., 1985. **113**(6).

Taylor, J. P., B. Wison, et al. (2002). "Comparison of microbial numbers and enzymatic activities in surface soils and subsoils using various techniques." Soil Biol. Biochem. **34**(3): 387-401.

Valocchi, A.J., *Theoretical analysis of deviations from local equilibrium during sorbing solute transport through idealized stratified aquifers.* J Contam Hydrol, 1988. **2**: p. 191-207.

Whitaker, S., *Diffusion and dispersion in porous media.* A.I.Ch.E. J., 1967. **13**: p. 420-427.

Whitaker, S. (1985). "A simple geometrical derivation of the spatial averaging theorem." Chemical Engineering Education **19**: 18-21, 50-52.

Whitaker, S., *The Method of Volume Averaging*. Theory and Applications of Transport in Porous Media, ed. J. Bear. 1999, Dordrecht: Kluwer.

Williams, P. J. (1973). "The validity of the application of simple kinetic analysis to heterogeneous microbial populations." Limnol. Oceanogr. **18**(1): 159-165.

Wood, B. D., M. Quintard, et al. (2002). "Calculation of Effective Diffusivities for Biofilms and Tissues." Biotechnology and Bioengineering **77**(5): 495-514.

Wood, B. D. and S. Whitaker (1999). "Cellular growth in biofilms." Biotechnology and Bioengineering **64**(6): 656-668.

Wood, B.D. and S. Whitaker, *Erratum to "Diffusion and reaction in biofilms" [Chemical Engineering Science 53 (1998) 397-425]*. Chemical Engineering Science, 2000. **55**: p. 2349.

Wood, B.D. and S. Whitaker, *Multi-species diffusion and reaction in biofilms*. Chemical Engineering Science, 2000. **55**: p. 3397-3418.

Wood, B.D., M. Quintard, and S. Whitaker, *Jump conditions at non-uniform boundaries: The catalytic surface*. Chemical Engineering Science, 2000. **Submitted**.

Wood, B.D., et al., *Comparison of Volume and Ensemble Averaging: Solute Transport in Porous Media*. Water Resour. Res., 2003. **39**: p. {doi:10.1029/2002WR001723}.